Doctoral Dissertation of MATTEO GRATTIERI
Matriculation Number 803170

POLITECNICO DI MILANO

**DEPARTMENT
OF
CHEMISTRY,
MATERIALS
AND
CHEMICAL ENGINEERING
"Giulio Natta"**

ENZYMATIC-SENSORS FOR MICROBIAL FUEL CELLS:
From bioelectrochemical mechanisms to electrodes development

**Doctoral Program in
Industrial Chemistry and
Chemical Engineering**

XXVIII cycle
2013-2015

Supervisor: prof. M. Bestetti
Assistant Supervisor: prof. S. P. Trasatti
Assistant Supervisor: dr. P. Cristiani
Tutor: prof. W. Navarrini

Doctoral Program Coordinator: prof. A. Frassoldati

Politecnico di Milano – PhD School
Doctoral Program in Industrial Chemistry and Chemical Engineering
Department of Chemistry, Materials and Chemical Engineering “Giulio Natta”

PhD Dissertation of Matteo Grattieri
Enzymatic-Sensors for Microbial Fuel Cells:
From bioelectrochemical mechanisms to electrodes development
Milan, 2016
192 pages

- "The disintegration of organic compounds by microorganism is accompanied by the liberation of electrical energy" -

M. C. Potter, 1911 [1]

This dissertation is dedicated to those who believed in me and in my dreams

Acknowledgements

There are so many people to thank for what I lived in the past three years. I will try to do not forget anybody. I will start with the "professional" acknowledgements and move forward to relatives and friends.

Special thanks go to Prof. Stefano Trasatti, to take me in his research group back in 2011, for the support during these years, for the time dedicated to me, for all the suggestions and explanation that I received. Thank you for the possibility to attend many international congresses and spend two visiting periods around the world.
Thanks to Dr. Pierangela Cristiani that encouraged me to do my best, to try and try again when something was not coming out. Your determination and optimism taught me to never give up.
Thanks to Prof. Massimiliano Bestetti to have been always available to help me along these three years of "external Ph.D" and for the support with the bureaucratic procedures.
Special thanks go to my two hosting professors: Plamen Atanassov and Ernesto Calvo. You received me in the USA and Argentina in a wonderful way. I felt great working in your groups and I had incredible experiences, both from the Academic and human points of view. Thanks for all the explanations and to help me even after my visiting periods. You have been essentials for my dissertation!
Thanks to Prof. Walter Navarrini for the discussions related to my research project and the visiting periods.

Many thanks go to my Mom and Dad. Along my life you support me to follow my dreams (no matter how "dangerous" they might be…and actually chemistry is not always so safe). You have always pushed me to be curious and fascinated of life. Thank you to have been close to me even when I was on the other side of the ocean! You are wonderful parents.
Thanks to my awesome brothers. You have been my "life coaches" and inspiration. I hope that I will be able to reciprocate for what I received helping my amazing nephew Alessandro (and the next to come!)
Thanks to Silvia for being with me during the happy and, (especially!!!), the sad and difficult moments. The challenges of these years were easier to overcome next to you. Thank you also for all the graphic design tips that made fantastic this dissertation :) The World is our, not even an ocean can separate us.

Thanks to my colleagues and friends Alessandra and Edoardo, for all the scientific and less scientific support, for the tea breaks and to bear me every day! I will miss you.
Thanks to my US roommate, colleague, friend and passenger/driver of our scooter, Carlo! Duuude it has been so funny! I'm coming back for a great barbecue.
Thanks to my US friend Jose, we had wonderful time in ABQ. Anodine will always be the best place for a good beer and Breaking Bad discussion (our "alternative shoot" of the final episode deserved at least one Emmy!!). We have to celebrate our graduation!
Thanks to Sofia to introduce me to the biosensors field.
Thanks to the Argentine/European craziest girls: Maria and Catherine. Buenos Aires would not be the same without you! Cath, Super Laccasa will always be the best :)
Thanks to Alvaro, Santiago, Matias and Walter for the time we had together and to teach me the Argentina culture (Santi I miss your empanadas!).
Thanks to the visiting PhD students, Pegah and Mahdi, to make me "discover" your country.

Thanks to the friends of so many years, Cristian, Iona, Ceki, Gale, Dario. It has been more than 13 years ago when we met for the first time, we were so young and we lived so many unforgettable moments, so many experiences…you will always have a place to stay wherever I will be in the world.
Thanks to Giuseppe, (or Prof. Di Grazia) to have been the first professor that made me love chemistry.
Thanks to the friends that I met during the University: Silvietta, Figio, Faggia, Gianni, Giorgione, Cecio, Scorzi, Enri. I can't imagine the past eight years without you!
Thanks to all the students that I met or helped in the lab during these years. Being with you has been helpful also for me!
To conclude, I thank all the other people that for room and time reasons I can't mention here. You know that.

It is time for me to take on a new challenge!

Milan, 2016

List of Pubblications

Part of this dissertation is based on the work contained in the following publications, ordered by most recent. (The Journals Impact Factors 2014 (IF) are reported)

[1] C. Adam; P. Scodeller; **M. Grattieri;** M. Villalba; E.J. Calvo, Revisiting Direct Electron Transfer in Nanostructured Carbon Laccase Oxygen Cathodes, UNDER REVIEW **October 2015**.

[2] **M. Grattieri**; P. Scodeller; C. Adam; E.J. Calvo, Non-Competitive Reversible Inhibition of Laccase by H_2O_2 in Osmium Mediated Layer-By-Layer Multilayer O_2 Biocathodes, *Journal of The Electrochemical Society*, 162(9) (**2015**) G82-G86. (IF: 3.266)

[3] E. Guerrini; **M. Grattieri**; A. Faggianelli; S.P. Trasatti; P. Cristiani, PTFE Effect on the Electrocatalysis of the Oxygen Reduction Reaction in Membraneless Microbial Fuel Cells, *Bioelectrochemistry*, 106 (**2015**) 240-247. (IF: 4.172)

[4] **M. Grattieri**; S. Babanova; C. Santoro; E. Guerrini; S. Trasatti; P. Cristiani; M. Bestetti; P. Atanassov, Enzymatic Oxygen Microsensor Based on Bilirubin Oxidase Applied to Microbial Fuel Cell Analysis, *Electroanalysis*, 27(2) (**2015**) 327-335. (IF: 2.138)

[5] E. Guerrini; **M. Grattieri**; S.P. Trasatti; M. Bestetti; P. Cristiani, Performance Exploration of Single Chamber Microbial Fuel Cell by Using Various Microelectrodes Applied to Biocathodes, *International Journal of Hydrogen Energy*, 39(36) (**2014**) 21837-21846. (IF: 3.313)

[6] B. Li; J. Zhou; X. Zhou; X. Wang; B. Li; C. Santoro; **M. Grattieri**; S. Babanova; K. Artyushkova; P. Atanassov; A.J. Schuler, Surface Modification of Microbial Fuel Cells Anodes: Approaches to Practical Design, *Electrochimica Acta*, 134 (**2014**) 116-126. (IF: 4.504)

[7] C. Santoro; K. Artyushkova; S. Babanova; P. Atanassov; I. Ieropoulos; **M. Grattieri**; P. Cristiani; S. Trasatti; B. Li; A.J. Schuler, Parameters Characterization and Optimization of

Activated Carbon (AC) Cathodes for Microbial Fuel Cell Application, *Bioresource Technology*, 163 (**2014**) 54-63. (IF: 4.494)

[8] E. Guerrini; P. Cristiani; **M. Grattieri**; C. Santoro; B. Li; S.P.M. Trasatti, Electrochemical Behavior of Stainless Steel Anodes in Membraneless Microbial Fuel Cells, *Journal of The Electrochemical Society*, 161(3) (**2014**) H62-H67. (IF: 3.266)

Congresses and Symposia

[1] **M. Grattieri**; S. Pellegrino; F. Secundo; M.L. Gelmi; P. Cristiani; S.P.M. Trasatti, Enzyme-based glucose electrode for MFC application, *European Fuel Cell Technology & Applications Conference (EFC 2015)*, December 16-18, **2015**, Naples (Italy).

[2] D. Perrino; P. Cristiani; **M. Grattieri**; A. Colombo; E. Guerrini; S.P.M. Trasatti, Degradation of organic waste in Microbial Fuel Cells, *Sigma-Aldrich Young Chemist Symposium (SAYCS 2015)*, October 27-29, **2015**, Rimini (Italy).

[3] E.J. Calvo; **M. Grattieri**; C. Adam; P. Scodeller; F.J. Williams, Revisiting Laccase Modified Electrodes for Oxygen Cathodes, *XXIII International Symposium on Bioelectrochemistry and Bioenergetics (BES 2015)*, June 14-18, **2015**, Malmo (Sweden).

[4] C. Adam; **M. Grattieri**; E.J. Calvo, Electrochemical Scanning Tunneling Microscopy (EC-STM) for the Study of Local Properties of Laccase at the Nanoscale, *XIX Argentinian Congress of Physical Chemistry and Inorganic Chemistry* (aaiFQ 2015), April 12-15, **2015**, Buenos Aires (Argentina).

[5] E. Guerrini; **M. Grattieri**; P. Cristiani; S.P. Trasatti, A Microelectrode Study for Anaerobiosis Profiles in Biofilms, *2014 European Corrosion Congress* (EUROCORR), September 8-12, **2014**, Pisa (Italy).

[6] **M. Grattieri**; S. Babanova; C. Santoro; E. Guerrini; P. Cristiani; S.P.M. Trasatti; P. Atanassov, Enzymatic Oxygen Micro-Probe for Analysis of Microbial Fuel Cells, *225th Electrochemical Society (ECS) Meeting*, May 10-15, **2014**, Orlando (Florida - USA).

[7] P. Cristiani; E. Guerrini; S.P.M. Trasatti; **M. Grattieri**, Meromictic Lakes as On-Field Laboratories for Microbial Fuel Cells, *225th Electrochemical Society (ECS) Meeting*, May 10-15, **2014**, Orlando (Florida - USA).

[8] E. Guerrini; P. Cristiani; S.P.M. Trasatti; **M. Grattieri**, A New Carbon-Based Paint For Low-Cost Cathodes in Microbial Fuel Cells, *Fifth European Fuel Cell Technology & Applications*

Conference (EFC 2013), December 11-13, **2013**, Rome (Italy).

[9] E. Guerrini; P. Cristiani; S.P.M. Trasatti; **M. Grattieri**, Evidence of Microbial Influenced Corrosion of Metallic Materials in Microbial Fuel Cell Applications, *2013 European Corrosion Congress* (EUROCORR), September 1-4, **2013**, Estoril (Portugal).

CONTENTS

List of Figures

List of Tables

Nomenclature

A	Electrode Area
A_e	Electrochemically Accessible Surface Area
C	Capacitance
C_{sp}	Specific Capacitance
C_S	Electroactive Species
D	Diffusion Coefficient
E	Potential
F	Faraday Constant
I	Current
i_k	Kinetic-limiting Current-density
i_l	Diffusion-limiting Current-density
L	Film Thickness

P	Power generation
Q	Electrical Charge
R	Resistance
b	Tafel Slope
k_f	Electron Transfer Rate Constant
r	Electrode–Solution Interface Resistance

Greek symbols

Ω	Ohm
α	Charge Transfer Coefficient
ε	Molar extinction coefficient (or molar absorptivity constant)
η	Overpotential
λ	Wavelength
ν	Kinematic Viscosity
ω	Rotation Speed
ζ	Electric efficiency
ζ_n	Stoichiometry Number

Acronyms

BOx	Bilirubin Oxidases
CV	Cyclic Voltammetry
DET	Direct Electron Transfer
E-DET	Extracellular-Direct Electron Transfer
E-MET	Extracellular-Mediated Electron Transfer
ET	Electron Transfer
GDL	Gas Diffusion Layer
LbL	Layer-by-Layer Technique
MCOs	Multi Copper Oxidases
MET	Mediated Electron Transfer
MFC	Microbial Fuel Cell
MPL	Micro-Porous Layer

NI	Native Intermediate
ocp	Open Circuit Potential
ORR	Oxygen reduction reaction
PAH-Os	Poly(allyl)amine Osmium polymer
PB	Phosphate Buffer
PEM	Proton exchange membrane
pI	Isoelectric Point
PTFE	Polytetrafluoroethylene
SCMFC	Single Chamber Microbial Fuel Cell
SEM	Scanning Electron Microscope
SHE	Standard Hydrogen electrode
sr	Scan-rate
WW	Wastewater

Abstract

Microbial fuel cell (MFC) has been one of the most attractive biotechnologies in the recent years since it was demonstrated that it can perform the degradation of organic matter with the concomitant production of electricity. The possible applications of the technology range from the self-powered wastewater treatment, self-powered sensors, production of electricity in remote regions and heavy metals recovery. This technology presents several issues and drawbacks, from fundamental to practical, which still limit the scale-up and the industrial application.

Single-chamber MFC (SCMFC) is a particular configuration that consists of a unique compartment where anode and cathode electrodes are exposed to the same solution, no polymeric membrane is placed between the two electrodes and protons produced at the anode can freely diffuse toward the cathode. This configuration is known as "air-breathing" MFC since one side of the cathode is directly exposed to the air while the other side is facing the same solution of the anode. The absence of a physical barrier between the electrodes of SCMFC brings colonization of the cathode by bacteria, obtaining a bio-catalyzed electrode. However, the absence of a barrier could theoretically increase the oxygen diffusion toward the anode, decreasing the columbic efficiency and the power production performances. There is a lack of studies related to the oxygen consumption in Single Chamber Microbial Fuel Cells, although the knowledge of bioelectrochemical mechanism occurring at the cathode is of primary importance for the operation of the device.

Air-breathing Cathodes are made with polytetrafluoroethylene (PTFE) on the air-side of the electrode, to avoid solution leakage. Thus, PTFE role on the oxygen reduction reaction (ORR) that takes place at the cathode should be considered. However, no detailed studies on its influence on the ORR performances are present in literature.

The application of enzymatic cathodes could improve the open circuit potential (*ocp*) and power production of SCMFC, but has to deal with enzyme inhibition due to the direct contact of the enzyme and the electrolyte of the anodic chamber, wastewater and several different ions that can bind to the actives sites of the enzyme, decreasing the amount of active sites available to the substrates.

A possible application of stainless steel as support for biocatalyzed anodes, to decrease the cost of SCMFC (AISI304 is a couple of orders of magnitude cheaper than Carbon cloth - CC), has to deal with microbial influenced corrosion.

Considering the above remarked issues, the research activity had both fundamental and practical goals and the research project has been focused to four main objectives.

The first objective was the study of the bioelectrochemical mechanism of oxygen consumption in Single Chamber Microbial Fuel Cells (SCMFC). A hand-made amperometric direct electron transfer enzymatic sensor based on bilirubin oxidase was developed and applied in SCMFC to study the oxygen content. Prior to the application in SCMFC, the enzymatic sensor was calibrated in phosphate buffer and wastewater, in different aeration conditions. The lifetime of the biosensor was studied by calibrating the same sensor over 14 days and evaluating the loss in current response.
The hand-made enzymatic microsensor helped clarify the bioelectrochemical mechanism of oxygen consumption in SCMFC. The cathodic biofilm developed on the air-breathing cathode plays a key role to maintain the anaerobic condition in the anode chamber. The biofilm acts as "natural barrier" for the oxygen diffusion to the anode.

The second objective was the study of the PTFE effect on the oxygen reduction reaction in air-breathing biocathodes. Four sets of MFCs were built, where the difference was in the composition of the external layer of the cathode (GDL), with PTFE content from 60 to 200% w/w (weight ratio is referred to the carbon powder). The effect of PTFE content on the cathodes of operating MFCs undergoing ORR was evaluated by electrocatalysis parameters. The results show that MFCs with the lower PTFE percentages in the GDL had a prompt startup and high current outputs. Electro-activation of the cathodes was shown by a change of the Tafel slope from 120 mV/decade of current (corresponding to no electrocatalysis), down to a lower limit of around 80 mV/decade of current (electrocatalytic behavior). Activation is reversible and related to the biological consumption of acetate in the MFCs. The ORR seems mostly related to biologically-assisted electron transfer activation, inhibited by the PTFE presence in the triple-contact zone.

To further improve the electrocatalytic performance of the biocathode, enzyme electrodes have to be developed. Thus, the third objective was the study of the H_2O_2 inhibition on laccase-based enzymatic biocathodes in mediated electron transfer (MET) and direct electron transfer (DET) configuration and the H_2O_2 inhibition mechanisms on the electrodes. The MET laccase-biocathode was made using osmium poly(allyl)amine as the redox mediator. The DET laccase-biocathode was made by adsorption of the enzyme on modified gold electrode with Vulcan® carbon. The study of H_2O_2 inhibition showed two different mechanisms depending on the wiring technique utilized for the sensor development. The inhibitor binds to the free enzyme or the enzyme-substrate complex, obtaining a non-competitive reversible inhibition for the MET biocathode. The inhibitor binds

preferentially to the enzyme-substrate complex in the case of the DET biocathode, obtaining an uncompetitive inhibition, especially at high H_2O_2 concentration.

The fourth and last objective was the study of the electrochemical behavior of AISI304 applied as anode electrode in a SCMFC. The suitability of AISI304 as anode support was investigated in different aeration conditions. AISI304 anode suffered from pitting corrosion due to the presence of residual oxygen in the anode chamber. Whereas, if strictly anaerobic conditions were ensured at the electrode surface, microbial corrosion did not occur. AISI304 and CC showed similarity in term of power generation, organic substances oxidation kinetics and dependence of the electrocatalytic properties on the biofilm settlement and stability.

1.

INTRODUCTION

1.1 Historical and Scientific context

The rapid increase of world population and the improvement of living standards during the last 60 years have dramatically increased the energy consumption and waste production [2]. Although fossil fuels are most likely expected to lead the energy-supply system in the next 30 years [3], renewable energies will rapidly increase their role. At the same time, recycling processes and biodegradation techniques are becoming more important in waste management [4]. Accordingly, considerable efforts of the scientific community have been devoted to study bioremediation and renewable energy technologies [5–8]. Particular interest is given to technologies capable of performing self-powered bioremediation of polluted water for niche application, such as at the small scale or in remote regions not served by industrial treatment plants or power grids [9], and technology for the local production of energy. At the same time, the continuous exchange of data and information is nowadays of primary importance, thus the possibility to develop self-powered remote wireless sensors for environmental, industrial or military application is crucial [10].

In this contest, microbial fuel cells (MFCs) have been one of the most attractive biotechnology for the self powered wastewater (WW) treatment since the capability to perform the oxidation of various organic compounds present in WW and wet wastes with the concomitant production of electricity has been demonstrated [11]. MFC is a challenging technology and several issues call for continuous and deep research in this field, as shown by the impressive increase of publications in the last 25 years (figure 1.1). The number of publications is not the only remarkable point in the propagation of MFC technology of the recent years. Figure 1.2 shows the allocation in the journals of publications related to MFC. It is interesting to note the inter-disciplinary nature of this technology, which ranges from biology and microbiology to bioelectrochemistry, from environmental engineering to materials science. Thus, a collaborative effort of biologists, electrochemists and engineers is required in order to optimize the technology and make it commercially viable.

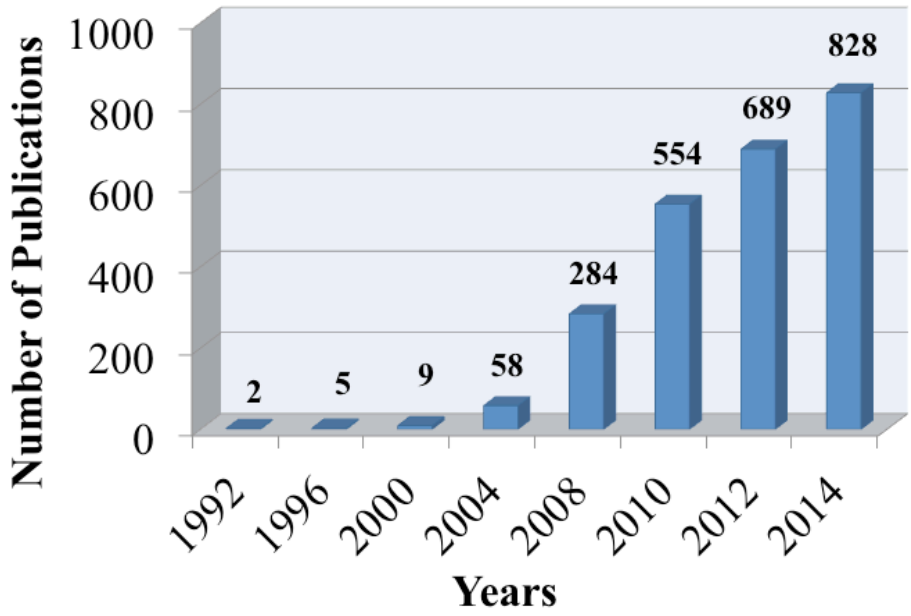

Figure 1.1 Number of publications related to Microbial Fuel Cells. Source Scopus at October 2015.

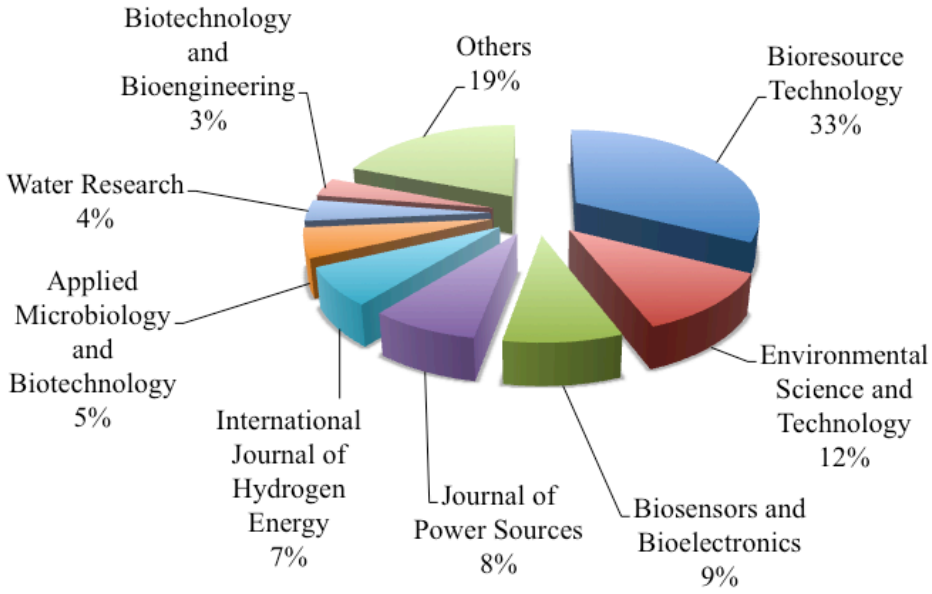

Figure 1.2 Graphical representation of the distribution of publications among the different journals. Source Scopus at October 2015.

1.2 Organization of the Dissertation

The chapters of the dissertation are organized as follow:

The state of the art in microbial fuel cell bioelectrochemistry, cell configurations and electrodes development are presented and the open issues of the technology remarked. Accordingly, the objectives of the dissertation, aimed to solve the presented issues are described and the experimental methods presented. The dissertation has then been divided in “Part 1” and “Part 2”, being the first dedicated to the study of the bioelectrochemical mechanism of oxygen consumption in Single Chamber Microbial Fuel. The latter has been dedicated to the study of bioelectrodes for Single Chamber Microbial Fuel Cell application, construction procedures, electrochemical behavior, performances and inhibition phenomena. At the end, the conclusions are presented. Enzymes and enzymes inhibition mechanisms are described in two appendices as supplementary information.

2.

STATE OF THE ART

2.1 Microbial Fuel Cell Technology

2.1.1 Microbial Fuel Cell Definition

A microbial fuel cell is an electrochemical system that consists of an anode, which accepts electrons produced by the anaerobic degradation of organic matter catalyzed by microbial culture, and a cathode which transfers electrons to an electron acceptor [9]. This technology is aimed to physically separate the oxidation and the reduction processes, as in batteries and fuel cells, forcing microbes to use electrons as intermediate in the electrode cascade processes [12]. When anaerobic conditions are present in the anodic chamber of the MFC, the electrons produced by the anaerobic oxidation of organic compounds (the electron donor) are transferred from the microorganism to the anode surface and flow in the external circuit that connect the anode to the cathode where they will be utilized for the reduction of the final electron acceptor.

2.1.2 Reactions in Microbial Fuel Cell

The communities of microorganisms adhering to the electrode surfaces are named a *biofilm* [13] and the pollutant (organic matter), named the *substrate*, is the carbon and energy source for the biological processes inside the biofilm. The chemical composition of the substrate can strongly affect the biodegradation process and the electricity production. Several substrates have been tested; some examples are reported in table 2.1.

Sodium acetate is the most used substrate for laboratory MFCs due to its high solubility in water and the peculiarity to be an “end product” in many metabolic pathways for higher order carbon sources that makes it readily usable by the microorganisms. Furthermore, it is inert towards microbial unwanted reactions at room temperature such as fermentation and methanogenesis [14].

Glucose is another substrate that has been widely studied [15]. It is a fermentable substrate and can be consumed by competing metabolism such as fermentation and methanogenesis that cannot

produce electricity. It has been found that glucose-fed microbial fuel cells show anodic biofilms with more diverse bacterial community compared with acetate-fed MFCs. This seems related to the presence of microbial species that do not produce electricity but participate in the degradation processes by breaking down the glucose into small molecules and, at a later stage, in less complex compounds that are utilized by electricigens species [16]. Due to the presence of a diverse microbial community, glucose-acclimated MFCs have shown good response to substrate switch. When propionate or acetate were injected in glucose-acclimated MFCs, a rapid increase in the power production was obtained and the maximum power was reached in a short time. Acetate-acclimated MFCs required a longer time to reach the maximum power production [16]. For practical applications, wastewaters have been tested as substrate for MFC to reduce decontamination treatment cost [17].

Table 2.1

Examples of different substrates used in Microbial Fuel Cells.

Substrate	Reference
Sodium Acetate	P. Clauwaert; D. Van Der Ha; N. Boon et al., 2007 [18]
Glucose	S. K Chaudhuri and D. R Lovley, 2003 [15]
Lactate	A. K. Manohar and F. Mansfeld, 2009 [19]
Wastewaters	S. Venkata Mohan; G. Mohanakrishna et al., 2008 [17]
Brewery wastewater	Y. Feng; Xin Wang et al., 2008 [20]
Landfill leachate	A. Gálvez; J. Greenmanb; I. Ieropoulos, 2009 [21]

If we consider glucose as electron donor and oxygen as electron acceptor, we may represent the reactions in a MFC as follow:

Anode Reaction:

$$C_6H_{12}O_6 + 6H_2O \rightarrow 6CO_2 + 24H^+ + 24e^- \qquad E^0 = +0.01V \qquad \text{(eq. 2.1)}$$

Cathode Reaction:

$$6O_2 + 24H^+ + 24e^- \rightarrow 12H_2O \qquad E^0 = +1.23V \qquad \text{(eq. 2.2)}$$

Oxygen is the most energetically favorable electron acceptor due to its high oxidation potential ($E°$= +1.23V at pH 0 and 25°C). However, the low reaction rate of the oxygen reduction reaction leads to high reduction overpotential and under practical conditions the biochemical standard potential for the oxygen reduction reaction (ORR) ($E°$= +0.81V at pH 7 and 25 °C) cannot be reached.

The overpotential (η) is defined as the additional potential, beyond the thermodynamic requirement, needed to drive a reaction at a certain rate [22]. The overpotential affects the electric efficiency (ζ) of the MFC, that is defined as:

$$\zeta = 1 - \frac{\eta_a + \eta_c}{\Delta E^0} \qquad \text{(eq. 2.3)}$$

where η_a is the overpotential for the anode reaction and η_b is the overpotential for the cathode reaction.

It is interesting to note that if ORR kinetics were fast on materials available over the earth's surface, a wide variety of oxidation reactions would occur spontaneously. Metallic materials would corrode very rapidly and non-metallic materials might be highly sensitive to oxidative deterioration. The reactive oxygen species resulting from fast oxygen reduction would exert incredibly high oxidative stresses on living organisms, resulting in accelerated aging and death [23].

2.1.3 How can a microbial fuel cell work?

One common question for a reader not familiar with the bioelectrochemical field is:

How can a MFC work? How is possible that microorganisms transfer electrons to an external collector? These are good questions, and several researches have been focused to clarify these points. Microorganisms are not designed to dispense energy and power a fuel cell. Their redox processes take place inside the microbial cells, thus in a microbial fuel cell the task is to transfer electrons from the inside of the cell membrane to the outside (and *vice-versa* at the cathode) since the electrodes cannot directly penetrate bacterial cells. Moreover, once the electrons have been transferred outside of the cell membrane they must reach the electrode surface via an extracellular electron transfer process. Two major mechanisms can be identified to accomplish the electron transfer between microorganisms and electrodes (figure 2.1) [24]:

Extracellular Direct Electron Transfer (E-DET) and Extracellular Mediated Electron Transfer (E-MET).

2.1.3.1 Extracellular Direct Electron Transfer (E-DET)

The E-DET proceeds via physical contact of the redox protein of the bacterial membrane with the electrodes and does not involve dissolved species. To accomplish E-DET the microorganisms must have electron transfer proteins bounded to the membrane that transfer electrons from the inside of the bacterial cells to the outside where an outer-membrane protein allows the electron transfer (ET) to a solid electron acceptor (the electrode) (figure 2.1 A). The outer membrane consists of c-type cytochromes, multi heme-containing proteins active in ET pathways. Heme is a molecule that forms a number of reduced and oxidized states. For cytochrome *c* the heme is partially exposed to the solution/electrode surface [25] and requires physical contact with the electrode.

It has been recently demonstrated by Lovley research group [26,27] that *Geobacter Sulfurreducens* can evolve electronically conducting molecular *pili*. These *pili* can be considered as microbial "nanowires" that perform carbon nanotube-like charge propagation (figure 2.1 B). Thus, nanowires allow higher microorganism density and consequent higher ET.

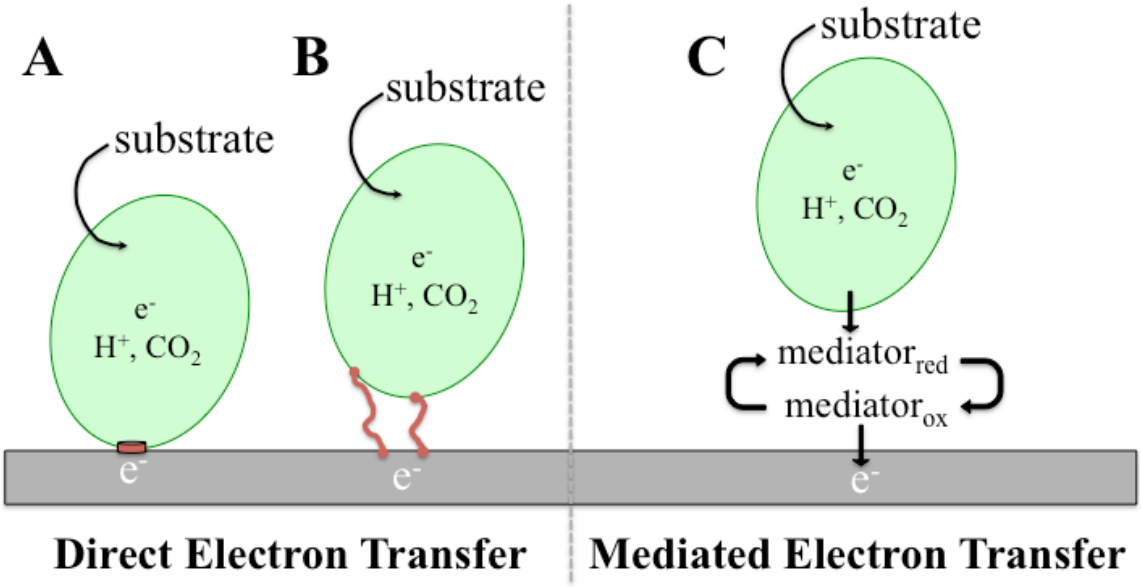

Figure 2.1 Schematic representation of electron transfer mechanisms between microorganism and anode in MFC. Direct contact between cytochromes of the microorganism and electrode surface (A); contact by mean of nanowires (pili) (B); mediated electron transfer via endogenous redox mediators (C).

2.1.3.2 Extracellular Mediated Electron Transfer (E-MET)

E-MET is based on dissolved redox species. Different E-MET mechanisms can be classified depending on the nature of the mediating redox species: i) *via* exogenous and ii) *via* endogenous redox mediators [28]. The E-MET *via* exogenous redox mediators was the object of many studies in the 1980s [29]. Accordingly to this approach, an artificial mediator should be introduced to support ET. Many compounds have been proposed, the majority based on phenazines, phenothiazines, phenoxazines and quinones, but the use of exogenous redox mediators were abandoned due to the necessity of regular addition of the redox compounds. Moreover, Newman and Kolter demonstrated in 2000 that *Shewanella Oneidensis* strain MR-1, formerly *Shewanella putrefaciens*, can excrete a quinone-like molecule that performs the extracellular electron shuttles [30] opening a new scenario: the E-MET *via* endogenous redox mediators.

Thus, E-MET *via* endogenous redox mediators (figure 2.1 C) is based on the capability of microorganism to produce low-molecular electron shuttling compounds [24]. Examples of endogenous redox mediators are bacterial phenazines like pyocyanine and 2-amino-3-carboxy-1,4-naphtho-quinone (ACNQ) [28]. The advantage of this class of redox mediators is that ET is independent of the presence of exogenous mediators.

Microbial extracellular ET is a fascinating area of research that calls for improvements. The majority of the studies until now was aimed to investigate the microbial electron transfer to the electrode surface, whereas for the reverse transfer only a few reports can be found [31–33]. Moreover, to the best of the writer's knowledge, only two microorganisms have been deeply investigated: *Geobacter Sulfurreducens* [26,27] and *Shewanella Oneidensis* [34–36]. Even if some studies have been intended to investigate ET in mixed species biofilms [37,38], further investigations are needed to clarify how other microorganisms, except *Geobacter* and *Shewanella*, contribute to the conductivity of biofilms.

2.2 Microbial Fuel Cell configurations

2.2.1 Two-chamber Microbial Fuel Cell

To lower the cathodic overpotential for the oxygen reduction reaction, materials and cell configurations coming from the well-established low temperature hydrogen fuel cell technology were adopted, where platinum is widely used as catalyst for ORR, especially supported on carbon electrodes [39]. Thus, MFC systems where initially designed with two-chamber configurations that mainly consist of an anodic chamber and cathodic chamber separated by a proton exchange membrane (PEM) (figure 2.2). Abiotic cathodes were used, chemically catalyzed with Pt-based materials as catalyst for the ORR [40]. The protons produced at the anode by the oxidation of the organic matter move through the PEM in the cathodic chamber where they react with OH^- to give water, at the same time the PEM limits the oxygen diffusion toward the anode [12]. The anode chamber can be filled using wastewater or bacteria inoculation whereas buffer solutions are used at the cathode chamber, where aeration must be added to provide oxygen to the cathode [41].

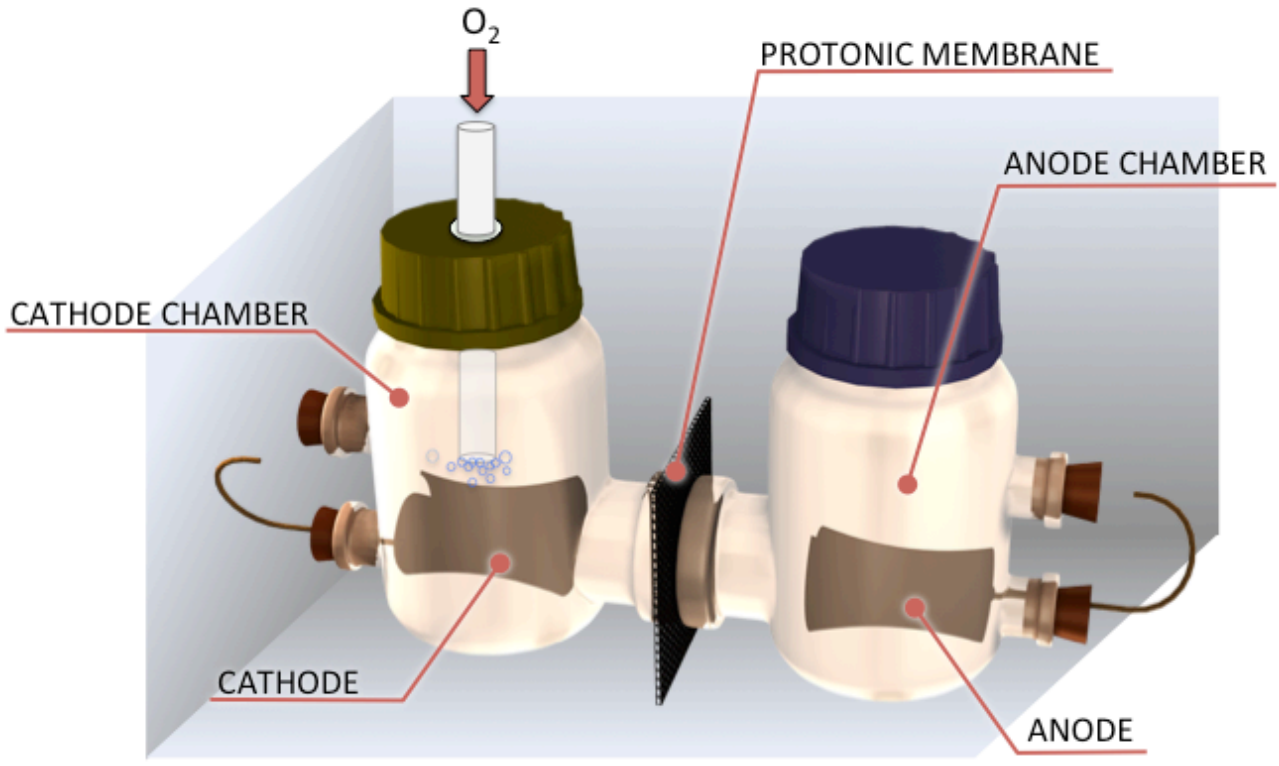

Figure 2.2 Schematic representation of a two chamber MFC with a proton exchange membrane and aeration system at the cathode chamber.

Good electrocatalytic performances were reported for Pt-based cathodes in acidic solution [42], but in the case of neutral or slightly alkaline condition (typical for MFC operation), the performances were lower. Experiments have been conducted using non-catalyzed carbon based cathodes adding final electron acceptors, such as ferricyanide, to avoid the aeration process [43], but the concentration of the electron acceptors needs to be restored, which limits this approach. Moreover, it was demonstrated that the PEM cannot totally prevent oxygen diffusion to the anodic chamber and different methods were investigated to ensure the anaerobic condition with increased costs [44]. The PEM also negatively affects the overall internal resistance of the system.

All the above mentioned issues strongly increase the capital and operating cost and act as bottleneck to the technology. Biocathodes as valid and cost-effective alternatives to platinum for the catalysis of the oxygen reduction for microbial fuel cells were first suggested by studies with marine sediment MFC, demonstrating that biofilm developing on metal electrodes can catalyze ORR [45]. Other preliminary studies reported that biofilm formation on the cathode of two-chamber MFCs, due to bacteria contamination from the anode chamber (or the air), increased the overall performances of the MFC [46]. Moreover, experiments conducted with the cathode chamber specifically inoculated with electrochemically active microorganism showed that the biofilm developing on the cathode acts as bio-catalyst (bio-cathode), and thus no expensive Pt-based catalysts are needed to catalyze the ORR [47]. Based on the presented achievements, researchers have focused on a different MFC configuration named Single-Chamber Microbial Fuel Cell (SCMFC), presented below.

2.2.2 Single-Chamber Microbial Fuel Cell

A single-chamber MFC consists of a unique compartment where anode and cathode are exposed to the same solution, no polymeric membrane is placed between the two electrodes and protons produced at the anode can freely diffuse toward the cathode. This configuration is known as "air-breathing cathode" MFC, since one side of the cathode is directly exposed to the air while the other side is facing the same solution of the anode (figure 2.3).

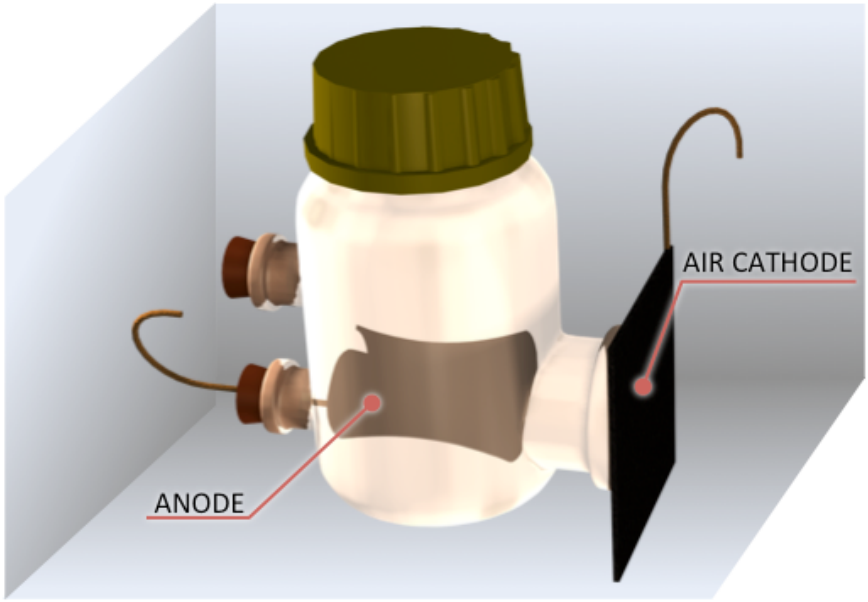

Figure 2.3 Schematic representation of a single chamber MFC.

2.2.2.1 "Air-Breathing" Cathode and Oxygen Diffusion in SCMFC

The absence of a physical barrier between the electrodes of SCMFCs brings colonization of the cathode by bacteria, which form the bio-catalyzed electrode. The biofilm that grows on the electrode is characterized by a complicated chemistry that is rarely investigated in literature. Preliminary studies conducted with hand-made potentiometric sensors evidenced that several reaction take place at the biocathode interface, in addition to the main ORR [48]. As an example, sulfate reduction and carbonate precipitation play a key role and dramatically affect the SCMFC performances.

The absence of a barrier between the biocathode and the bioanode of SCMFC could theoretically increase oxygen diffusion toward the anode, decreasing the columbic efficiency and the power production performances. Conversely, removing the PEM led to increased performances in

preliminary experiments with carbon paper cathodes containing platinum [49]. Further studies demonstrated that SCMFCs based on Pt-free carbon cloth biocathodes can achieve performances similar to the Pt-based cathodes [50,51]. These apparent conflicting results call for new and detailed studies about the bioelectrochemical mechanism that allow the anode to reach anaerobic conditions, as the oxygen consumption in single chamber microbial fuel cells is not well discussed in literature and needs to be clarified.

2.2.2.2 Cathodes for SCMFC

As previously introduced, cathodes for SCMFCs were initially based on carbon cloth electrodes modified with Pt and PTFE to prevent the leakage of liquid electrolyte while allowing the transport of oxygen [52]. Furthermore, Pt-free cathodes with PTFE and Micro Porous Layers (MPLs), consisting in carbon black particles that facilitate the biofilm growth, have been tested [51]. Activated carbon has also been tested together with Pt-free carbon cloth electrodes utilizing PTFE based Gas Diffusion Layers (GDLs) [53].

Among the numerous publications present in literature describing methodology for cathodes preparation [51,54,55], many extremely different amounts of PTFE are used for the construction of the GDL but the effective influence of this compound on the ORR and the biocathode performances is seldom or never discussed.

2.2.2.3 Anodes for SCMFC

At the anode, unmodified carbon cloth electrodes have been commonly applied in SCMFCs due to their ideal characteristic of biocompatibility, high surface area that provides an excellent support for the biofilm settlement, chemical stability and good electrical conductivity [11,20,51,56]. Chemical and electrochemical modification of the carbon cloth anodes have also been investigated aiming to enhance the immobilization of microorganism and increase the surface charge-transfer properties [57]. Chemical modification such as acid attack and thermal treatment were effective to introduce functional groups on the surface to increase the bacteria attachment, but these modifications involve complex steps or harsh conditions that increase the pretreatment cost and can also modify the basic properties of the carbon materials. Electrochemical oxidation is simpler to perform, but the effectiveness of the introduced modifications along SCMFC operation is not clear as most studies were focused on the start up of the cell [57,58].

Moreover, the carbon cloth fragility and its price make it not suitable for the scale up of the technology. Thus, different materials have been tested, such as metal electrodes, nanomaterials and

conductive polymers [59]. Stainless steel electrodes are of great interest due to the extremely low cost of this material if compared to carbon cloth. The main disadvantage of stainless steel is that it can suffer of corrosion problems due to the complex environment of SCMFCs. More research is needed in order to clarify if AISI304 can be applied as anode material in SCMFCs.

2.3 Enzyme-based Amperometric Biosensors for Microbial Fuel Cells

2.3.1 Enzyme-based biocathodes

It has been previously discussed that the overpotential for oxygen reduction is significant even when platinum or other metal-based electrodes are used, showing the critical role of the cathodic reaction for the power generation of MFCs, as the overpotential decreases the electric efficiency (ξ) of the cell. Moreover, it has been demonstrated that Pt-based cathodes suffer from poisoning by compounds in a bacterial solution. The microbial reduction potential of oxygen catalyzed by the biofilm developing in SCMFCs on carbon electrodes was reported at values similar to the Pt-based electrodes for long time operating MFCs, with open circuit potential (*ocp)* in the range of 0.15/0.25 V vs. SHE [18,50,56,60], thus a strong contribution of the overpotential was still present.
A promising approach to decrease the overpotential and consequently increase the *ocp* in MFCs is the use of redox enzymes (see Appendix One – Enzymes, pp. 145) that can catalyze ORR at the cathode, while a microbial anode is present. This type of MFC is named as hybrid-microbial fuel cell. The great advantage of utilizing hybrid systems is that higher *ocp* can be reached. Using redox enzymes of the multicopper oxidase family, it was possible to perform ORR under physiological conditions at high electrode potential (c.a. 0.7 V vs. SHE) [61–63].

2.3.2 Multicopper oxidases

Multicopper oxidases (MCOs) constitute a large family of redox enzymes that coupled the oxidation of different organic substrates with the four-electron reduction of O_2. These enzymes are evolutionarily and structurally related to pigmentation, morphogenesis, detoxification and lignin degradation. The activity of MCOs is due to a minimum of four copper ions (per monomer of a protein molecule) that can be classified in a mononuclear type I copper site (T1) and a trinuclear copper cluster (TNC) T2/T3 depending on their magnetic and optical properties [64]. The T1 site is the primary acceptor of the electrons from the substrate or from the electrode surface. The reduction of the T1 Cu(II) site proceeds with further internal electron transfer to the trinuclear T2/T3 cluster where the reduction of molecular O_2 to water takes place. The T1 site imparts a light blue color to

the enzyme solutions and it is characterized by a distinctly pronounced band of optical absorption at the wavelength of 600 nm (ε ~ 5000 $M^{-1}.cm^{-1}$) [65]. The MCOs can be divided in two classes, depending on the substrate specificity of the T1 site, classified as broad specificity (class 1) and high substrate specificity (class two).

2.3.2.1 Laccases (MCO class 1)

Laccases (E.C. 1.10.3.2; benzenediol: oxygen oxidoreductase) are the most abundant sub-group of MCOs and belong to the broad specificity class (class 1). They are able to catalyze the oxidation of different organic compounds (especially aromatics) including phenols, diamines and some inorganic compounds. Due to the broad substrate specificity, ease of cloning and high catalytic activity, laccases have been the enzyme of choice for many industrial applications [66].

Laccases can have plant or fungal origin, the latter is the most described in literature. Fungal laccases are typically monomeric proteins with a molecular weight of approximately 60−70 kD. They have good heat tolerance and isoelectric point (p*I)* values that range between 3 and 5. Fungal laccases are involved in degradation pathogenesis and detoxification of lignin, but their role during the delignification is not well understood. It was initially suggested that they participate in lignin degradation due to their ability to oxidize various polyphenolic compounds. It was later demonstrated that laccases can catalyze the *in vitro* degradation of lignin, but the produced low molecular weight components can repolymerize. The enzymatic decomposition of lignin results in some toxic products dangerous for the fungal mycelium. Thus, it has been proposed that laccase detoxifies these low molecular weight phenolic components converting them to polymers nontoxic for fungal hyphae [67].

The application of laccases to develop biocathodes in mediated electron transfer (MET) and direct electron transfer (DET) configuration has been extensively demonstrated using carbonaceous and gold electrodes [68–72]. The optimum pH for the majority of fungal laccases is in the slightly acid pH range, due to the binding of hydroxide ions to the T2/T3 site at high pH that prevents the electron transfer from the T1 site to the T2/T3 cluster and decreases the enzyme activity. It has been found that some laccases have poor stability in the presence of chloride [73].

2.3.2.2 Bilirubin Oxidases (MCO class 1)

Bilirubin oxidases (EC 1.3.3.5; bilirubin: oxygen oxidoreductase) are another sub-group of MCOs that oxidize bilirubin to biliverdin with the concomitant reduction of O_2 to H_2O (2.4) [74].

$$Bilirubin + \tfrac{1}{2}O_2 \rightarrow Biliverdin + H_2O \qquad \text{(eq. 2.4)}$$

Bilirubin oxidases (BOx) are attractive since the detection of bilirubin is of great importance for the medical field. In addition, BOx have been immobilized on electrodes surfaces to make oxygen biocathodes and the capability to exchange electrons at the electrode surface in MET and DET electrodes was repeatedly demonstrated using various carbonaceous electrodes [75–78]. Similar to laccases, BOx contains four copper atoms, classified by a T1 and the T2/T3 trinuclear cluster and have a molecular weight of approximately 60 kD. Unlike laccases, BOx display high stability and activity at neutral pH and tolerance towards chloride anions, which makes them a good candidate for the reduction of oxygen in physiological conditions [73,79].

2.3.3 Hybrid-Microbial Fuel Cell with MCO-based Biocathodes

Hybrid-MFCs were studied in a two chamber configuration with laccase coated on a Pt electrode and an *ocp* up to 1.1V was reported [80]. Another study described a two-chamber hybrid-MFC equipped with a cathode utilizing laccase mixed with carbon nanoparticles in a polymer matrix directly on sole carbon paper as support [81]. A *Shewanella* MR1 anode was coupled with a carbon black cathode with adsorbed laccase in a two chamber MFC reaching 1 V *ocp* [82]. An enzymatic cathode was tested in Single Chamber MFC utilizing a bilirubin oxidase-based carbon cloth cathode reaching a maximum *ocp* of 0.690V vs. SHE for the cathode and 1.05 V for the cell [83]. Thus, enzymatic cathodes demonstrated to be extremely useful to enhance the power production of microbial fuel cells. However, one challenge in the application of hybrid-MFC is the stability of the enzymatic cathode due to the presence of the microbial anode, a complex electrolyte and the operation at neutral/slightly alkaline pH. Small inorganic anions, such as hydroxyde, fluoride and chloride, can bind to the TNC of laccases, inhibiting the enzymes. Thus, the enzymatic cathode could suffer of deactivation and inhibition problems (see Appendix Two: Enzyme Inhibition, pp. 155). Moreover, it has been demonstrated that laccase and bilirubin oxidase are inhibited by H_2O_2 [84,85]. Later studies further underlined that the H_2O_2 produced by glucose oxidase-bioanode can inhibit the performance of laccase biocathode with a consequent loss in performances of the full

device [86]. It was found that H_2O_2 irreversibly affect the electrocatalytic activity of bilirubin oxidase, whereas reversible inhibition was found in the case of laccase biocathode [85], but the inhibition mechanism is not well described in literature, calling for detailed investigations.

2.4 Construction of Enzyme-based Amperometric Biosensors

When constructing an enzyme-based amperometric biosensor, or "enzyme electrode", the electron transfer between the enzyme and the electrode surface is the primary goal. In order to achieve this result, different techniques have been developed to produce the electrodes. Adsorption, covalent binding, crosslinking and entrapment of the enzyme in redox polymer hydrogels are some examples [87–89]. Moreover, polymer matrixes have been tested to improve sensor stability and lifetime [90,91]. In the last decade, enzyme engineering has been of great interest and several efforts were devoted to maximizing the stability of enzymatic electrodes, facilitating the electron transfer and improving their performances [92–94]. Depending on the type of electronic coupling between the redox enzymes and electrodes for the construction of enzyme electrodes or biosensors, three generations of amperometric biosensors can be described [25]:

- First-generation biosensor: a substrate or a product of the enzymatic reaction (i.e. H_2O_2) diffuses to the transducer and causes the electrical response.
- Second-generation biosensor: the enzyme delivers the electrons produced by the enzymatic reaction to an artificial mediator that communicates with the transducer, obtaining the electrical response.
- Third-generation biosensor: the enzyme directly delivers the electrons produced by the enzymatic reaction to the electrode.

2.4.1 First-generation biosensor

First-generation biosensors are based on the electrochemical detection of the decrease of a substrate or the increase of an enzymatically generated product (figure 2.4) [95]. Basically, the oxygen consumption or the hydrogen peroxide productions are measured for oxidase enzymes. The latter has been preferred due to a better reproducibility (O_2 concentration may vary during the measurement) and the possibility to decrease interfering reactions. Redox inorganic mediators capable to catalyze the oxidation or reduction of hydrogen peroxide are of great interest as they decrease the applied potential and, thus, avoid many electrochemical interferences. Prussian Blue (ferric hexacyanoferrate) has found large application for this purpose [96–98].

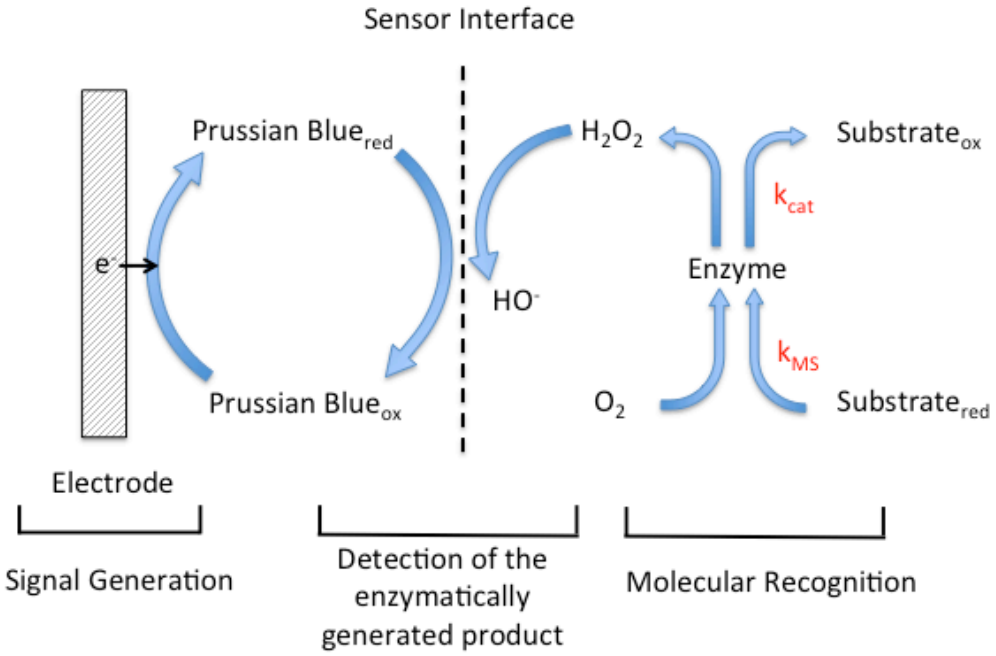

Figure 2.4 Schematic representation of an amperometric biosensor of first-generation.

2.4.2 Second-generation (MET) biosensor

Small redox active molecules (mediators) can react with the enzyme active sites and the electrode, shuttling the electrons between the enzyme and the electrode surface (figure 2.5). Electrostatic complexing of the enzyme with redox active molecules is of remarkable interest particularly in the case of large enzymes, like glucose oxidase (186 kD), where the prosthetic group is buried inside the protein structure. Thus, MET biosensors have the advantage to greatly facilitate the enzyme-electrode communication [89]. Figure 2.5 depicts from right to left the three processes that take place in a second generation biosensor: the molecular recognition, the redox mediation and the signal generation. The mediator is regenerated at the electrode surface with no overpotential. The redox molecules (redox shuttles) can be organized in redox polymers (or redox hydrogels), obtaining an electron-conducting phase where the permeation of water-soluble reactants and products are rapid. In these redox polymers, the electrons can diffuse by several mechanisms as self-exchange between immobile redox centers or collision between mobile reduced and oxidized redox centers [63].

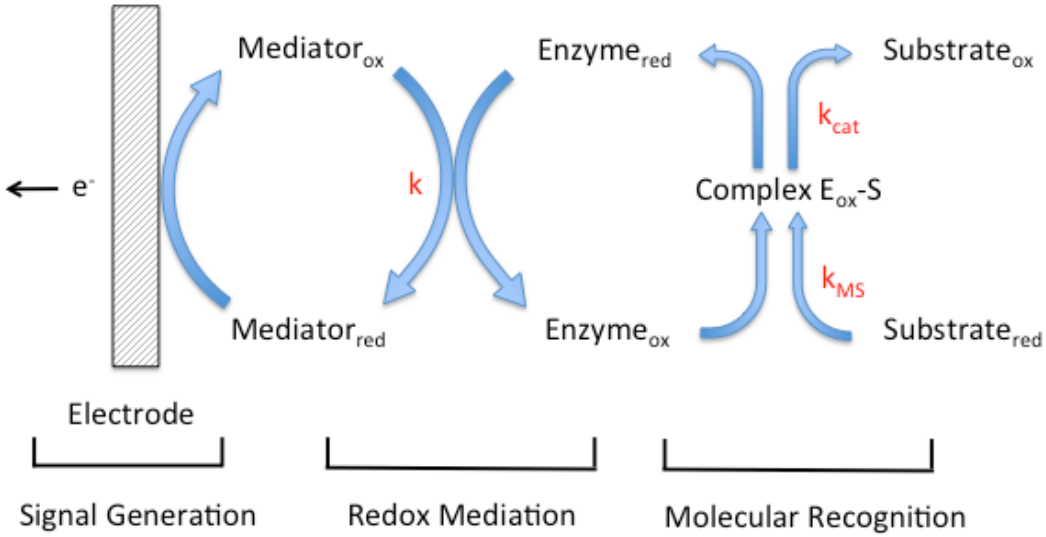

Figure 2.5 Schematic representation of an amperometric biosensor of second-generation.

2.4.3 Third-generation (DET) biosensor

Direct electron transfer (DET) occurs through the enzyme's ability to oxidize or reduce a substrate while transferring the electrons to or from the electrode surface, without the need for an external mediator. Thus, electrons are transferred from the enzyme active site to the electrode, or vice versa (figure 2.6) [99].

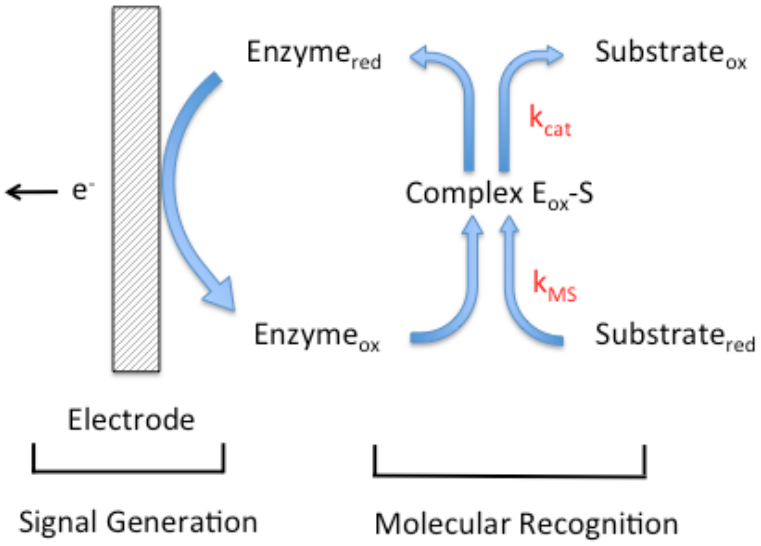

Figure 2.6 Schematic representation of an amperometric biosensor of third-generation.

The absence of the mediator provides the advantage to operate in a potential window closer to the redox potential of the enzyme itself [25]. Following Marcus' theory, the kinetics of electron transfer between two redox species is determined by the driving force (e.g., the potential difference), the reorganizational energy and the distance between the two redox centers [100]. Thus, the unfavorable orientation of enzyme molecules on electrode surface may block the electron exchange between the electrode and the electroactive redox center of enzyme via a tunneling mechanism. In order to ensure DET, the enzyme active center must be placed in the proximity of the electrode surface and properly oriented. Over the past years extensive research on the DET between enzymes and electrodes has been carried out. Experimental evidences for DET were reported using different redox enzymes and applying various strategies to orientate enzymes and minimize the enzyme-electrode distance, thus, promoting the DET [101–106].

The efficient DET remains a scientific challenge due to the location of the active sites of enzymes, which in many cases are situated deeply in the apoenzyme structure [89].

3.

OBJECTIVES OF THE DISSERTATION

Despite the results achieved in the recent years and presented in the previous chapter, several issues still affect the microbial fuel cell technology, ranging from fundamental to more practical problems. It is important to remark the lack of studies related to the oxygen consumption in Single Chamber Microbial Fuel Cells, although the knowledge of bioelectrochemical mechanisms occurring at the cathode is of primary importance for the operation of the device. The use of PTFE to make Gas Diffusion Layer in Open-Air Cathodes with no detailed study about the PTFE influence on the oxygen reduction reaction performances is another point to be considered. The applicability of hybrid-microbial fuel cells with enzymatic cathodes could improve the *ocp* and power production of the devices, but there are only few detailed studies on the inhibition mechanisms of enzyme-based biocathode. A possible application of stainless steel as a support for biocatalyzed anodes, to decrease the cost of SCMFC, has to deal with microbial influenced corrosion. Considering the above issues, the research activity had both fundamental and practical goals and the PhD project has been focused to four main objectives:

One: *Study of the bioelectrochemical mechanism of oxygen consumption in Single Chamber Microbial Fuel Cells.*

Two: *Study of the PTFE effect on the oxygen reduction reaction in air-breathing biocathodes.*

Three: *Study of H_2O_2 role and inhibition mechanisms on laccase-based oxygen biocathodes in mediated electron transfer (MET) and direct electron transfer (DET) configuration.*

Four: *Study of the electrochemical behavior of AISI304 applied as anode in SCMFC.*

To accomplish objective one, a hand-made amperometric enzyme sensor based on bilirubin oxidase was developed. The sensor construction and application for oxygen measurement in SCMFC is described in Part 1 – Bioelectrochemical mechanisms, chapter 5 of the dissertation. The experimental activity related to objectives two, three and four is reported in the Part 2 of the dissertation – Electrode Development, chapter 6, 7 and 8 respectively.

4.

METHODS

4.1 Fundamentals of the applied techniques

4.1.1 Electrochemical techniques

Electrochemical techniques are applied to study redox processes in the heterogeneous phase, thus the chemical species that react on the electrode surface, taking or releasing electrons. The majority of the electrochemical techniques required three electrodes: a working electrode (WE), a counter electrode (CE) and a reference electrode (RE) connected to a potentiostat. The WE is the electrode where the electrochemical processes of the test take place. The current flows between the WE and the CE that is characterized by a bigger area than the WE, to avoid polarization and interference on the WE response. The electric circuit is closed by means of the electrolytic solution. The potential of the WE is referred to the RE, which has a fixed potential. No current flows between the WE and the RE.

The international accepted primary reference electrode is the *standard hydrogen electrode* (SHE) that has all components as unit activity:

$$Pt / H_2(a=1) / H^+(a=1, aqueous) \qquad \text{(eq. 4.1)}$$

However, SHE is not very convenient from an experimental standpoint, thus potentials are often measured and quoted with respect to other reference electrodes. A common reference electrode is the *silver-silver chloride electrode*:

$$Ag / AgCl / KCl\ (saturated) \qquad \text{(eq. 4.2)}$$

with a potential of +0.197V vs. SHE;

or:

$$Ag / AgCl / KCl\,(3M) \qquad \text{(eq. 4.3)}$$

with a potential of +0.210V vs. SHE.

Another common reference electrode is the *saturated calomel electrode* (SCE), which is:

$$Hg / Hg_2Cl_2 / KCl\,(saturated) \qquad \text{(eq. 4.4)}$$

with a potential of +0.242V vs. SHE [22].

In this dissertation, the potentials are referred to *silver-silver chloride (3M)* or *saturated calomel electrode* as specified in each chapter.

4.1.1.1 Polarization

In electrochemistry, a polarization consists of a technique that allows applying a potential to the working electrode to shift the potential from the equilibrium value upon passage of faradic current. The extent of the polarization is measured by the applied overpotential η:

$$\eta = E - E_{eq} \qquad \text{(eq. 4.5)}$$

It is possible to distinguish between potentiostatic polarization and potentiodynamic polarization.
In the case of the potentiostatic polarization, the WE is polarized to a fixed potential and the current between the WE and the CE is recorded as a function of time. This technique is also named as chronoamperometry, which is the most common technique used for the operation of amperometric sensors. It annihilates the influence of the capacitive current on the sensor reading and thus the performed measurement. In a potentiodynamic polarization, the potential applied to the WE is changed linearly in the time, with a scan rate ($mV \cdot sec^{-1}$), following a potential ramp, while the current is measured. This is referred to as voltammetry.

4.1.1.2 Cyclic Voltammetry

Cyclic voltammetry (CV) is a potentiodynamic electrochemical technique where the potential of the WE is changed linearly in the time between potential E_1 and E_2, according to a characteristic triangular diagram (figure 4.1). To obtain the cyclic voltammogram the current at the WE is plotted versus the applied potential (i-E curve).

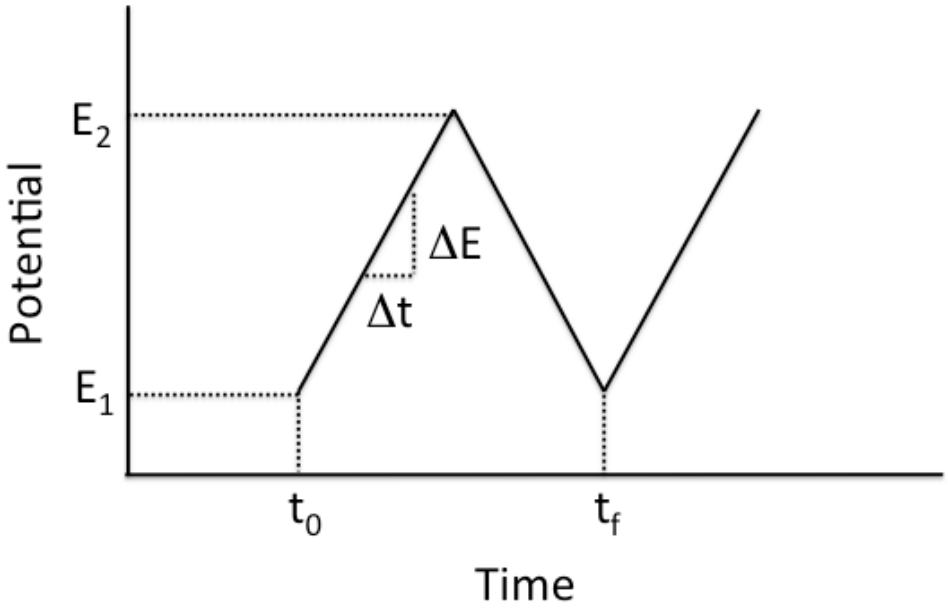

Figure 4.1 Potential-time diagram for a cyclic voltammetry.

4.1.1.3 Rotating Disk Electrode

The Rotating Disk Electrode (RDE) is a fundamental tool that allows controlling the mass transport towards the working electrode. The mass transport is accelerated by the application of a mechanic force that produces a forced convection. Thus, RDE allows to control and to define the hydrodynamic conditions of the experiments. The RDE consists of a conductive disk of the desired material for the working electrode, embedded in an inert non-conductive polymer. The plate is connected to an electric motor to control the electrode's rotation speed (ω). The Levich equation predicts the current observed at the RDE and shows that the current is proportional to the square root of the rotation speed when no kinetic limitation is present:

$$i_l = 0.62nFAD^{2/3}\omega^{1/2}\nu^{-1/6}C_s \qquad \text{(eq. 4.6)}$$

where i_l is the measured current, n is the number of electrons transferred, F is the Faraday Constant, A is the electrode area, D is the diffusion coefficient, ω is the rotation speed, ν is the kinematic viscosity of the solution and C_S is the electroactive species.

When there is a kinetic limitation, the current is predicted by the Koutecky-Levich equation:

$$\frac{1}{i} = \frac{1}{i_k} + \frac{1}{i_l} = \frac{1}{i_k} + \frac{1}{0.62nFAD^{2/3}\omega^{1/2}\nu^{-1/6}C} \qquad \text{(eq. 4.7)}$$

where i_k and i_l are the kinetic-limiting and diffusion-limiting current densities respectively;

i_k is: $$i_k = nFAk_fC \qquad \text{(eq. 4.8)}$$

where k_f is the electron transfer rate constant.

Figure 4.2 depicts the variation of the current with the rotation speed of the RDE for a reaction with kinetic limitation.

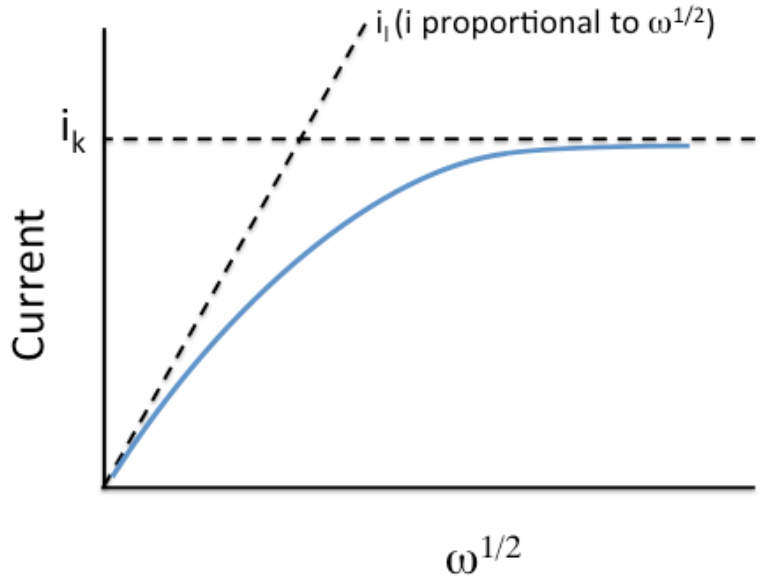

Figure 4.2 Relation of the current with the rotation speed ($\omega^{1/2}$) for a rotating disk electrode polarized at a fixed potential in the case of slow kinetic.

4.1.2 Microscopy Technique

4.1.2.1 Scanning Electron Microscopy

The utility of the Optical Microscopy in nanotechnology is severely limited by its resolution (close to 150nm) due to the diffraction limit of the light. Electron microscopy overcame this problem thanks to wavelengths between 10^{-2} and 10^{-3} nm [107]. The Scanning Electron Microscope (SEM) utilizes focused beams of electrons to obtain information. When the incident electrons come in contact with the specimen, energetic electrons are released from the surface. The scatter patterns made by the interaction yields information on size, shape, texture and composition of the specimen.

A variety of detectors are used to attract different types of scattered electrons, including secondary and backscattered electrons as well as x-rays.
The specimens need to be conductive; non-conductive specimens undergo to sputter coating to be covered with a thin layer of conductive material (typically gold/palladium alloy).

4.2 Calculations

4.2.1 Single Chamber Microbial Fuel Cell productivity

The Single Chamber MFCs were polarized with a constant resistance (R) of 100Ω and the cell potentials (E) across the resistance were monitored. E was recorded using multichannel data loggers. The current was calculated based on Ohm's law $I = E/R$ and power generation (P) was calculated using the formula $P = E \cdot I$.

4.2.2 Tafel slopes

Processing of data from quasi-stationary polarization curves permits the calculation of the Tafel slope (b) and the electrode–solution interface resistance (r) of the electrodic process. Basically, two methods are applicable for the Tafel slope experimental determination [108]. The first is based on one of the forms of the Tafel equation:

$$E = a + b\log(I) \qquad \text{(eq. 4.9)}$$

where E is the electrode potential, I is the current, and a is a parameter connected with the experimental conditions of the electrochemical process under evaluation. Under activation control, an electrochemical half-reaction can show a linear section in a graph of E vs. log(I), whose slope is b. This method is prone to subjective evaluation, and on highly porous materials might bring to modifications of the expected Tafel slope, due to microporosity, channel length and width [109]. The derivative method gives more reliable and objective Tafel slope values. The empirical Tafel equation is first added with the ohmic drop term ($r \cdot I$). Since the total current I is the product of the current density i and the surface area A, the below equation is derived:

$$E = a + b\log(I) + r \cdot I = a + b\log(i \cdot A) + r \cdot i \cdot A \qquad \text{(eq. 4.10)}$$

The differentiation of Eq. (4.10) with respect to the current gives:

$$\frac{\partial E}{\partial I} = 0 + \frac{b}{I \cdot \ln(10)} + r \qquad \text{(eq.4.11a)}$$

for the total current (I), and

$$\frac{\partial E}{\partial i} = 0 + \frac{b}{i \cdot \ln(10)} + r \cdot A \qquad \text{(eq.4.11b)}$$

for the current density (i).

From Eq. (4.11a), a graph of $\partial E/\partial I$ vs. $1/I$ gives a straight line, where the slope is proportional to the Tafel slope b, and the intercept gives the ohmic resistance r of the electrode. From Eq. (4.11b), a graph of $\partial E/\partial I$ vs. $1/i$ gives the Tafel slope and the resistance multiplied by the surface. Evaluation of $\partial E/\partial I$ and $1/I$ is easily obtained from numerical methods.

4.2.3 Capacitance and Electrochemical Accessible Surface Area

Electrochemically active area is defined as the extent of surface capable of producing a faradaic current. As a rule, the extent of electrochemical surface area differs from the geometric (total) accessible area, and from the projected surface area. The difference is particularly pronounced for highly porous materials, as it is the case of the GDL and MPL layers of the cathodes of MFC systems.

The definition of the capacitance C is:

$$C = \frac{\Delta Q}{\Delta E} \qquad \text{(eq. 4.12)}$$

where ΔQ is the electrical charge supplied to the capacitor and ΔE is the resulting potential variation. Based on the definitions of current (I) and scan-rate (sr), it is possible to obtain the following equation:

$$sr \cdot C = I \qquad \text{(eq. 4.13)}$$

where I is the average between the anodic and cathodic currents, in the purely capacitive zone of the voltammograms. A graph of I vs. scan-rate gives a straight line, whose slope is an estimation of the total capacitance C of the electrodic double-layer capacitor.

The total capacitance C is related to the specific capacitance (c_{sp} / μF cm^{-2}) by the equation

$$C = c_{sp} \cdot A_e \qquad \text{(eq. 4.14)}$$

where A_e is the real conductive surface wetted by the electrolyte, also called electrochemically accessible surface area [110,111]. Therefore, the experimental determination of the capacitance C gives a quantity that is proportional to the electrochemical surface area. At constant temperature, c_{sp} changes with electrolyte concentration. As a consequence, C depends on both surface extent and electrolyte concentration. An increase in electrolyte concentration produces a more compact electric double layer, generating a higher capacitance.

4.3 Amperometric enzyme biosensors

In this dissertation second and third-generation enzyme biosensors are presented. The techniques applied to make the sensors are following described.

4.3.1 Second-Generation (MET) Enzyme Biosensor

4.3.1.1 Redox mediator

To make the second-generation biosensors Osmium bipyridine poly(allyl)amine (PAH-Os) was used as redox mediator (figure 4.3C).

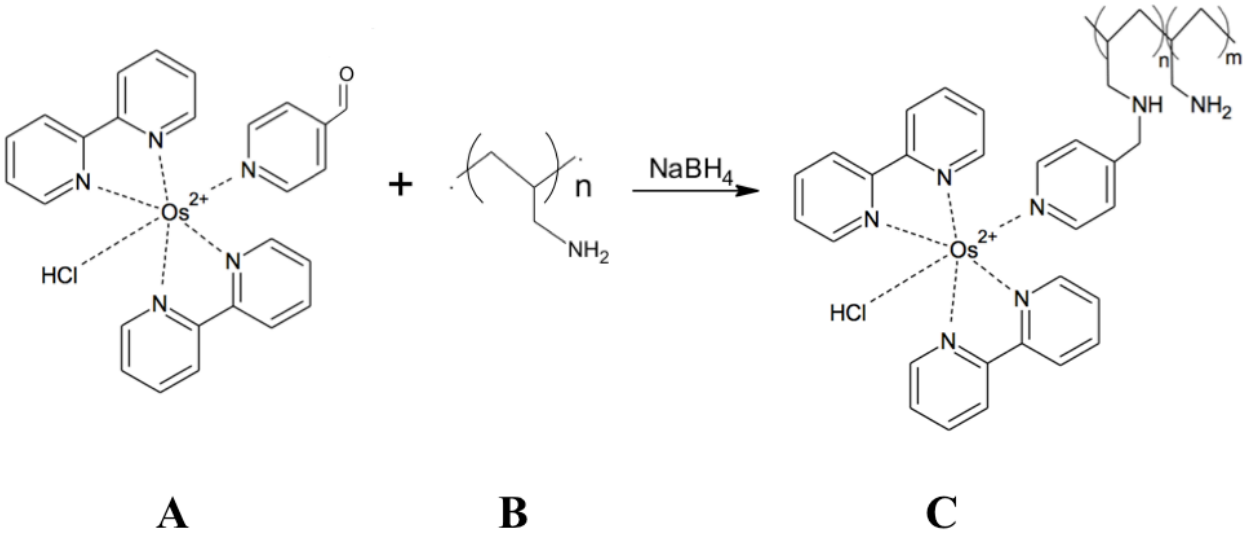

Figure 4.3 Osmium bypiridine modified poly(allyl)amine (C) redox polymer synthesis. $[Os(bpy)_2Cl(pyCHO)]^+$ complex (A); poly(allyl)amine (B).

The PAH-Os is a redox polymer obtained from the reaction of the complex $[Os(bpy)_2Cl(pyCHO)]^+$ (figure 4.3A) with the amino groups of the poly(allyl)amine (figure 4.3B) [112]. The osmium complex anchored to the polymer has sufficient mobility to mediate the electron transfer with different enzymes as extensively demonstrated [70,113]. The redox mediator was immobilized onto the electrode surface of a modified gold electrode, together with the enzyme, using the self-assembled, layer-by-layer technique.

4.3.1.2 Self-assembled Layer-by-Layer Technique

The self-assembled layer-by-layer technique (LbL) consists in the alternate deposition of macromolecules, polycations and polyanions, on solid surfaces as schematized in figure 4.4 [114]. The deposition process is due to the overcompensation of charges. When the charged polyelectrolyte is adsorbed on the modified electrode surface, the charge is not balanced, but overcompensation is obtained and the polarity of the topmost layer is inverted. Thus, the adsorption of a new layer of opposite charge is possible. The thickness of the multilayers electrode is exponentially increased by increasing the layers number [115].

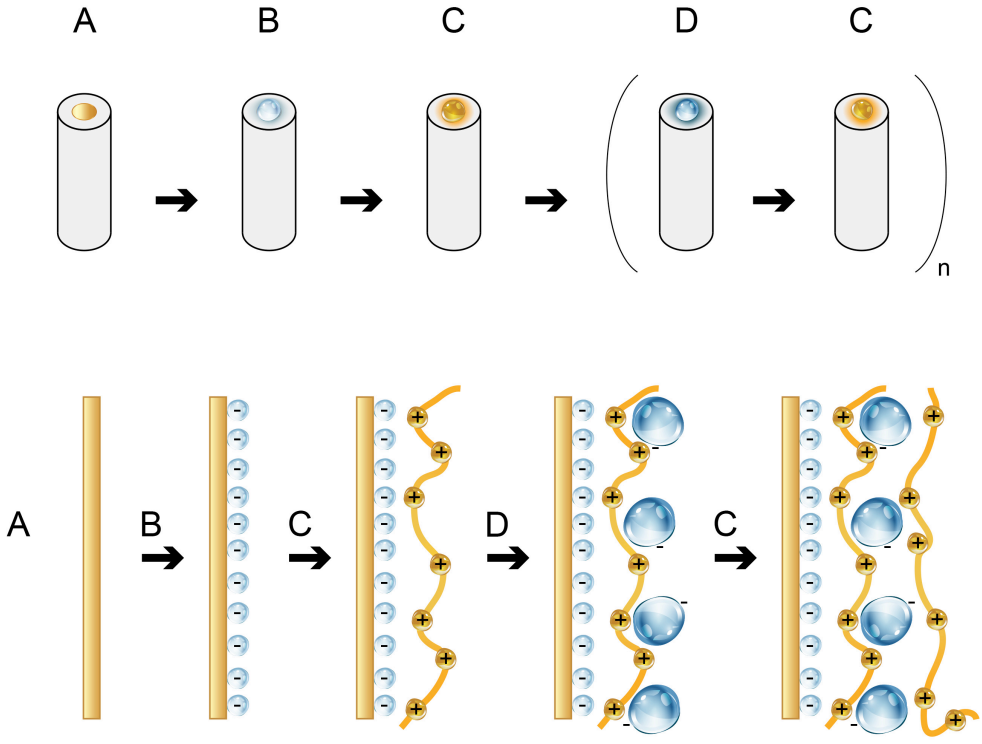

Figure 4.4 Self-assembled layer-by-layer technique steps diagram. Gold electrode (A); gold-surface modification (B); polycataion deposition (C); macromolecule deposition (D). Steps C and D can be repeated until the desired number of layers.

4.3.2 Third generation (DET) biosensor

The DET biosensors were made in two different ways: 1) by cross-linking on carbon electrodes using 1-pyrenebutyric acid, N-hydroxysuccinimide ester (PBSE) as "tethering" agent (figure 4.5), which provides stable and effective enzyme immobilization and orientation. This technique allowed to develop an amperometric oxygen biosensor based on bilirubin oxidases; and 2) by simple adsorption on modified gold electrode with Carbon Vulcan® for the H_2O_2 inhibition study on Laccase-based biocathode.

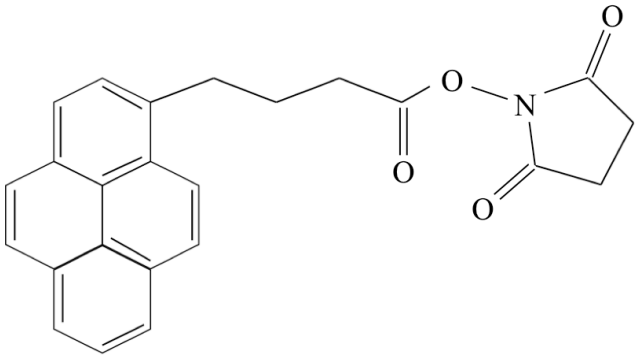

Figure 4.5 1-pyrenebutyric acid, N-hydroxysuccinimide-ester (PBSE)

The pyrene moiety of PBSE interacts with the aromatic-like structure of carbon materials through irreversible π-π stacking. This allows the functionalization of the electrode surface with succinimidyl ester groups that are highly reactive to nucleophilic substitution by primary and secondary amines that exist on the surface of the enzyme molecule [104,106]

Part 1

BIOELECTROCHEMICAL MECHANISMS

5.

OXYGEN CONSUMPTION IN SINGLE CHAMBER MICROBIAL FUEL CELL

From: ***M. Grattieri**; S. Babanova; C. Santoro; E. Guerrini; S. Trasatti; P. Cristiani; M. Bestetti; P. Atanassov, Enzymatic Oxygen Microsensor Based on Bilirubin Oxidase Applied to Microbial Fuel Cell Analysis, Electroanalysis, 27(2) (**2015**) 327-335.*

5.1 Introduction

In a microbial fuel cell, the direct contact of oxygen with other reactants confined in the anode compartment must be avoided, in order to divert electrons and utilize them in an external load. If oxygen can reach the anode, short circuit of the system is obtained. In a two-chamber microbial fuel cell, the separation between oxygen and reactants at the anode is ensured by the presence of a PEM. In the case of Single Chamber MFCs, no physical barrier is placed between anode and cathode. Thus, the presence of oxygen at the anode could significantly, or totally, decrease the kinetics of the involved processes and the efficiency of the electron transfer between microorganisms and electrode surface. Therefore, the diffusion of oxygen is an unwanted environmental factor, which should be diminished to negligible values if cannot be completely avoided. Conversely, the concentration of oxygen at the cathode needs to be maximized, as it is often the limiting reagent for efficient MFC operation [13,116].

Based on the above context, a selective and localized measurement of oxygen content in SCMFCs would clarify the bioelectrochemical mechanism of oxygen consumption and would be of primary importance for understanding the processes and the mechanisms involved in MFC operation [117]. Nevertheless, current MFC studies rarely report oxygen concentration measurements [118]. Most frequently, the presence/absence of oxygen is just assumed. Commercial oxygen microsensors are relatively “cheap” in comparison to other advanced analysis techniques [119] but considering the cost of the equipment to use common microsensors, the price can be significant. Moreover, the

characteristic application in MFC of the existing microsensors is generally difficult due to the complex geometry of the cell. Therefore hand-made microsensors with high selectivity, high sensitivity and a flexible structure has to be developed [120].

As previously introduced, enzymatic molecules are reported as highly active and selective towards a specific and unique reaction [121], which makes them useful for many industrial applications [122], as well as catalysts in the design of biofuel cells and biosensors [101,123,124]. The enzymatic microsensors have several important features and the most important ones are selectivity and substrate specificity. Among the broad and diverse list of proteins, the enzymes belonging to the family of multicopper oxidases (MCOs) are one of the most extensively studied and explored enzymes in the design of bio-electrochemical systems. This is mainly due to their capability for direct oxygen reduction to water, performing in nature and when incorporated in the design of enzymatic electrodes [70,78,85].

Two possible electron-transfer mechanisms exist, by which MCOs can perform oxygen reduction reaction (ORR) at the electrode surface [61,76–78]:

i) a four-electron transfer

$$O_2 + 4H^+ + 4e^- \rightarrow 2H_2O \quad \left(E^0 = 1.23V \; vs. \; SHE\right) \qquad \text{(eq. 5.1)}$$

ii) or a two-electron transfer producing hydrogen peroxide

$$O_2 + 2H^+ + 2e^- \rightarrow H_2O_2 \quad \left(E^0 = 0.69V \; vs. \; SHE\right) \qquad \text{(eq. 5.2)}$$

The formation of H_2O_2 decreases the number of electrons transferred per molecule of oxygen reacted and thus decreases the Columbic efficiency of the bioelectrode. In addition the produced H_2O_2 can have negative impact on living cells.

Bilirubin oxidase (BOx) was chosen to develop the hand-made biosensor for the study of SCMFCs. For application of BOx in the design of amperometric biosensors to monitor MFC, reaction (5.1) is the most favorable, since it extracts the maximum number of electrons, increasing the recorded current and avoids the release of toxic products [78]. A key advantage of BOx and all MCOs is their ability to reduce oxygen by carrying out direct electron transfer avoiding the need of mediator utilization. In order to achieve DET, the enzyme active center should be placed in the proximity of the electrode surface. One strategy to promote the DET is the modification of a carbon support with 1-pyrenebutyric acid, N-hydroxysuccinimide ester (PBSE), which provides stable and effective enzyme immobilization. A PBSE-modified carbon cloth electrode was reported to support faster and more complete bio-electrochemical oxygen reduction than unmodified electrodes with only

physisorbed BOx, generating higher current densities. According to Ramasamy [106], this effect can be related to the formation of a covalent bond between the amino group of the enzyme and the PBSE-tether that reduces the electron tunneling distance between the enzyme and the electrode, facilitating DET. Moreover, it has been demonstrated that by cross-linking the enzyme to the electrode with PBSE, four-electron transfer mechanism of oxygen reduction reaction takes place (Equation 5.1) [78]. BOx displays high activity and stability at neutral pH and high tolerance towards different anions, such as F^- and Cl^- [125]. Therefore BOx has been used in physiological conditions as a bilirubin or DNA sensor [126,127] and as a catalyst for the ORR in biofuel cells including MFC [77]. Constructing enzymatic oxygen microsensor based on the utilization of bilirubin oxidase will provide specific oxygen reduction avoiding the influence of other electrochemically active species. In fact, the electrochemical active species are very likely to be present in wastewater or to be produced as intermediates or final metabolic products of organics oxidation during MFC operation. The developed sensor was further explored for localized oxygen measurements, carried out in an operating MFC. Based on the sensor readings, an oxygen profile from the anode surface to the cathode and through the cathodic biofilm was created.

5.2 Materials and Methods

5.2.1 Sensor construction

A sheet of carbon cloth (Fuel Cell Earth) (Figure 5.1A) was used as a source for the bundle of carbon cloth fibers (CC) (Figure 5.1B) (average diameter for a bundle of fibers ≤ 100 μm; 10 μm single fiber diameter). The bundle (ohmic resistance between 6 and 10 Ω) was used as support for the construction of the enzymatic oxygen microsensor that at the end, as specified below, itself composed of only one fiber. In order to electrically connect and make the sensor more robust, the bundle of carbon cloth fibers was linked with a nickel wire (200 mm diameter) using a bi-component (A – monomer; B – hardener) silver conductive epoxy resin (H22 EPO-TEK) with a mixing ratio of 100A : 4.5B w/w. The volume resistivity of the paste is reported as <0.005 Ω·cm. Curing of the conductive epoxy resin was performed at 80°C for 50 minutes. The obtained device (ohmic resistance between 15 and 30Ω) was placed inside of a micropipette tip (200 mL Yellow Universal Pipette Tip, Figure 5.1C) leaving only one carbon fiber out of the tip at a certain extent. A bi-component nonconductive epoxy resin (3M Scotch-Weld Epoxy Adhesive DP100 Clear) with a curing time of 8 hours at 25°C was used to insulate the fiber and leave only the tip uncovered (Figure 5.1D). The tip was then lapped with abrasive paper, thus the sensor exposed to the

electrolyte was the end part of the single carbon fiber with a diameter of 10 μm ($7.85 \cdot 10^{-7}$ cm^2). Only this portion was further subjected to enzyme immobilization.

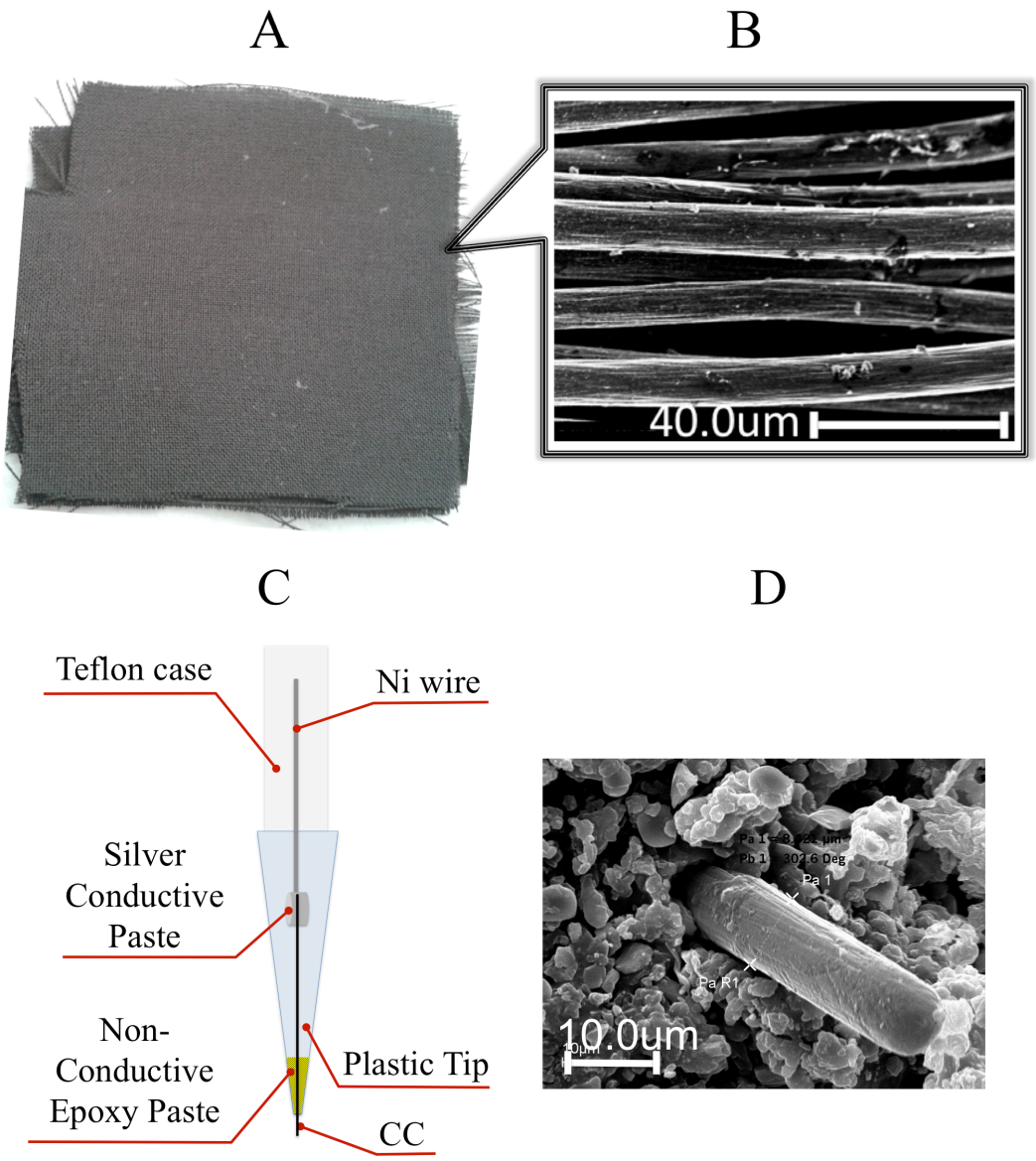

Figure 5.1 Sensor construction. Carbon cloth sheet (A); SEM image of selected CC fibers bundle (B); schematic description of the device (C); SEM frontal view of a detail of the sensor tip before the lapping procedure (D).

Bilirubin oxidase enzyme used in the present work was purchased from Amano Enzyme Inc. with a specific activity of 2.53 U/mg of protein. The enzyme was immobilized onto the carbon fiber surface via 1-pyrenebutyric acid, N- hydroxysuccinimide ester (PBSE, Sigma Aldrich). To accomplish that, the tip of the sensor was immersed in 0.01 M PBSE solution in dimethyl sulfoxide (DMSO) and left for 1 hour. The sensor was then washed, placed in $2 mg \cdot mL^{-1}$ solution of BOx,

dissolved in 0.1M phosphate buffer (PB) (pH 7.5) and kept at 4ºC for 16–18 hours to obtain enzyme attachment. After enzyme immobilization the biosensor was ready for calibration or further steps such as silica encapsulation.

To increase sensor stability and introduce a diffusional barrier, the tip of the sensor was encapsulated using a chemical vapor deposition technique (CVD) as previously reported by Gupta et al. [91]. The silicate matrix was obtained by hydrolysis of tetramethyl orthosilicate (TMOS) as alkoxide precursor, followed by condensation to yield a polymeric oxo-bridged SiO_2 network. Encapsulated sensors were prepared by positioning the wet sensor after the enzyme immobilization in a closed petri dish with two small containers having 200 μL of tetramethyl orthosilicate (TMOS) and 200 μL of water, respectively, for five minutes at 30ºC. Only the liquid on the sensor surface is transformed into a silica gel. The additional water container serves to capture the excess of TMOS vapors.

5.2.2 Electrochemical Tests

A three-electrode setup was used for all electrochemical experiments, where the sensor was connected as working electrode (WE), a platinum wire was the counter electrode (CE) and a Ag|AgCl (3M) electrode (3mm diameter) was the reference electrode (RE) (all potentials in this chapter are referred to this reference electrode). The electrochemical response of the device with and without immobilized BOx was studied by cyclic voltammetry at three different aeration conditions under controlled flow: air-saturated solution ([O_2 in solution]= 6.91 $mg \cdot L^{-1}$), 60 sec purging oxygen (purity 96%, [O_2 in solution]= 20 $mg \cdot L^{-1}$) and 30 min purging nitrogen (purity 90%, [O_2 in solution]= 0.66 $mg \cdot L^{-1}$). The cyclic voltammetry was recorded from 0.7 V to - 0.4 V at 100 $mV \cdot sec^{-1}$ in a 0.1M PB (pH 7.5) + 0.1M KCl. Based on the performed CVs, a potential of -0.4 V was selected for sensor calibration and operation. The sensors were calibrated by chronoamperometry in four different aeration conditions: air-saturated solution ([O_2 in PB]= 6.91 $mg \cdot L^{-1}$ and [O_2 in WW]= 3.74 $mg \cdot L^{-1}$), 60 sec purging oxygen (purity 96%, [O_2 in solution]= 20 $mg \cdot L^{-1}$), 1 min purging nitrogen (purity 90%, [O_2 in PB]= 5.47 $mg \cdot L^{-1}$ and [O_2 in WW]= 3.38 $mg \cdot L^{-1}$) and 30 min purging nitrogen ([O_2 in PB]= 0.66 $mg \cdot L^{-1}$ and [O_2 in WW]= 0.63 $mg \cdot L^{-1}$). The oxygen concentration in the calibration solutions was determined by a commercial DO probe (HQ440d, Hanch). The chronoamperometry was performed after 30 seconds of equilibration time with 120 seconds of current recording at -0.4 V. The current value was recorded every second and the steady state current observed at the end of the measurement was taken as the sensor reading. Calibration curves were obtained for both encapsulated and not encapsulated sensors in triplicate.

The best performing sensor in terms of sensitivity and linearity of the response was chosen for monitoring a MFC system. The chosen sensor was further calibrated in wastewater using the same, previously described procedure in order to investigate an eventual matrix effect. The lifetime of the sensors was also studied. One and the same sensor was calibrated in wastewater at day one right after it has been prepared and then at different days (i.e. days 1, 3, 4, 5, 8 and 14). The sensor was kept at 4°C between measurements.

5.2.3 SCMFC Setup

A membraneless single chamber MFC with air-breathing cathode, having a volume of 125 mL was used in this study. A AISI304 stainless steel anode [30] and activated carbon (AC) based cathode [31] were used as electrodes in the SCMFC. The stainless steel anode (diameter of 4 cm, area of 12.6 cm^2) was connected to a plastic-insulated copper wire and the connection was insulated by at least 5 layers of high-viscosity epoxy resin (MAPEI Epojet). The anode was placed at the bottom of the SCMFC (see chapter 8, pp. 103). Electrical connection was tested for internal resistance and fluid contact/leakage by prolonged exposure to distilled water. The geometrical surface area of the AC based cathode exposed to the solution was a disk of 2 cm in diameter. The electrical connection to the external circuit was made with a copper wire in the case of the anode and by direct connection of the carbon cloth for the cathode. In the external circuit, a resistance of 100Ω connected the anode and cathode poles. The electrolyte was urban wastewater (pH around 7) coming from the treatment plant of Albuquerque (NM, USA). The wastewater was used as received, without any pretreatment step. During SCMFC operation, sodium acetate (Sigma Aldrich) was added to the electrolyte as substrate (carbon source) for bacteria.

5.2.4 Determination of oxygen profiles in SCMFC

In order to reduce eventual interference in the sensor response, profiles of oxygen concentration in proximity of both anode and cathode surfaces (Figures 5.2A and 5.2B, respectively) were determined under open circuit conditions of the MFC. Preliminary experiments (not reported here) demonstrated that the presence of a current flow could considerably increase the noise of the amperometric sensor response.

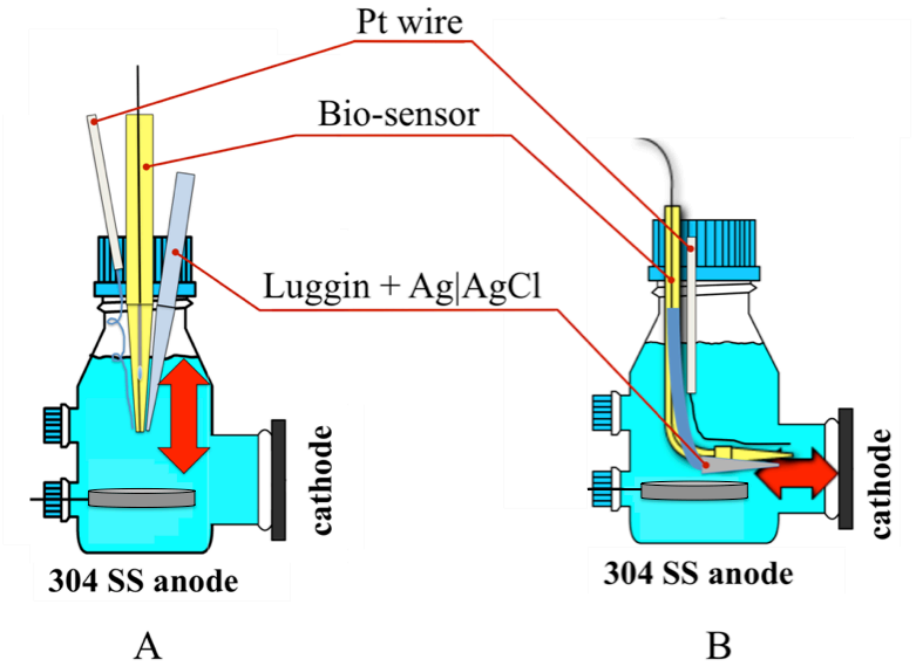

Figure 5.2 Schematic analysis-setups approaching the anode (A) and the cathode (B).

The microsensor along with Ag|AgCl (3M) reference and Pt-wire counter electrodes were inserted from the upper cap of the MFC and moved down from the level of the solution towards the anode (Figure 5.2A). For the cathode monitoring, the microsensor was bent to reach the cathode surface and it was moved from the anode towards the cathode creating oxygen profile between the two electrodes (Figure 5.2B). The position and movement of the oxygen microsensor was controlled by a computer-controlled stage (NLE Series Precision Linear Stage, Newmark Systems Inc.) having a maximum spatial resolution of 100 nm.

5.3 Results and Discussions

5.3.1 Electrochemical Performances

The electrochemical performance of the BOx-based microsensor was examined via cyclic voltammetry (CV), carried out at 100 $mV \cdot s^{-1}$ in 0.1M PB + 0.1M KCl solution (pH 7.5) (Figure 5.3). The potential window of the cyclic voltammetry was selected between 0.7 and -0.4 V in order to avoid enzyme denaturation and ensure enzyme function. Control electrode, containing only carbon fiber and no enzyme showed almost flat response over the investigated potential window. After the enzyme immobilization, increased capacitance and current output were observed.

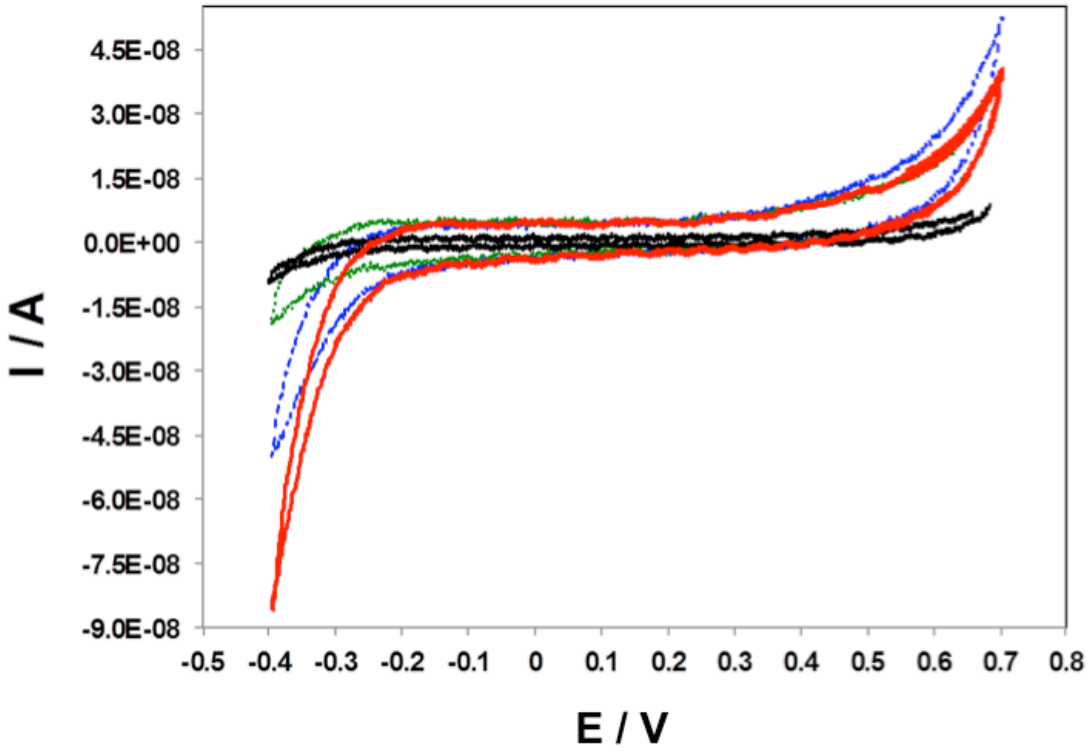

Figure 5.3 CVs. Scan rate: 100 mVs^{-1}; CE: Pt; RE: Ag|AgCl (3M). WE: carbon cloth fibers in oxygen saturated solution (black); BOx microsensor electrode in oxygen depleted solution (green), in air-saturated solution (blue) and in oxygen saturated solution (red).

The highest difference in the sensor response as a result of different oxygen content in the electrolyte was recorded at -0.4 V; therefore, this potential was consequently chosen as a proper potential for the subsequent chronoamperometry analyses. One of the main problems of enzymatic biosensors and biological systems in general is their low stability. This constraint can be overcome

with encapsulation of the enzyme in silica matrix [128]. Silica encapsulation is a simple, fast and effective method for entrapment of biological specimens. This encapsulation process involves low-temperature hydrolysis of appropriate monomeric precursors. The polymeric framework grows around the biomolecule, creating a cage and thus protecting the enzyme from aggregation and unfolding. These silica matrixes are chemically inert, hydrophilic, and inexpensive to synthesize. Their porous nature provides an efficient design that restricts movement of the enzyme but allows free access of the analytes [129]. In addition to the increased stability, the silica matrix creates a diffusional barrier, which ensures operation of the sensor at mass transport controlled mode. In this condition the sensor has a linear response from the concentration of an analyte [130].

In order to test the effect of the silica layer on the performance of the developed enzymatic oxygen sensor, a comparison between encapsulated and not encapsulated sensors was also performed. Chronoamperometry measurements of the sensor response at various oxygen concentrations were carried out in 0.1M PB + 0.1 KCl (pH 7.5) solution at the chosen potential of -0.4 V.

These measurements were executed with two sensor types:

I: not encapsulated;

II: encapsulated with silica-layer.

Each measurement was carried out in triplicate (Figures 5.4A and 5.4B). Considering that low oxygen concentrations have been previously reported for biofilms [117], the calibration graphs are presented without the current values obtained for the solutions where oxygen was added ([O_2 = 20 $mg \cdot L^{-1}$]). In this way, it is possible to visualize the graphs in the range of interest.

Both sensor types showed a good linear current response as a function of oxygen concentration with a coefficient of determination $R^2 > 0.97$. The sensitivity of the type *I* sensor was higher since the electrode was directly exposed to the electrolyte. At the same time, the reproducibility of the sensor response was lower in comparison to the encapsulated sensor (type *II*), especially at small oxygen concentrations, which we expect to have in MFC. Therefore, the encapsulated sensor was selected for further implementation in determining MFC's oxygen profile due to its higher response reproducibility. The next step was calibration of the type *II* (encapsulated) sensor in wastewater (WW) solution in order to avoid eventual matrix effect (Figure 5.4C). The sensor showed linear response in both PB and WW. The response in terms of current intensity and sensitivity was lower in the latter. There are two possible reasons for the decreased sensor performance:

i) the conductivity of the wastewater is significantly lower than the phosphate buffer, which introduces ohmic losses and thus leads to decreased current densities;

ii) although BOx shows good resistance towards halogens, the complicated chemistry of the wastewater (used as received) creates a matrix effect that can modify the enzyme performances and behavior.

Therefore, the MFC analyses were performed after calibration of the sensor in WW solution. The presence of sludge in the murky solution did not affect the sensor linearity.

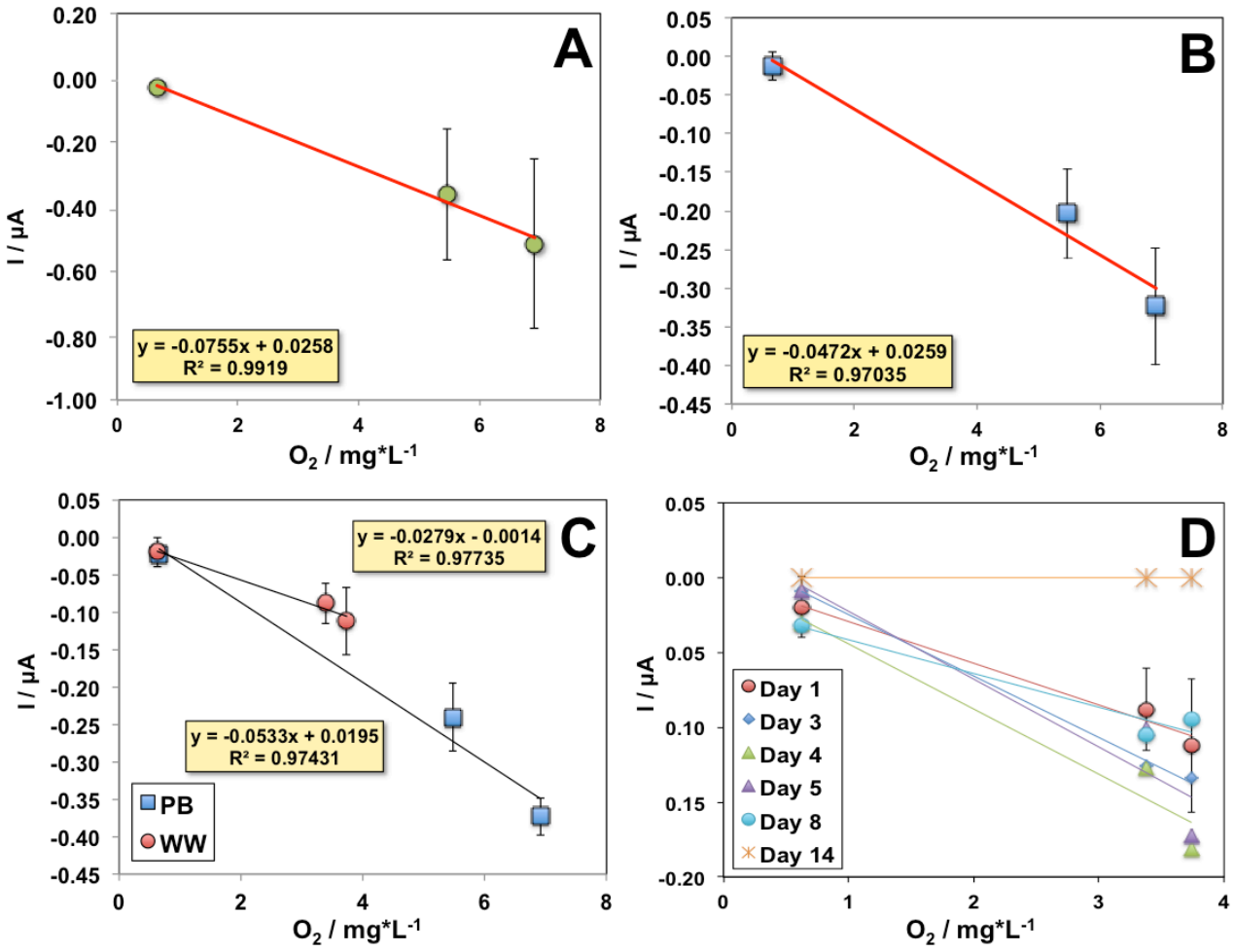

Figure 5.4 Calibration curves. Not encapsulated sensor (A) and encapsulated sensor (B) in 0.1M PB + 0.1M KCl. Encapsulated sensor in 0.1M PB + 0.1M KCl and in WW (C); lifetime in WW from day 1 to day 14 (D).

Figure 5.5 depicts the calibration graph for encapsulated sensors in PB and WW considering the four oxygen concentrations described in chapter 5.2.2. It is important to note that the biosensor maintains a linear response also at high oxygen concentration.

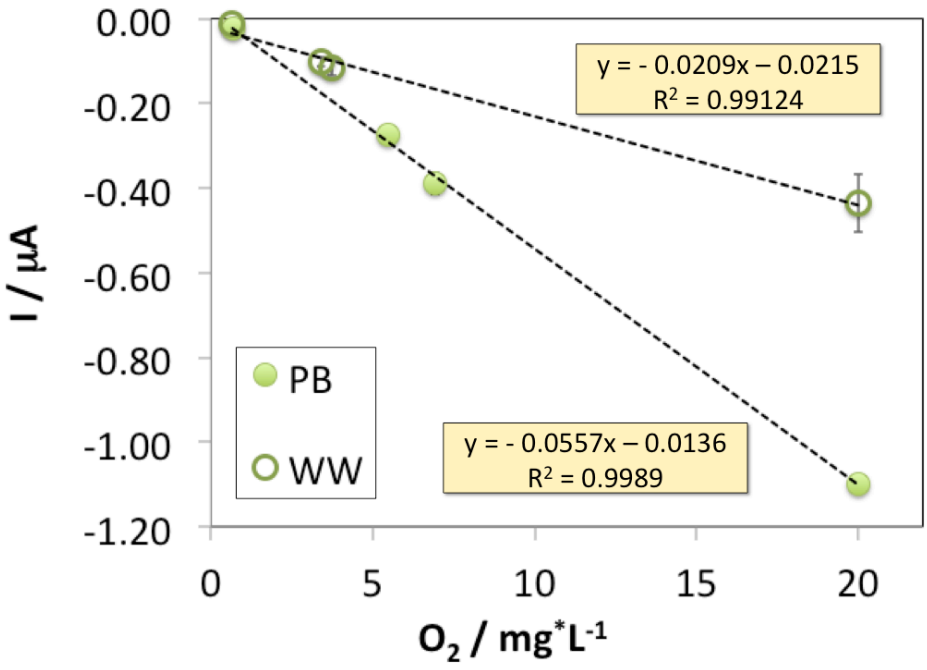

Figure 5.5 Calibration curves for encapsulated sensor in 0.1M PB+0.1M KCl (pH 7.5) and in WW using four oxygen concentrations.

In order to study the sensor lifetime, the calibration procedure was repeated at different days (Figure 5.4D). In terms of linearity and reproducibility, the sensor performance was maintained for 8 days for the encapsulated biosensor. After that time, the response was no longer linear and became totally flat (Figure 5.4D – Day 14). It is interesting to remark that the enzyme showed only slight gradual deactivation over time. The deactivation of the enzyme was faster for not encapsulated sensors: after 2–3 days unacceptable responses were obtained. This phenomenon most likely was a consequence of the direct contact of the enzyme with pollutants in the wastewater that decreased significantly the enzymatic activity. Silica encapsulation stabilized the enzyme and quadrupled the sensors life.

5.3.2 SCMFC Analysis

Membraneless single chamber microbial fuel cell equipped with an activated carbon (AC) based air-breathing cathode and a AISI304 stainless steel anode was inoculated with fresh urban wastewater at the beginning of the test. Sodium acetate was added to the electrolyte as a substrate (3 $g \cdot L^{-1}$) for bacteria. The SCMFC was polarized with a constant resistance of 100 Ω and the corresponding cell potential was recorded and recalculated in terms of power. The power generated from the SCMFC over time is shown in Figure 5.6 A. The SCMFC was unproductive for five days, as power values close to zero were observed. At day 6, the cell started to produce power, reaching 10μW, which dropped to zero at day 7. It has to be taken into consideration that at the startup both the anode and the cathode of the SCMFC where clean, un-colonized, electrodes. Thus, the initial delay is needed to allow bacteria colonizing the surfaces, obtaining the bio-catalyzed electrodes. Bacteria consume acetate to grow and, as explained below in chapter 5.3.3, to establish anaerobic conditions inside the SCMFC. At the end of day 9, the 3 $g \cdot L^{-1}$ sodium acetate concentration was re-established by addition of acetate in the solution. Three days later (day 12), the power production started again and constantly increased until day 18 (80 μW), when the experiment was terminated.

5.3.3 Oxygen Profiles Towards the Anode Surface

Profiles of oxygen concentration in the proximity of the anode were determined under MFC open circuit conditions. The microsensor was inserted into the MFC and moved down from the level of the solution to the anode surface (Figure 5.2A). The position of the oxygen microsensor was controlled by a computer-controlled stage with a maximum spatial resolution of 100 nm. The oxygen profiles approaching the anode surface were measured at different time intervals: after day 1, 3, 8 and 15 of MFC operation (Figure 5.6B). At the startup of the MFC operation (day 1), the oxygen concentration was approximately constant along the entire path, with the exception of the first millimeters close to the solution surface where the concentration of oxygen was higher. After 3 days, the concentration was still constant but at a slightly lower value. The oxygen consumption during these first days is associated with the microbial aerobic processes taking place in the SCMFC during the startup process with no power production. As a result of oxygen consumption, anaerobic conditions establish inside the bulk solution, from the solution surface towards the proximity of the anode [56]. The lower oxygen concentration detected in the SCMFC at day 8 shows that oxygen was progressively consumed over this period. The SCMFC started to produce power at day 6, and when all the acetate was consumed, it fell dramatically to zero. A very low oxygen concentration at 10 mm from the solution surface was detected at day 15, consistent with the highest power

production. These results remark that the absence of oxygen in the region close to the anode of the SCMFC plays a key role in the cell productivity.

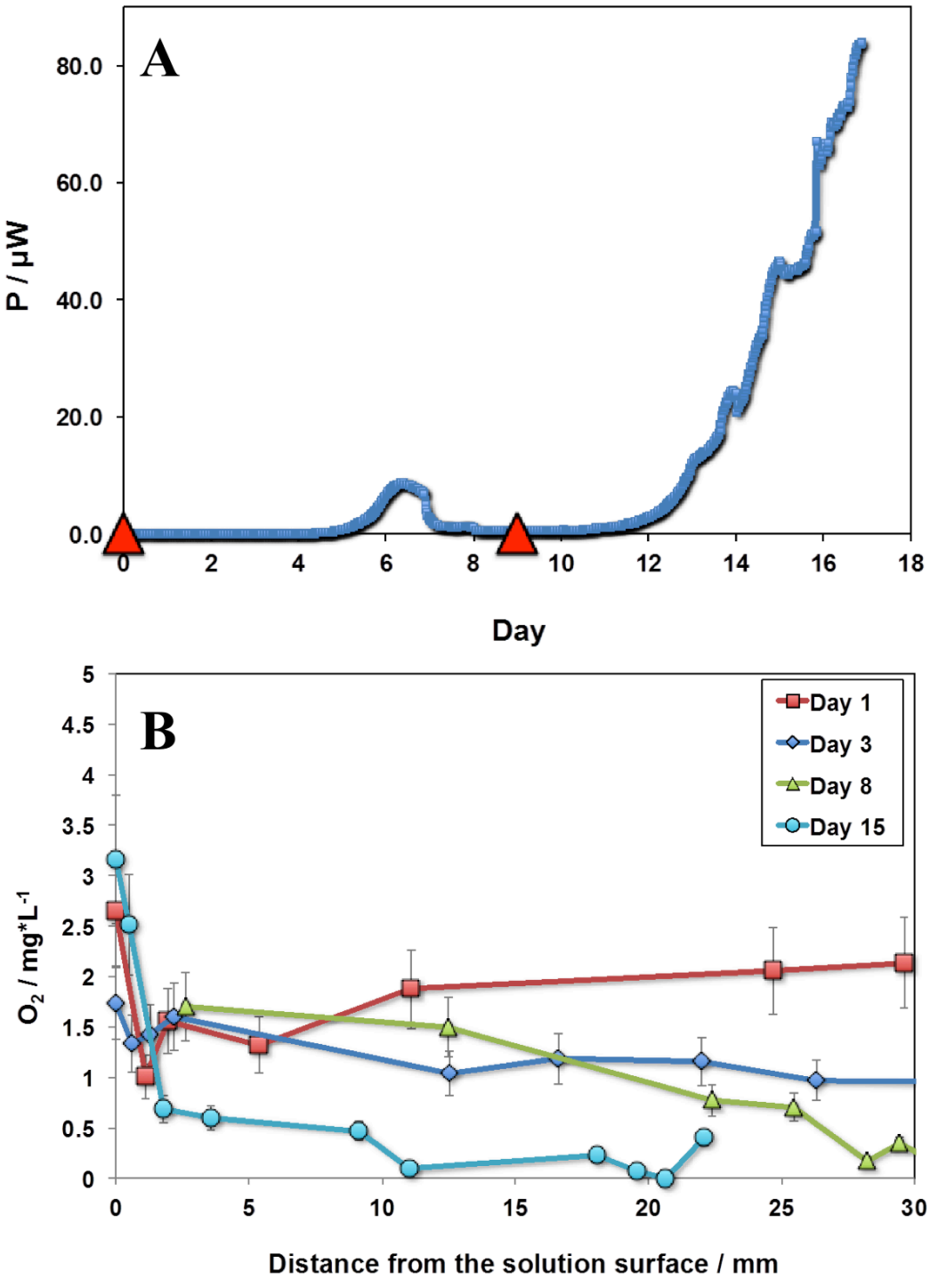

Figure 5.6 Power generated by the SCMFC over time (A), triangles indicate acetate addition. Oxygen profile to the anode surface at days 1, 3, 8 and 15 (B).

5.3.4 Oxygen Profiles Towards the Cathode Surface

For the cathode analyses, the microsensor was moved from the anode towards the cathode (Figure 5.2B). The oxygen profiles measured approaching the cathode surface are shown in Figure 5.7 A at two different days (8 and 15).

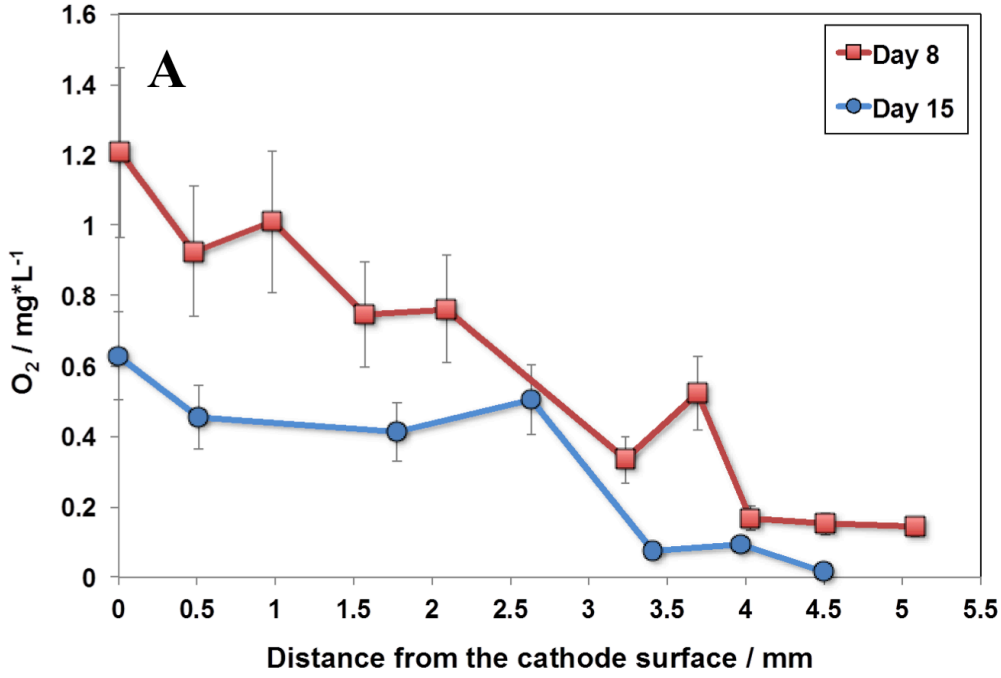

B

Figure 5.7 Oxygen profiles to the cathode surface at days 8 and 15 (A); cathodic biofilm after 18 days of operation (B).

The oxygen content at 4.5 mm far away from the cathode surface was almost equal to that measured close to the anode at the same days of MFC operation. Moving the sensor closer to the cathode surface, the oxygen concentration tended to increase. At day 8, oxygen continuously increased towards the electrode surface, reaching 1.2 $mg \cdot L^{-1}$ in the proximity of the cathode. The curve at day 15 exhibits a practically flat profile from 2.5mm to the cathode surface, where the oxygen content was 0.6 $mg \cdot L^{-1}$. This concentration was half of value observed for day 8. The results confirm that the biofilm developed at the cathode surface (figure 5.7 B) acts as barrier for oxygen diffusion as previously hypothesized, but never directly measured [48,51,118] and further demonstrates that the power production was strictly connected to the oxygen consumption in the SCMFC. Based on the oxygen-profile measurements, it can be proposed that the cathode biofilm has a thickness around 3 mm.

Part 2

ELECTRODE DEVELOPMENT

6.

BIOCATHODE DEVELOPMENT

From: *E. Guerrini; **M. Grattieri**; A. Faggianelli; S.P. Trasatti; P. Cristiani, PTFE Effect on the Electrocatalysis of the Oxygen Reduction Reaction in Membraneless Microbial Fuel Cells, Bioelectrochemistry, 106 (**2015**) 240-247.*

6.1 Introduction

Similar to any other chemical fuel cell, in SCMFCs the most energy-demanding process is the electroreduction of oxygen (ORR) at the cathode [23] and great efforts have been devoted in the last decades to find electrode materials with lower overpotential for this half-reaction [131–134]. Oxygen reduction reaction is critical as it can produce, locally, very reactive compounds such as hydrogen peroxide and hydroxyl radicals, according to a two-electron path, or specific intermediates as a result of a four-electron path [135]. Carbon-based materials are conventionally used as components of cathodes in the form of composites or thin layers normally kept in place with organic binders. The most common binders are Nafion® when a hydrophilic layer is required (Micro-Porous Layer, MPL) and PTFE if hydrophobicity is necessary (Gas Diffusion Layer, GDL) [136,137]. Both materials come from the low-temperature fuel cell field. These two binders are widely used for electrodes of MFCs, but different performances and optimal concentrations are sometimes reported [55,138,139]. Compression of the GDL is usually applied during the thermal treatment to increase the electrical conductivity of the carbon powder.

ORR electrocatalysis was attempted by means of different routes [140,141] and several advantages were already pointed out by using microbial biofilm as catalyst (biocathode) on carbon matrix [45,50,142–145], capable of continuously producing enzymes [146,147]. Bacteria colonize the wet surface with a hydrophilic biofilm. Consequently, open-air biocathodes must meet:

i) hydrophobicity on the air side, to prevent solution leakage from the cathodic compartment, with high oxygen diffusion [148];

ii) hydrophilicity on the water side, as the catalysts of the electrochemical process act at the interphase between liquid and solid electrode.

In order to discuss these aspects, an electrochemical approach is herein applied based on the analysis of the polarization curves (ohmic drops, Tafel slope and mass transport issues). Tafel slopes (*b*) in biological systems are seldom calculated. In some cases, *b* is calculated on the linear sweep voltammetry [149,150]. In these cases, polarization resistances, Tafel slopes and exchange currents are calculated to evaluate the electrical current passing through the cathode. Together with Tafel slope calculations, the capacity (*C*) of the electrochemical double layer was determined and used as a parameter proportional to the electrochemically accessible surface area. Close scrutiny of results led to a deeper understanding of the real role of PTFE in the environment of a microbial fuel cell. GDL was prepared under atmospheric pressure, using PTFE content in the range of 60 to 200%, with the aim to specifically stress the PTFE role in the oxygen reduction reaction.

6.2 Materials and methods

6.2.1 SCMFC design

Single chamber MFCs were operated in batch mode at room temperature (22 ± 2 °C). A Pyrex bottle of 125mL was equipped with a large Pyrex flange on one side, to accommodate the air-breathing cathode. On bottle top, a hermetic plastic screw cap was used to prevent air exchange with the electrolyte. Raw inlet from a wastewater treatment plant (Nosedo Milan, Italy) was used as medium and inoculum. The wastewater had buffer power (pH around 7) and low initial COD (up to 500 $mg \cdot L^{-1}$ of O_2). Sodium acetate (Sigma-Aldrich ACS reagent, 99.0%) was periodically added during the experiment as fuel for bacterial metabolism (36.5$mmol \cdot L^{-1}$ acetate for each addition). Anodes were made of 2×5 cm carbon cloth (SAATI C1), without any pretreatment or additional layer on the surface. Carbon cloth was electrically connected to a plastic-insulated copper wire by a carbon-based conductive paste (TIMCAL). The connection was then insulated by at least 5 layers of high-viscosity epoxy resin (MAPEI Epojet). The anode was mounted in the lower opening by a rubber plug. Electrical connection was tested for internal resistance and fluid contact/leakage by prolonged exposure to distilled water. Cathodes were built from a square 3×3 cm carbon cloth (SAATI C1) modifying the procedure described from Santoro et al. [50] by the addition of:

a) one layer of carbon (TIMCAL ENSACO 350G)+Nafion® ink on the internal surface (MPL) and

b) one layer of carbon (TIMCAL ENSACO 350G)+PTFE ink on the external surface in contact with air (GDL).

The geometric surface area exposed to the solution was a disk of 2 cm in diameter. The electrical connection to the external circuit was made with a copper wire in the case of the anode and by direct connection of the carbon cloth for the cathode. In the external circuit, a resistance of 100Ω connected the anode and cathode poles. Four sets (triplicates) of SCMFCs were built. The difference was only in the composition of the external layer of the cathode (GDL). The fabrication of the GDL begun by heating at 100 °C for 24h a given amount of carbon powder (TIMCAL ENSACO 350G) and carbon cloth to completely remove humidity. GDL layer was constructed by room temperature spreading of a carbon powder–PTFE suspension ink on one face of the carbon cloth. A thermal treatment at atmospheric pressure was then carried out to ensure the fixing of the layer. Working at atmospheric pressure limited the PTFE content in the ink to a minimum percentage of 60% weight with respect to the carbon powder, as lower percentages exhibited mechanical instability. The PTFE ink was prepared by adding 1 g of dehydrated carbon powder with 7 g of deionized water (18.2MΩ, MilliQ) and thoroughly mixed. 0.67 g of Triton®X100 was added to the mixture as surfactant, together with the needed mass of PTFE suspension, and briefly mixed. The prepared ink was then bar-coated over the pre-treated carbon cloth. The resulting material was heated at 290 °C for 15 min, to promote the evaporation of the surfactant, and then at 330 °C for 30 min to melt the PTFE.

6.2.2 Experimentation

Four types of cathode were built, with PTFE varying from 60 to 200%w/w (60, 80, 100, 200%) with respect to carbon powder content (GDL composition only). For each composition, three identical SCMFCs were built and remained operational for more than two months in batch mode. The potential difference across a 100Ω resistance was continuously recorded, and electrochemical experiments were performed. The potential *E* was recorded every 10min, using a multichannel Data Logger (Graphtec midi LOGGER GL820). The generated current (*I*) was calculated as previously indicated. Polarization curves were recorded in-situ at a low scan rate (0.166 $mV \cdot s^{-1}$) [108], using a three-electrode configuration. The cathode was connected to the working terminal of the potentiostat, a Pt wire was connected to the counter, and a SCE reference electrode (Amelchem) (all potentials in this chapter are referred to this reference electrode) was equipped with a Luggin capillary and positioned close to the working electrode, so that no compensation of the ohmic drops was necessary. After equilibration at the open-circuit condition, a linear potential ramp was applied from the open circuit potential of the electrode, down to appreciable currents (higher than −500 μA). The separation of electro-kinetic factors and electrodic ohmic resistances was performed by a

further evaluation of the data (see chapter 4.2, pp. 35). The double layer capacitance was measured by cyclic voltammetry (CV) at different potential scan rates (4, 25, 64, 121 and 196 $mV \cdot s^{-1}$). The same three-electrode configuration as used for the polarization curves was employed. The potential window was selected from −50mV to +50mV vs. the open circuit potential (*ocp*) of the cathode. In this potential interval, no Faradaic currents or redox peaks were observed.

6.3 Calculations

6.3.1 Tafel Slope

To calculate the Tafel Slope from the quasi-stationary polarization curves, both interpolation and derivative methods were applied (chapter 4.2.2 pp. 35) and the mean value was used.

6.3.2 Capacitance from cyclic voltammetry

Cyclic voltammetries (CVs) were conducted on the cathodes at different operating times of the SCMFCs in order to obtain an evaluation of the total surface area accessible to the electrolyte. The potential window of the CV was chosen to be in a zone where no faradaic processes were expected to occur. The electrochemical response was then approximated to a capacitor [110].

6.3.3 Normalization of current production by electrochemical surface

In literature, the calculation of surface area was recently implemented using a value of 35 $\mu F \cdot cm^{-2}$ for the carbon specific capacitance c_{sp} [111]. Assuming C proportional to the real, wetted, electrochemical surface, the normalization of the exhibited ORR currents by C gives an estimation of the specific electrocatalytic activity of the electrodic material. Capacitance changes were estimated and used to compare the relative performances of the different cathodes.

6.4 Results and discussion

6.4.1 SCMFC current output

The evolution over time of the current (I) of the four types of SCMFCs is reported in Fig. 6.1. One curve for each SCMFC is shown, as current outputs of triplicates were very similar. The triangles along the abscissa indicate the addition of 36.5 $mmol \cdot L^{-1}$ (3 $g \cdot L^{-1}$) of sodium acetate. The trend of

current shows higher values in the SCMFCs with lower PTFE contents at cathode. All SCMFCs started productivity in a few days and settled at a first plateau corresponding to a current less than 400 μA. The SCMFCs with the lowest content of PTFE (60%) showed a prompt power production, but the SCMFCs with 80% PTFE had a similar trend and currents. Higher contents of PTFE gave a different response: the SCMFCs with 100% PTFE in the cathode started slowly to produce current, and settled at ~250 μA; the SCMFCs with 200% PTFE in the cathode did not show an appreciable current production after the first addition of acetate. After a second addition of acetate, at day 18, the SCMFCs with 60 and 80% PTFE in the cathode showed comparable currents. The SCMFCs with 100% PTFE slightly increased current. The SCMFCs with 200% PTFE showed a hint of current production up to a maximum and then a slow decay from the 23rd to the 37th day. Another addition of acetate at day 37 increased current production, especially in the SCMFCs with the lower PTFE concentrations. After the last addition of acetate, at day 52, the SCMFCs with 60 and 80% PTFE started a prompt current production, with a maximum plateau of ~700 μA for the lowest composition. At the same time, 200% SCMFCs showed no significant production of current despite the additions of acetate.

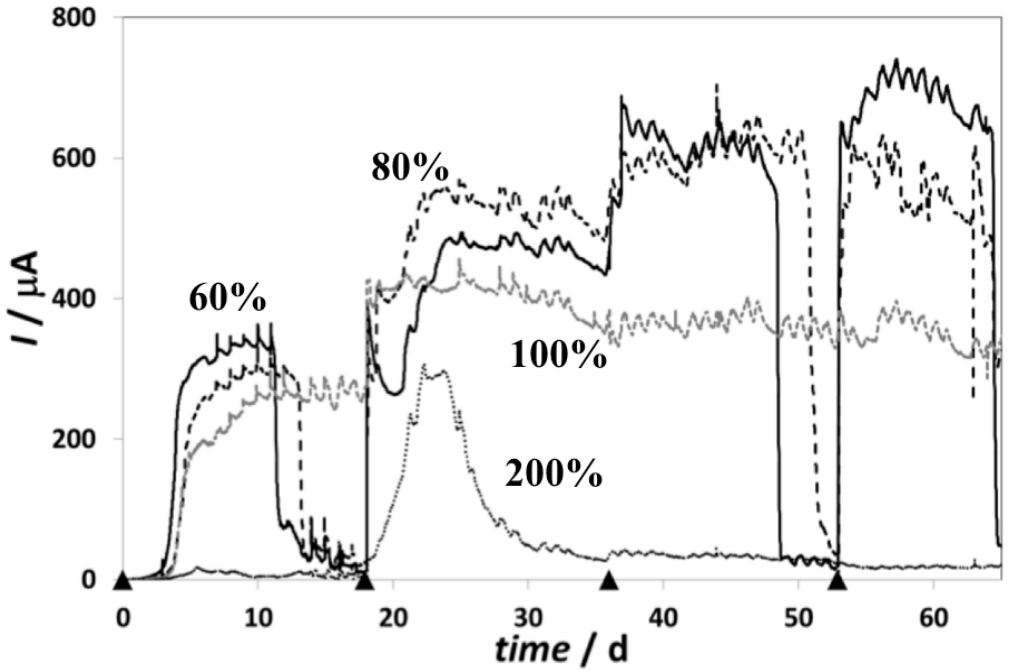

Figure 6.1 Current trends of SCMFCs with different PTFE contents in the cathode. Triangles indicate acetate additions.

6.4.2 Polarization curves

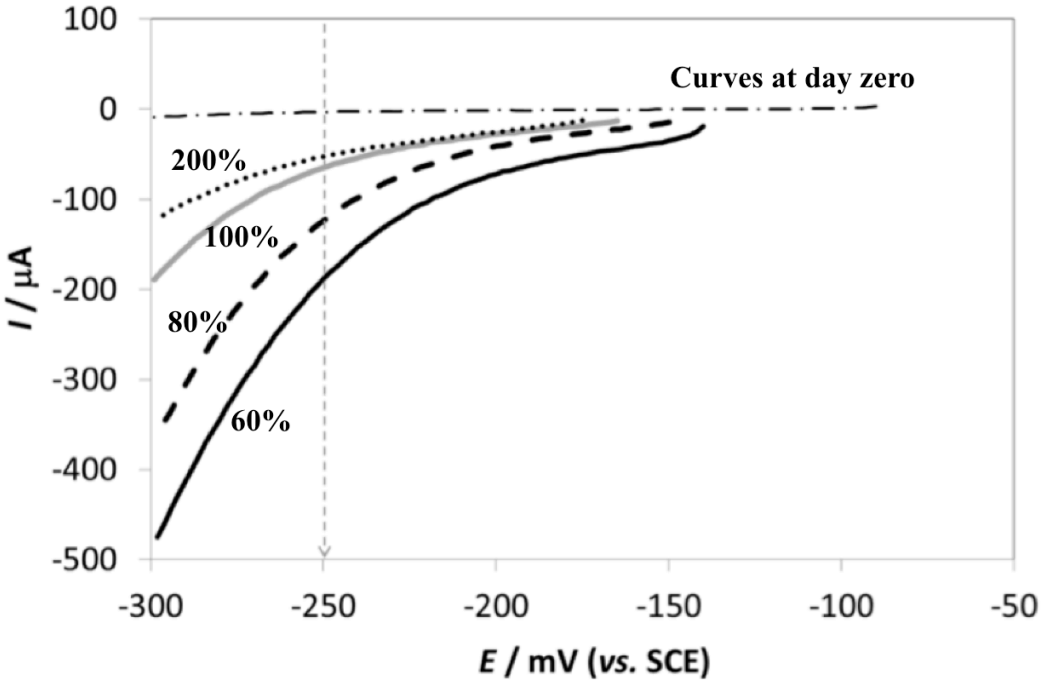

Figure 6.2 Polarization curves of cathodes with different PTFE contents (%) at days zero (overlapped) and 61 operating.

Fig. 6.2 shows quasi-stationary polarization curves, recorded at day 61 on cathodes of well operating SCMFCs (each curve is the average of experiments conducted on the three identical MFCs) and for simplicity only one of the polarization curves at day zero (all very similar). The graph documents the transformation of a non-electrocatalytic carbon-based electrode (day zero, practically no current) into a more active electrode, exhibiting higher currents as PTFE content was decreased. This correlated well with the SCMFC current trends in Fig. 6.1. All the cathodes showed a continuous increase of current as the potential became more negative, without diffusion-related plateau. This trend demonstrated that, in this potential window, oxygen concentration on the electrode was not the limiting factor, in agreement with the results of previous experiments [51]. Moreover, Fig. 6.2 shows that, although very low current was produced in 200% PTFE SCMFCs, a capability of the electrode to produce currents was increased in respect to day zero. High PTFE cathodes appeared to be lightly influenced by the biological activity in the SCMFC. To emphasize the evolution of ORR catalytic biocathodes consistently with the SCMFC productivity, the exhibited currents (media and standard deviation of points taken from polarization curves at the same days) at a potential of −250mV (vs. SCE) are reported in Fig. 6.3 vs. the lifetime of each SCMFC.

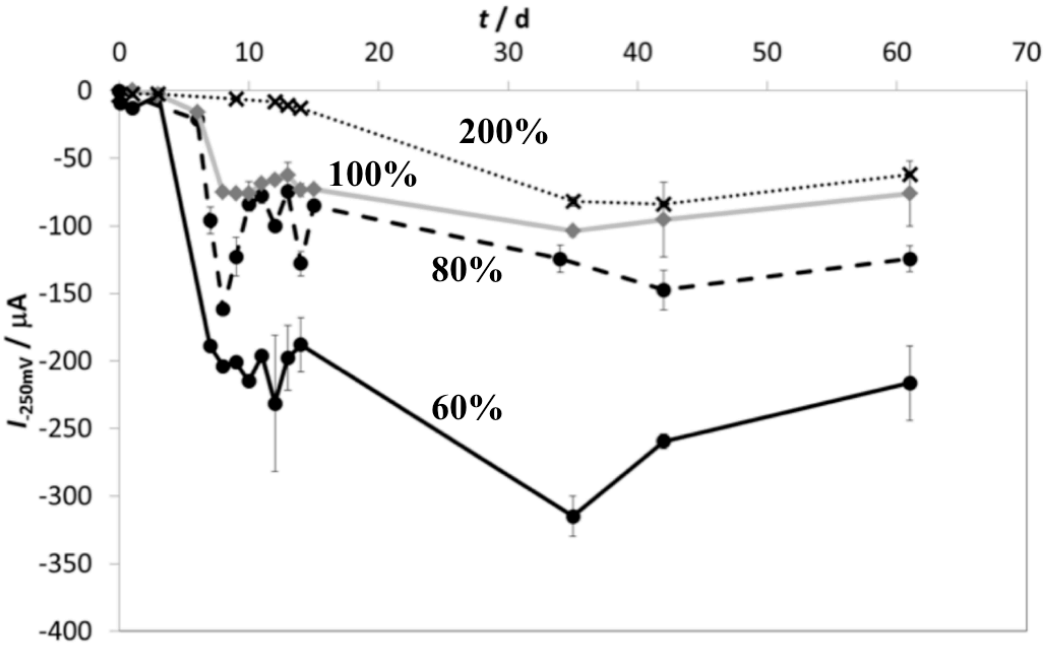

Figure 6.3 Faradaic currents extracted from polarization curves of cathodes at a potential of −250 mV (vs. SCE) vs. time. Mean values and standard deviations of the triplicates are reported.

At the selected potential (−250mV vs. SCE), polarization curves of all SCMFCs showed the linearity typical of Tafel plot calculations. Averages of the triplicates, together with standard deviations, are reported. As for the productivity of the SCMFCs, the cathodes supported very low currents from the start, up to day 3. At this time, only the 60% PTFE cathodes activated quickly showing increases in current production. The activation quickly followed in 80% and 100% PTFE cathodes, then slowly and less in 200% PTFE cathodes. A small tendency to decrease current output was evident in the final part of the experimentation for all the cathodes. It is worth noting that the current showed a high standard deviation, together with higher scatter of the average, during the unproductive days (see Fig. 6.1, days 12–18) especially for 60–80% PTFE concentrations. This is consistent with the deactivation of bacteria metabolism in the biocathode in the periods of acetate depletion. Current did not decrease in the case of the 100% PTFE SCMFCs, pointing to a minor bacteria activity that never depleted completely the acetate in the SCMFCs.

The currents finally decreased in the 200% PTFE cathodes after a hint of productivity of the SCMFCs, in consequence to the second acetate dosage.

6.4.3 Tafel slopes and resistances

The exhibited currents *I* in the graphs of Figs. 6.2 and 6.3 can be related to two different parameters:

i) an increase in current might be due to an increase in electrochemically accessible surface area, maintaining the electrocatalytic characteristics of the pristine materials;

ii) an increase in current might be due to real-electrocatalytic effects.

In this last case, a modification of the path (or rate determining step) occurs, with an increase of the ORR reaction rate on the same extent of electrochemical surface. Similarly, a decrease in the exhibited current might be due to an increase in the intrinsic ohmic resistance of the electrodic interface (*r*). The method used for the evaluation of these parameters is the calculation of the Tafel slopes *b* and the resistance *r*, as described in the theory/calculation section. Application of the derivative method to the quasi-stationary polarization curves is synthetized in Fig. 6.4. The Tafel slopes *b* for the four PTFE concentrations are reported on the primary ordinate axis. The resistance *r* for the two outmost concentrations is reported on the secondary ordinate axis vs. days of operation. In all cases, the mean of triplicate measurements is reported.

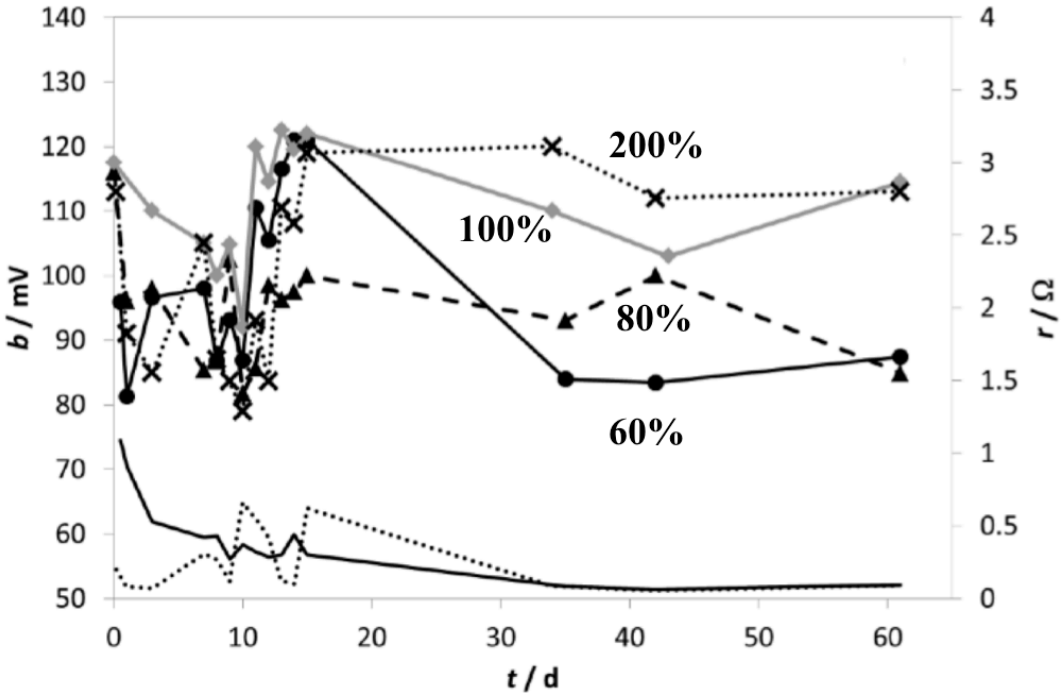

Figure 6.4 Calculated Tafel slopes (primary axis) and cathode ohmic resistances (60% continuous line; 200% dashed line, secondary axis) vs. time of single cathodes with different PTFE contents.

The resistance *r* of the electrode interface showed a very low value in both cases, pointing to a quite conductive electrode–solution interphase. Furthermore, this parameter decreased from 1 to 1.5 Ω down to near 0.1 Ω at 61 days. The increase of electrical conductivity could be due to a build-up of ion concentration in the developing biofilm [48]. Although minimal, differences between 60% and 200% compositions are evidenced. In particular, 200% PTFE cathodes did not show appreciable resistance contribution from the beginning of the experiment. 60% PTFE cathodes showed a higher resistance at the beginning. Consequently, the marked differences in current productivity and quasi-stationary cathodic polarization curves cannot be ascribed to variations of *r*. Fig. 6.4 also reports the calculated Tafel slopes *b* of the four concentrations and their variation with time. With an invariant *b*, electrocatalytic effects cannot be ruled out, but a variation of *b* is a sufficient condition to call for electrocatalysis. *b* is an intensive parameter: a decrease in *b* is ascribed to electrocatalytic activation; an increase of *b*, calls for electrocatalytic deactivation of the electrochemical process. Cathodes approached an initial Tafel slope of 120mV/decade of current, indicative of an uncatalyzed ORR. Lower PTFE contents showed a lower Tafel slope even at the startup of the cell, indicating a prompt activation of the electrode. Nevertheless, a general decrease of this parameter down to a value near 80mV/decade of current was clearly visible for all the cathodes within the first week. From days 10 to 18, deactivation occurred, in connection with the decay of MFC performance (Fig. 6.1). The 120mV/decade of current value was reestablished for the most productive (60%), as well as the less productive (200%) and slightly productive (100%) cathodes. *b* remained high for the two higher PTFE percentages, even after the second acetate addition at day 18, while it moved again to 80 mV/decade of current for the 60% cathode. The 80% content cathode moved slowly from 100mV/decade of current, down to 80 mV/decade of current at day 61. The variation of *b* appeared to be strictly connected with the acetate availability. Consequently, it seemed most related to the biocathode development and activity. A first period was associated to the evolution of the abiotic, uncatalyzed cathode into a catalyzed cathode with a lower *b*. The differences in the current trends point out that this is a crucial step for the stimulation of SCMFC productivity. The electrocatalytic properties of an active biofilm on the cathode are supported by the anodic oxidation of acetate, supplying the electron flow from the anode through the external circuit. Deactivation of electrocatalysis happens when acetate is consumed and the lack of acetate inhibits the bacterial metabolism. Reversal of the deactivation is possible by a new acetate addition. The reversibility of the process is more evident with the lowest PTFE composition, once the acetate is fed to the SCMFC. Too high concentrations of PTFE act against this process of electrochemical re-activation, resulting in a permanent deactivation of the electrocatalytic electron transfer process in few days, as proved by the general increase in Tafel slope from days 10 to 15. The lowest value of 80

mV/decade of current is, however, higher than the conventional chemical electrocatalysts (30–60 mV/decade of current) [131]. This value calls for a limited electrocatalytic activity of the biocathodes.

6.4.4 Capacitance and normalized current production

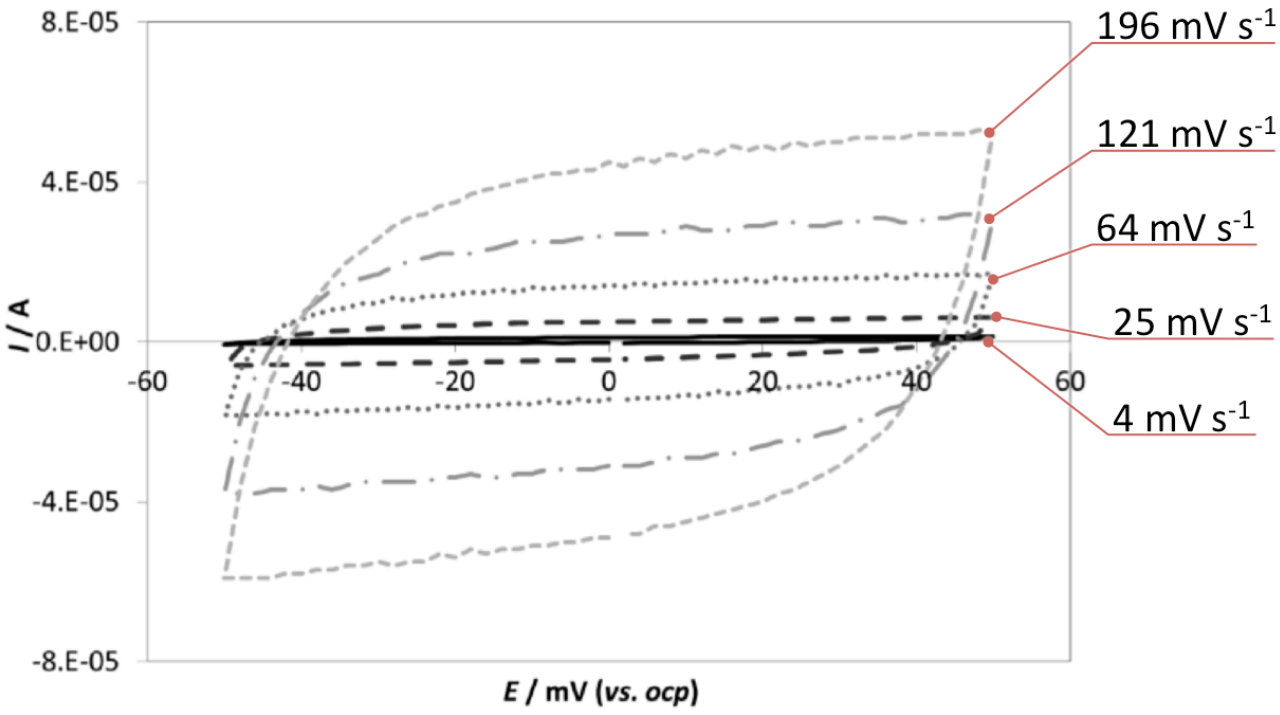

Figure 6.5 Cyclic voltammetries at different scan rates in the capacitive zone of a cathode with 60% PTFE content.

The calculation of electrochemical double-layer capacitance *C* from cyclic voltammetry gave an evaluation of the surface-active area changes of the cathodes. Fig. 6.5 shows an example of the voltammograms for a 60% PTFE cathode, recorded at different scan rates at day zero. Curves did not show any faradaic peak, thus resembling the behavior of a capacitor. Potential window was selected large enough (from −50 to +50mV) to estimate the capacitive currents. The mean capacitances of the cathodes at the four different PTFE contents were reported in Fig. 6.6 as a function of time. Standard deviation was shown in the plot, too.

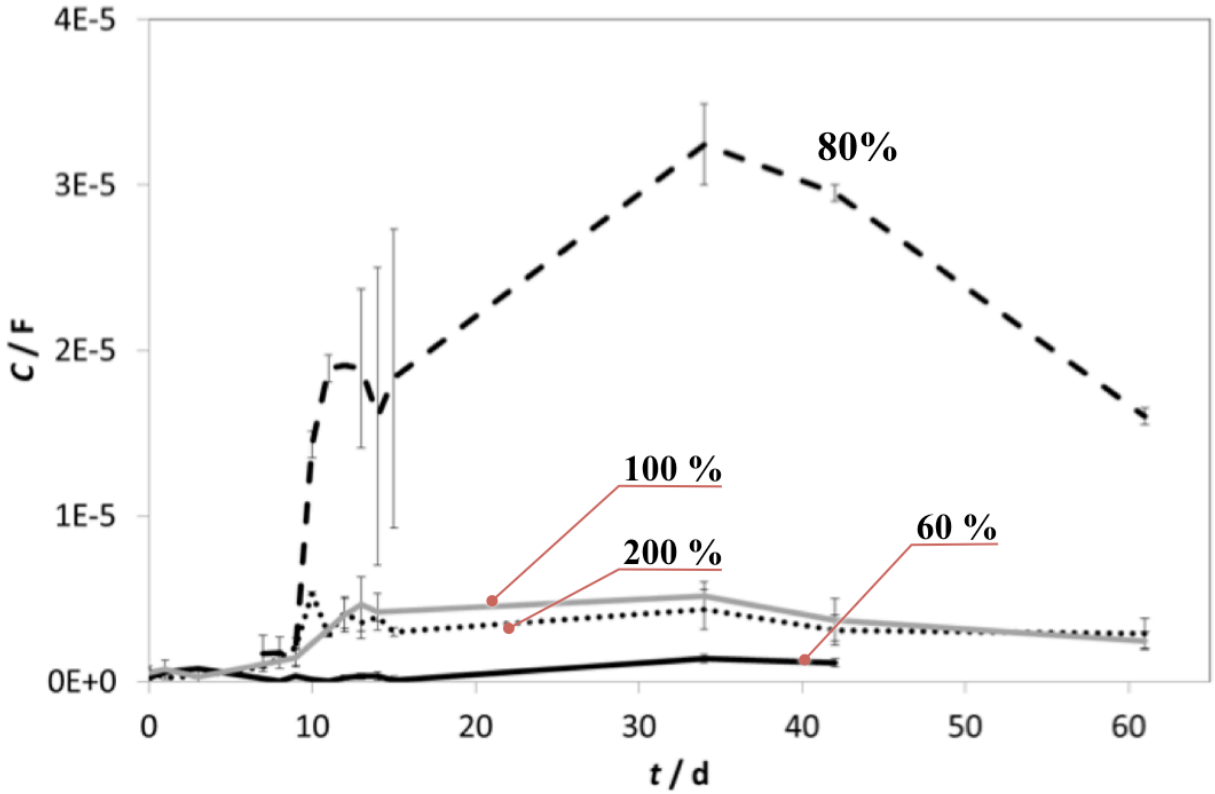

Figure 6.6 Double layer capacitance trends (average with standard deviation) of the cathodes with different PTFE contents.

The capacity of the 80% PTFE cathode was definitely higher than the others. Wetting of the GDL increased at the beginning of the experiment, promoted by the relatively low PTFE content. In the case of 60% PTFE cathodes, wetting resulted in no capacitance increase. This apparently contrasting result can be explained in terms of poor mechanical stability of this GDL: carbon particles detach from the carbon cloth as the cathode gets wet during the first days. Leakages cause the loss of the GDL carbon particles, which are responsible for the increase of active surface area. Nevertheless, the great difference in capacitances between the 60 and 80% PTFE cathodes did not affect the current trends (Fig. 6.1). The trend of each curve was quite similar: after the first days, *C* increased up to a maximum (day 34th in the graph) and then decreased again. The final decrease might be due to fouling (carbonate precipitation [50,51]). To quantify the relation between cathode capacity and current, calculation of the normalized currents was attempted. In Fig. 6.7, the absolute values of the ratio between the cathodic currents *I* at −250mV of Fig. 6.3 and the capacitance *C* of Fig. 6.6 are reported.

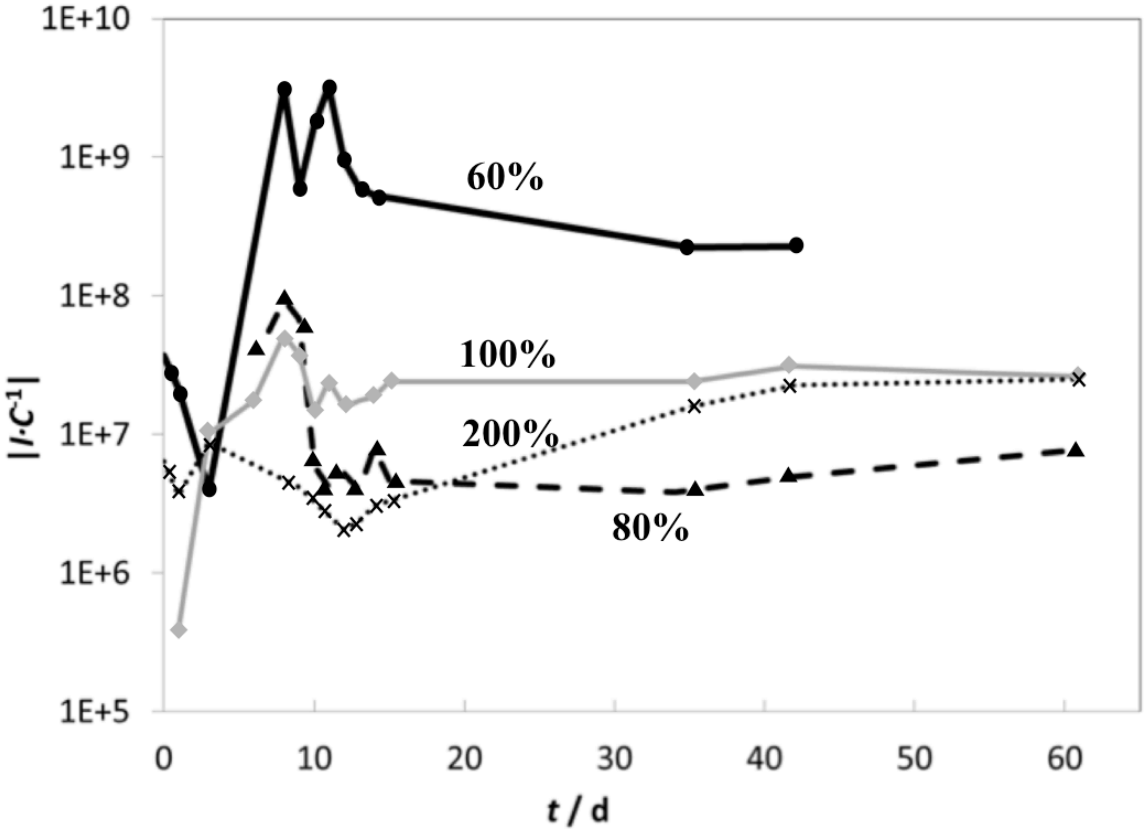

Figure 6.7 ORR currents normalized by the double layer capacity vs. time of the cathodes with different PTFE contents.

The y-axis is expressed in logarithmic scale. The lowest PTFE concentration, reaching a maximum value of $3.18 \cdot 10^9$, was two orders of magnitude higher than the others ($9.3 \cdot 10^7$, $5.2 \cdot 10^7$, $2.5 \cdot 10^7$ for the 80, 100 and 200% PTFE, respectively). A peak of activity was visible for the three lower concentrations, around the days from 7 to 13. It has to be taken into consideration that during these days the SCMFCs with the lower concentrations started to produce current, whereas the 200% PTFE was unproductive, in agreement with the absence of the peak in figure 6.7. Conversely, no peak of activity is present for the following days, despite the current production of the 60, 80 and 100% PTFE SCMFCs. This behavior is discussed in chapter 6.4.5.

6.4.5 Electrocatalysis and electrochemical active surface

Observing the behavior of normalized currents shown in Fig. 6.7, it is possible to discuss the trends with two different suppositions:

1) the evolution of very active ORR sites on the surface of the electrode took place at the beginning of SCMFC life, then these active sites undergo permanent deactivation when the electrode wetting was completed;
2) the evolution of ORR active sites is not related to the electrochemically accessible surface area.

The first hypothesis is not supported in the light of the data shown in Fig. 6.4, as well as the current trends in Fig. 6.1. 80mV/decade of current Tafel slopes point to a more efficient ORR, occurring until the day 61. The current trends in Fig. 6.1 are consistent with the increase of cathodic polarization curves in Fig. 6.2, which was maintained during that time. Deactivation, observable after the peaks in Fig. 6.7, does not reflect in a decrease of currents, polarization curves, or Tafel parameters during the rest of the experiment. The second hypothesis is corroborated by the high activity documented before the dramatic increase of the capacity of 80% PTFE cathodes, shown in Fig. 6.6. It is possible to conclude that the permeation of the solution into the pores not covered effectively by the PTFE in the GDL allowed the increase of its electrochemical surface area, although unconnected with an actual enhancement of the ORR electrocatalysis. In fact, 60% PTFE cathodes exhibited even higher currents, together with the lowest electrochemical surface area. Based on the results achieved by the electrochemical tests, the cathode activation during the first days of the SCMFC operation was clearly documented by the decrease of the kinetic Tafel slope parameter. This is a sufficient condition to call for electrocatalysis. Efficient active sites for ORR due to the biocathode development [50,51,146] explain at best the superior performance of SCMFCs with low PTFE contents. ORR occurs in the hydrophilic MPL in contact with the water inside the SCMFC, as the mechanical instability destroyed the GDL layer during its wetting. These sites go through activation and deactivation phases during the SCMFC's life, coherently with the acetate addition and consumption. The lower productivity of the high PTFE content cathodes is consequently explained. Cathodes with 200% PTFE did not show any significant activity during the SCMFC's life, and the calculated ratio I/C poorly increased over time. An intrinsic inertness of the PTFE to sustain the biocathode and ORR is inferable. In fact, the highest PTFE cathode does not show significant current production and, after an attempt of electrocatalytic activation that might be attributed to incomplete wetting of the electrode MPL during the first days of operation, a permanent deactivation is demonstrated by the constant, high Tafel value. Based on the fact that the ORR can take place in the proximity of the triple-contact zones, where electrolyte, electronic conductor (carbon powder) and air (oxygen) coexist, the following steps might summarize the mechanism of ORR in the MFCs tested:

- biological ORR active molecules (mediators) are produced inside the cathodic biofilm;

- if the PTFE content is low, grafting of these active molecules occurs on the carbon surface and the ORR occurs with a 80mV/decade of current Tafel slope;
- if PTFE covers the large percentage of carbon surface near the triple-contact zone, grafting of the active molecules is inhibited and the ORR occurs on the cathode with a 120 mV/decade of current Tafel slope.

This mechanism is also consistent with the decrease of the Tafel slope during the first days of the experiment. Before the complete wetting of the cathode, the three phase interface is presumably in the MPL where the electronic conductors are carbon particles and carbon cloth. Long-term permeation of the water in the GDL moves the triple-contact in the zone where PTFE on carbon particles inhibits the ORR. This inhibition is permanent and proportional to the capability of the PTFE of covering the carbon particles with a homogeneous and thick veil. The mechanical instability of GDL in the 60% PTFE cathode showed a virtually PTFE-free triple-contact zone in the MPL with a low electrochemical surface area, but large enough to fully sustain the ORR electrocatalysis of the SCMFC.

Fig. 6.8A reports a SEM micrograph of a 60% cathode after three days of operation, showing the exposure of the carbon cloth fibers in the cracks underneath the GDL. Fig. 6.8B shows a detail of the 60% GDL, evidencing its friable nature at high magnifications (12,500×). The other cathodes with a higher PTFE content did not show similar erosion processes. Operating the SCMFCs in batch condition, the pH of solution increased over the value of 8.5, allowing the precipitation of carbonates at the cathode, MPL side, as already documented in previous experiments [50,51]. The deposition of a carbonate layer might decrease the electrochemical-active area, acting as a barrier to the waterfront, like the PTFE does in the GDL. It has to be underlined that the expected results for SCMFCs operating in flow is not far to that obtained in batch, because the stagnant condition in the porous MPL should be preserved. The solution permeates the porous media depending on the hydraulic conductivity that, in turn, is a function of the porous medium properties and hydraulic properties (acceleration, pressure, gravity etc.) following a hydraulic gradient governed by the Darcy law [151]. Biofilms in porous media grow, occupying pore space and obstructing fluid flow through pore gorges. In general, the structure of a biofilm can vary a lot depending on a number of factors including hydrodynamic conditions, nutrient availability, bacteria species, and cell communication [152]. Erosion occurs due to shear stress exerted by the bulk fluid on the biofilm-fluid. Operating in turbulent flow, the biofilm should be inhibited outside the MPL solid matrix at velocity higher than $2 m \cdot s^{-1}$ [153].

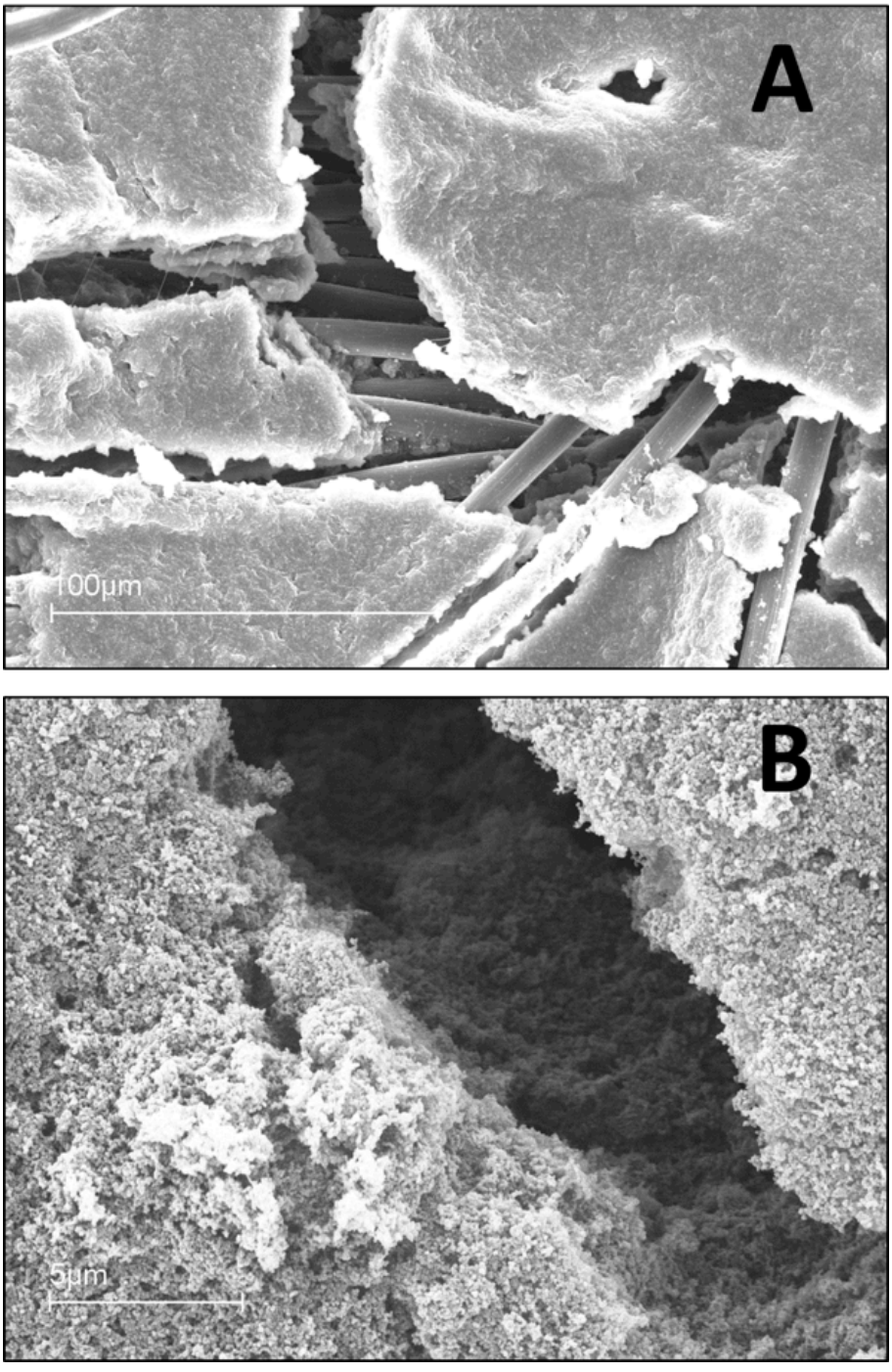

Figure 6.8 SEM micrograph of a 60%cathode, GDL side, after three days of operation (A). Detail of the 60% GDL at 12,500× magnifications (B).

7.

LACCASE-BASED BIOCATHODE

From:

1) ***M. Grattieri**; P. Scodeller; C. Adam; E. Calvo, Non-Competitive Reversible Inhibition of Laccase by H2O2 in Osmium Mediated Layer-By-Layer Multilayer O2 Biocathodes, Journal of the Electrochemical Society, 162 (9) (**2015**) G82-G86*

2) *C. Adam; P. Scodeller; **M. Grattieri;** M. Villalba; E.J. Calvo, Revisiting Direct Electron Transfer in Nanostructured Carbon Laccase Oxygen Cathodes, Submitted*

7.1 MET Laccase-based Biocathodes

While preparing a biocathode, the maximum current production is the primary goal. Key factors to achieve this goal are the increased enzyme concentration and its capability to communicate with the electrode surface. Entrapping the enzyme in a polymeric film is a possible approach to maximize the enzyme loading. In order to achieve reproducible enzyme electrodes, it is essential to control film thickness, enzyme and mediator surface loading, variation of oxygen partial pressure, convective-diffusion mass transport in the liquid electrolyte, and the charge of the topmost layer [154]. This can be achieved by using the layer-by-layer (LbL) electrostatic adsorption technique pioneered by Decher [114]. The advantage of the LbL self-assembly over hydrogels of same composition is that the electrodes can be designed and built choosing from different variables such as thickness, enzyme loading, osmium concentration and charge of the topmost layer. Unlike randomly oriented redox hydrogels, cast or electropolymerized films, organized nanostructured thin films allow control over the film thickness, the enzyme loading and the mediator concentration. While one assumes homogeneous composition in the x-y plane at any normal distance z from the metal surface, there is a normal distribution of species, electrostatic potential and vector electron transfer given by a redox concentration gradient.

The LbL technique allows coating alternate layers of enzyme and a polymer redox mediator until a desired amount. Thus, the enzyme concentration can be greatly increased and utilizing a mediator, such as the poly(allyl)amine osmium, the enzyme-electrode communication is increased, facilitating the electron transfer.

During the catalytic reduction of oxygen by laccase mediated by the osmium complex tethered to the poly-electrolyte, PAH-Os, the reactions occurring in the film can be written as:

$$4PAH-Os\left(II\right)+\mathrm{Lac}\left[4\mathrm{Cu(II)}\right]\xrightarrow{k}\mathrm{Lac}\left[4\mathrm{Cu(I)}\right]+4PAH-Os\left(III\right) \quad \text{(eq. 7.1)}$$

$$\mathrm{Lac}\left[4\mathrm{Cu(I)}\right]+O_2+4H^+\underset{}{\overset{K_{M,S}}{\rightleftharpoons}}\mathrm{ES}\xrightarrow{k_{\mathrm{cat}}}\mathrm{Lac}\left[4\mathrm{Cu(II)}\right]+H_2O \quad \text{(eq. 7.2)}$$

Where ES is the complex formed between Lac and molecular oxygen. At the electrode surface:

$$4\left\{PAH-Os\left(III\right)+\mathrm{e}^-\left(electrode\right)\rightarrow PAH-Os\left(II\right)\right\} \quad \text{(eq. 7.3)}$$

with further redox charge propagation by electron hopping between adjacent osmium redox sites covalently bound to the polymer back-bone in the normal direction to the electrode surface in the multilayer film assisted by segmental motion of the polymer strands. In Eq. 7.9 the stoichiometry number is $\zeta_n = 4$, since four moles of osmium complex are needed to fully reduce the 4-copper sites of Lac, while the number of electrons is n = 1 for the osmium redox mediator [155]. The substrate O_2 undergoes partition between the bulk solution and the film (we assume a partition coefficient K_S = 1 for oxygen since the thin enzyme films are highly hydrated) and then diffuses within the film with a diffusion coefficient D_{O2}. The mediator is assumed to be confined within the film, PAH-Os, covalently attached to the polyelectrolyte backbone. Charge propagation occurs by electron hopping self-exchange between adjacent sites of the reduced and the oxidized forms of the mediator described by a diffusion coefficient De [156,157]. Michaelis-Menten kinetics is assumed for the enzyme-substrate reaction with the association constant K_{MS} and enzyme turnover, k_{cat}. The reduced mediator, PAH-Os(II) regenerates the enzyme from the "Native Intermediate", NI, into the "Fully Reduced Laccase" Lac[4 Cu(II)] and Lac[4 Cu(I)] respectively [158] by exchanging 4 electrons with a mediator-enzyme constant k, according to the conventional "ping-pong" mechanism. It should be noted that under physiological conditions these four electrons are exchanged sequentially

through the T1 copper site of the enzyme and further transferred by internal electron transfer (ET) to the tri-nuclear T2-T3 cluster [158]. The second-order differential equations describing the system in the steady state are given by Eqs. 7.4 and 7.5 [159,160]. The symbols in brackets refer to the concentrations of the corresponding species, which vary across the film. Equations 7.4 and 7.5 are non-linear second order differential equations and have no closed analytical solutions.

$$D_{\mathrm{e}} \frac{d^2\left[\mathrm{PAH\text{-}Os}\right]}{dx^2} = \frac{\xi k k_{\mathrm{cat}} \left[\mathrm{PAH\text{-}Os}\right] \left[\mathrm{O_2}\right] \left[\mathrm{Lac}\right]_{\mathrm{TOT}}}{k\left[\mathrm{PAH\text{-}Os}\right] \left(K_{\mathrm{MS}} + \left[\mathrm{O_2}\right]\right) + k_{\mathrm{cat}} \left[\mathrm{O_2}\right]} \qquad \text{(eq. 7.4)}$$

$$D_{\mathrm{O_2}} \frac{d^2\left[\mathrm{O_2}\right]}{dx^2} = \frac{k k_{\mathrm{cat}} \left[\mathrm{PAH\text{-}Os}\right] \left[\mathrm{O_2}\right] \left[\mathrm{Lac}\right]_{\mathrm{TOT}}}{k\left[\mathrm{PAH\text{-}Os}\right] \left(K_{MS} + \left[\mathrm{O_2}\right]\right) + k_{\mathrm{cat}} \left[\mathrm{O_2}\right]} \qquad \text{(eq. 7.5)}$$

Pratt and Bartlett [160,161] have described a kinetic case-diagram for approximate solutions of the differential Eqs. 7.4 and 7.5, with the boundary conditions for multilayer enzyme electrode with self-contained immobilized redox mediator and freely diffusing enzyme-substrate (cases I to VII). These approximations have been recently verified experimentally for glucose oxidase and PAH-Os in LbL films [162].

7.1.1 MET Laccase-biocathode construction

In LbL films, the film thickness, Os surface concentration and enzyme loading grow with the number of adsorption steps. The catalytic current varies with the film thickness (L) since charge propagates within the film by electron hopping and the charge increases with thickness [156]. At high bulk oxygen concentrations, the model predicts that the current will be limited by the kinetics of the reaction between the mediator and the enzyme T1 Cu site, cases I and II in Bartlett-Pratt model for thin and thick films respectively [160].

$$I\left(caseI\right) = \zeta_n nF\left[PAH-Os\right]_{TOT} k\left[Lac\right]_{TOT} L \qquad \text{(eq. 7.6)}$$

$$I\left(caseII\right) = nF\left[PAH-Os\right]_{TOT} \sqrt{\zeta_n D_e k\left[Lac\right]_{TOT}} \qquad \text{(eq. 7.7)}$$

Therefore at high oxygen concentration, the catalytic current increases linearly with the film thickness (number of enzyme bilayers), the [PAH-Os(II)] follows a Nernstian dependence on the electrode potential:

$$\ln\left[\frac{i_L}{i}-1\right]=\frac{F\left(E-E_{1/2}\right)}{RT} \qquad \text{(eq. 7.8)}$$

At low oxygen concentration, cases V and VII in Bartlett-Pratt model describe the biocathode current density for thin and thick films respectively [160]:

$$I\left(caseV\right)=\xi_n nF\frac{L\left[Lac\right]_{TOT}k_{cat}K_S\left[O_2\right]_\infty}{K_{MS}+K_S\left[O_2\right]_\infty} \qquad \text{(eq. 7.9)}$$

$$I\left(caseVII\right)=nF\sqrt{\frac{2\xi_n D_e\left[PAH-Os\right]_{TOT}k_{cat}\left[LAC\right]_{TOT}K_S\left[O_2\right]_\infty}{K_{MS}+K_S\left[O_2\right]_\infty}} \qquad \text{(eq. 7.10)}$$

Figure 7.1 depicts a plot of the catalytic current density at p_{O2} = 1 atm at the plateau potential (0.15 V) as a function of the number of laccase layers and PAH-Os, i.e. the film thickness. For the thinnest films (corresponding to the lower coverage), the current increases linearly as the film thickness increases (case I). For the thicker films, on the other hand, the current density reaches a constant value, i_{max} (case II). This is in excellent agreement with the predictions of the model: in case I, for the thinnest films, the current dependence in film thickness is first order while for thicker films, case II predicts a current density independent of film thickness. It is noteworthy that evidence for the transition of the limiting cases of Pratt-Bartlett model for amperometric enzyme electrodes could be obtained because of the unique features of the LbL enzyme multilayer strategy, i.e. the ability to vary the film thickness in a controlled way at the nanometer scale. In both cases, for the enzyme-mediator rate determining step, one expects a Nernstian dependence of the catalytic current that follows the Os^{II} redox mediator concentration dependence on electrode potential (Eq. 7.9) giving rise to a catalytic wave in Figure 7.7 [160].

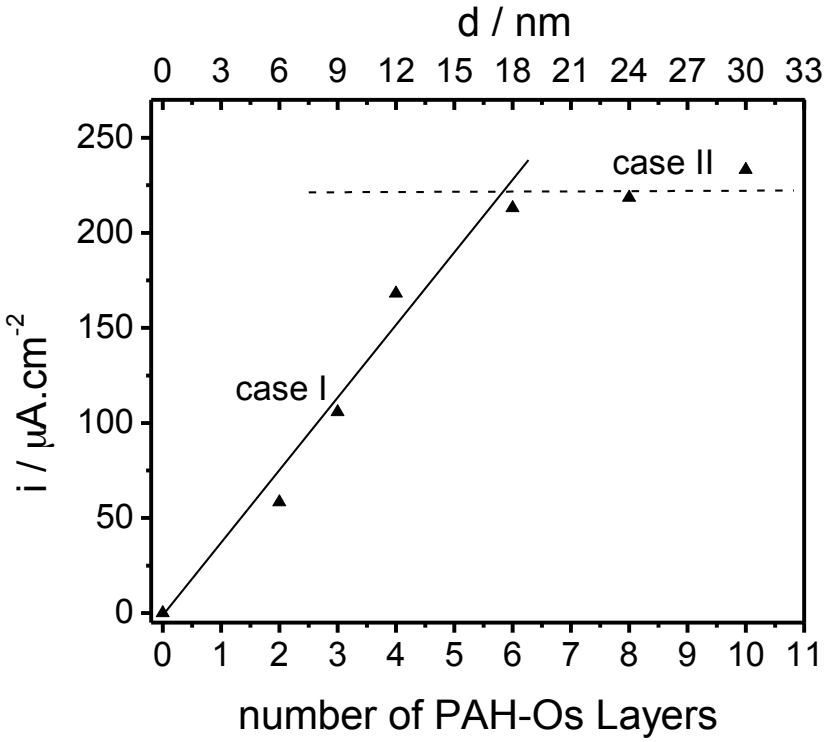

Figure 7.1 O_2 reduction catalytic current at 0.15 V vs. Ag/AgCl as function of number of PAH-Os/Laccase layers; measured by cyclic voltammetry ($v = 5\ mV{\cdot}sec^{-1}$) in O_2 saturated 0.1 M acetate buffer 0.2 M KNO_3 pH 4.7; RDE: $\omega = 9$ Hz. Ellipsometric thickness d.

It should be noted that $E_{1/2}$ shifts from the reversible potential of the Os^{II}/Os^{III} surface redox couple, 0.35 V, toward less positive potentials as the number of layers increases, approaching the redox potential of the surface Os^{III}/Os^{II} couple under these experimental conditions, i.e. 0.31 V [160]. At low O_2 concentration with $[O_2]_\infty << K_{MS}$, case V predicts a Michaelis Menten dependence on O_2 concentration, while for case VII, square root dependence is expected. Notice the different laccase concentration dependence for thin (Eq. 7.9) and thick films (Eq. 7.10), i.e. linear and square root, respectively, because of electron diffusion limitations in thick films. We can approximate the current density to the enzyme reaction rate only for thin films.

7.1.2 MET Laccase-biocathode response

Purified enzyme laccase from *Trametes trogii* has been employed in this study [163]. Strain 463 (BAFC: Mycological Culture Collection of the Department of Biological Sciences, Faculty of Exact and Natural Sciences, University of Buenos Aires) of *Trametes trogii* (Funalia trogii) (Polyporaceae, Aphyllo phora-les, Basidiomycetes) was used in these experiments. Stock cultures

were maintained on malt extract agar slants at 4◦C. Details of culture conditions and purification of the enzyme laccase have been reported elsewhere [84].

Figure 7.2 shows the CVs obtained for $Lac_n|PAH\text{-}Os_m$ biocathodes, with n values from 1 to 4 and m from 2 to 5. The electrode responses in N_2 saturated solution (7.2A) remark that the progressive osmium deposition brought to an increased load of Os redox molecules as can be seen by the increased current peaks related to the redox couple Os^{II}/Os^{III} (at 0,3V vs. Ag|AgCl). At the same time, the current responses in O_2 saturated solution (figure 7.2 B) increased, until current values close to the previously presented for a $Lac_4|PAH\text{-}Os_5$ biocathode.

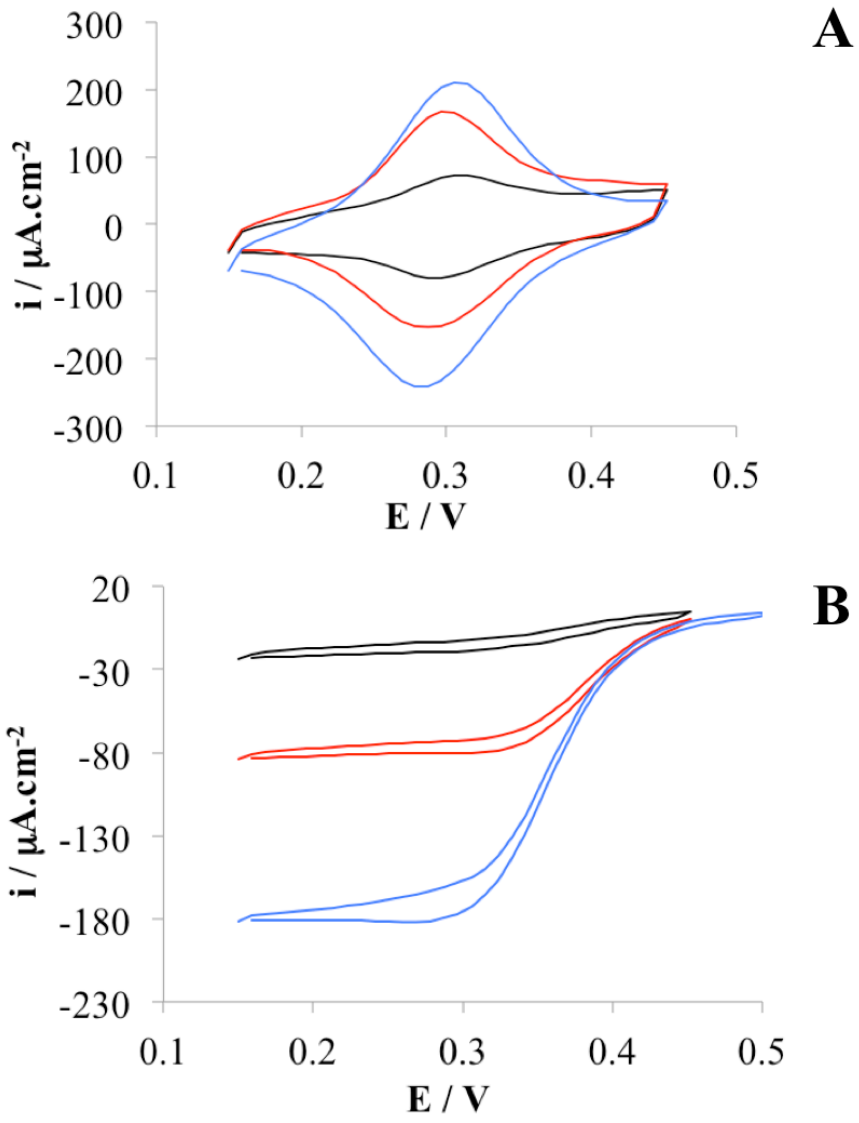

Figure 7.2 Cyclic voltammetry of $(Lac)_n(PAH\text{-}Os)_m$ biocathodes with n = 1 and m =2 (black line), n=2 m=3 (red line), n=4 m=5 (blue line), RDE: ω = 16 Hz at p_{O2}=0 in N_2 saturated acetate buffer of pH4.7 + 0.2 M KNO_3 at 500 $mV.s^{-1}$ (A) and at p_{O2} =1 in O_2 saturated acetate buffer of pH4.7 + 0.2 M KNO_3 at 5 $mV{\cdot}s^{-1}$ (B).

7.2 Role of H_2O_2

Laccase biocathodes have been intensively studied for biofuel cells [70,90]. In 2010, it was reported the first evidence that laccase can be inhibited by H_2O_2 produced by the enzymatic reduction of oxygen in osmium mediated biocathodes [84]. Later, it was shown that biofuel cells based on a laccase cathode suffer a dramatic loss in performance due to the H_2O_2 produced by glucose oxidase immobilized at the anode [86]. The inhibition mechanism of H_2O_2 on mediated laccase electrodes was unclear until recently, when Milton and Minteer reported the reversible inhibition of laccase by hydrogen peroxide in mediated electron transfer by (2,2'-azino-bis(3-ethylbenzothiazoline-6-sulfonic acid) ABTS [164]. Since hydrogen peroxide can be formed at the anodes of biofuel cells and also be accumulated during oxygen reduction in laccase-modified electrodes, it is imperative to understand the mechanism of inhibition.

7.3 H_2O_2 Inhibition in MET Laccase-based biocathodes

7.3.1 Materials and Methods

3-mercaptopropane sulfonate (MPS) was purchased from Sigma-Aldrich Argentina. Poly(allyl)amine (PAH), sodium acetate and acetic acid (100%) were obtained from Fluka. All reagents were analytical grade and used without further purification except PAH which was dialyzed against Milli-Q water. Ultra pure water was obtained from a Milli-Q purification system (nominal resistivity 18.2 MΩ at 25°C) and used to prepare all solutions. The complex osmium poly(allyl)amine (PAH-Os) was synthesized as described elsewhere [112]. The osmium content was evaluated spectrophotometrically at λ = 475 nm ($\varepsilon = 8100 M^{-1} cm^{-1}$). A gold electrode primed with 20 mM 3-mercaptopropane sulfonate in 0.01 M H_2SO_4 was further modified on top with a layer of Os bipyridine covalently tethered to poly(allyl)amine cationic polyelectrolyte followed by adsorption of laccase from a solution of a suitable pH value (around 5) where the protein carries a net negative charge (pI = 3.3). This process was repeated with rinsing between each adsorption step to yield an all-integrated enzyme-mediator system as previously reported [70]. The enzyme laccase (Lac) was co-immobilized with 100 μL of 0.44 mM osmium bipyridine redox polyelectrolyte mediator (PAH-Os, pH 8) via layer-by-layer (LbL) electrostatic self-assembly technique. After rinsing the electrode with Milli-Q water, the following layer was deposited covering the modified

electrode with 100 μL of 8 μM laccase solution in Milli-Q water for 20 minutes. In every case the LbL self-assembled electrode structures was covered with a topmost layer of PAH-Os.

7.3.1.1 Electrochemistry

Cyclic voltammetry was performed using an Autolab PGSTAT 30 potentiostat in a three-electrode cell with a platinum gauze as counter electrode and Ag|AgCl (3M) as reference electrode (all potentials in this chapter are referred to this reference electrode). The working electrodes were rotating gold discs (d = 5 mm) embedded in KelF polymer. All measurements were performed in 0.1 M acetate buffer of pH 4.7 containing 0.2 M KNO_3. Before measurements, all solutions were degassed with pure nitrogen or saturated with gas mixtures of nitrogen/oxygen in different ratios. In order to control the oxygen partial pressure, the N_2/O_2 ratio of this gas mixture was controlled by means of precision flow meters and flow regulators (G. Bruno Schilling, Argentina). Calibration of the N_2/O_2 gas mixtures was performed with the rotating disc electrode (RDE) convective-diffusion limiting current density

7.3.2 Results

The adsorption of laccase on the PAH-Os layers was monitored with the quartz crystal microbalance obtaining an average surface concentration of 1.34×10^{-11} mol·cm^{-2} in each adsorption step, while the thickness of the enzyme-mediator multilayer thin films was monitored by in-situ ellipsometry at 632 nm. As shown by XPS [165], the enzyme multilayer films are comprised of alternate layers of Lac and osmium polyelectrolyte mediator with some intermixing and interpenetration of the layers contributing to a flexible wiring of the enzyme due to segmental motion and electron hopping between adjacent redox centers and the enzyme Cu(T1) center [84,166].

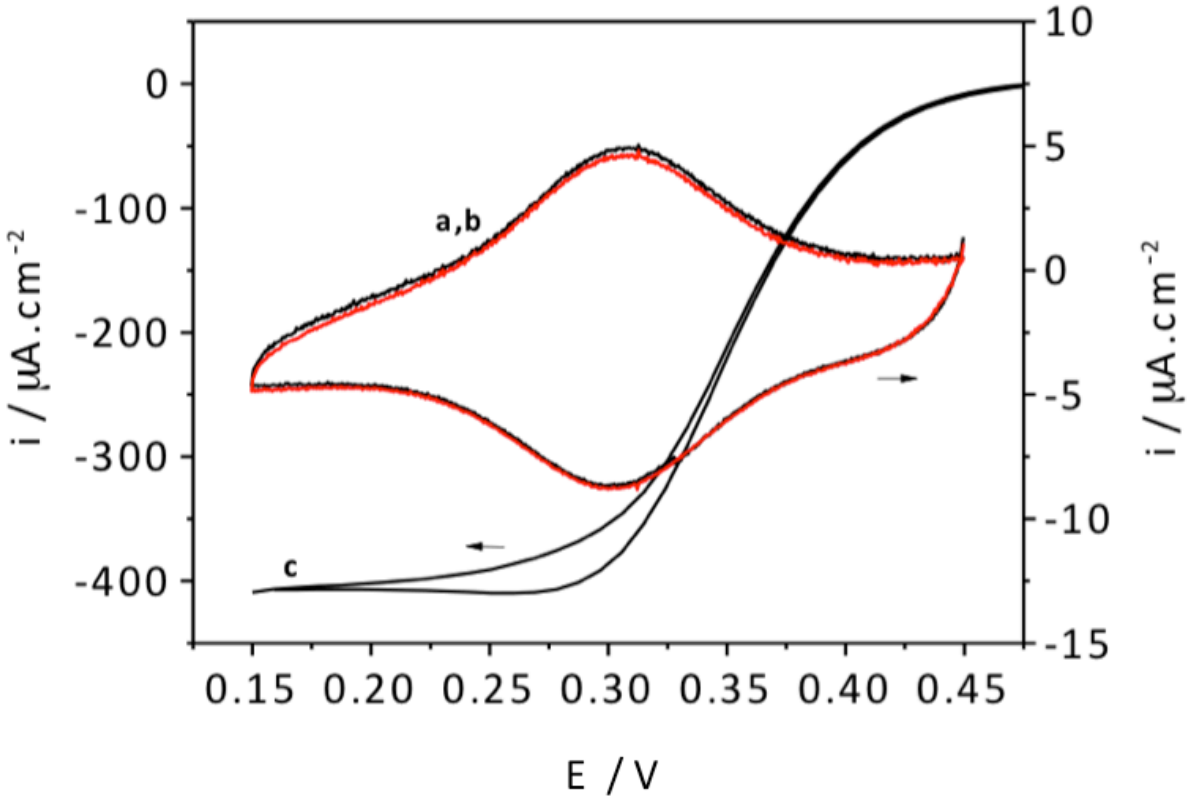

Figure 7.3 Cyclic Voltammetry of $(Lac)_3(PAH\text{-}Os)_4$ biocathode in 0.1 M acetate buffer (pH 4.7)+0.2M KNO_3 in absence of oxygen (curve a and b), and at p_{O2} = 1 atm (curve c), without H_2O_2 (curves a, c) and with 1 mM H_2O_2 (curve b). The right axis corresponds to curves a, b and the left axis to curve c.

Figure 7.3 depicts the electrochemical response of the biocathode in the absence and presence of oxygen. Under anaerobic conditions, the characteristic redox wave due to the surface confined osmium complex can be clearly identified. In the presence of oxygen, the Nerstian shape of the laccase mediated O_2 reduction catalytic current clearly develops.

Figure 7.4 shows the O_2 reduction current evolution after addition of H_2O_2 from 1 µM to 1 mM final concentrations. In all cases, the current drops to a steady state value at each peroxide concentration. Notice in the inset that for the highest peroxide concentration, a steady current density value is reached after more than two hours. The long time needed to reach a stationary current in the case of the highest concentration of H_2O_2 is indicative of an irreversible damage of the enzyme for high peroxide concentrations as previously reported [167,168]. This result is indicative of a reversible inhibition by peroxide since a steady state current arises from a balance between the inhibition rate, which increases with peroxide concentration, and the rate of the enzyme inhibitor release. Irreversible enzyme inhibition would result in a drop to zero of the catalytic O_2 reduction current at all peroxide concentrations (as the H_2O_2 concentration can be always assumed

as higher than the enzyme concentration). Thus, at each peroxide concentration, a fraction of the enzyme molecules is inactivated while there is a population of remaining active enzyme for each inhibitor concentration.

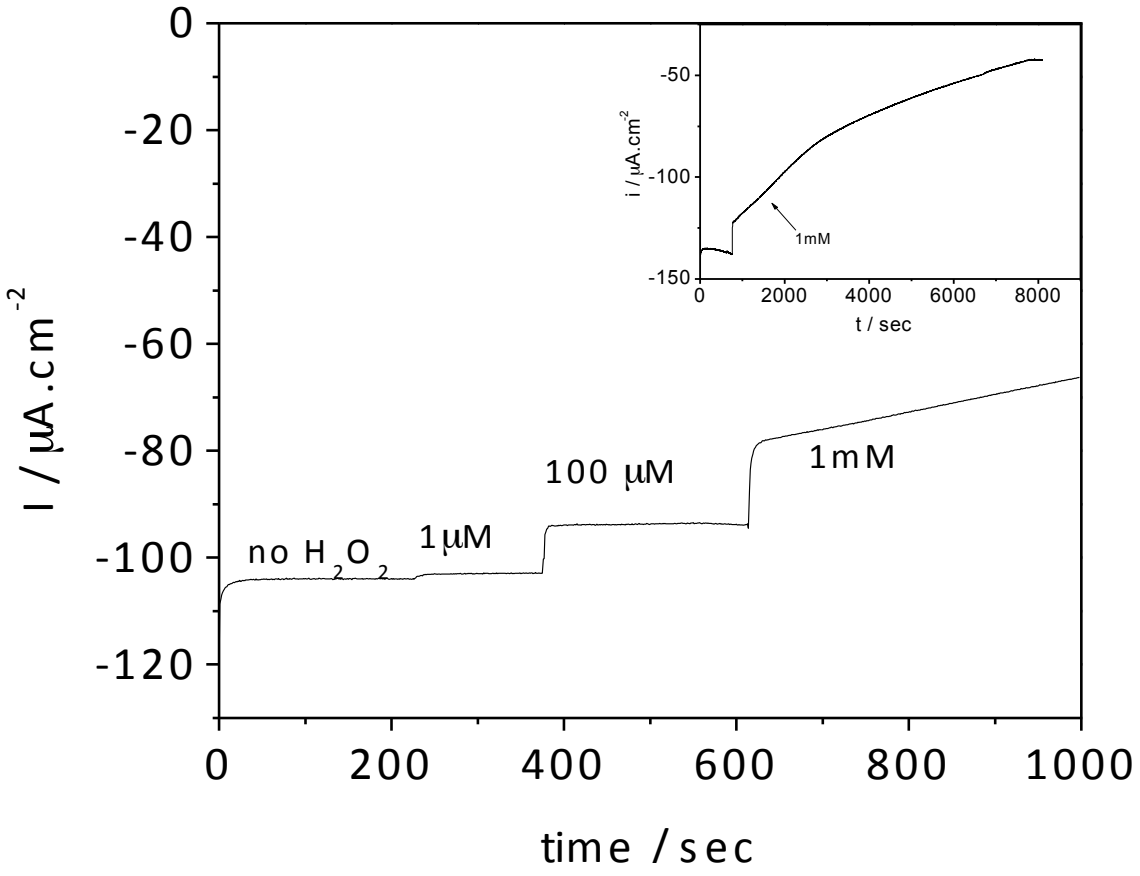

Figure 7.4 Chronoamperometry of $(Lac)_3(PAH\text{-}Os)_4$ biocathode at p_{O2} =0.2 atm with added H_2O_2 in 0.1 M acetate buffer (pH 4.7) + 0.2 M KNO_3 at E = 0.15 V, RDE: ω = 16 Hz. Inset: expanded plot for 1 mM.

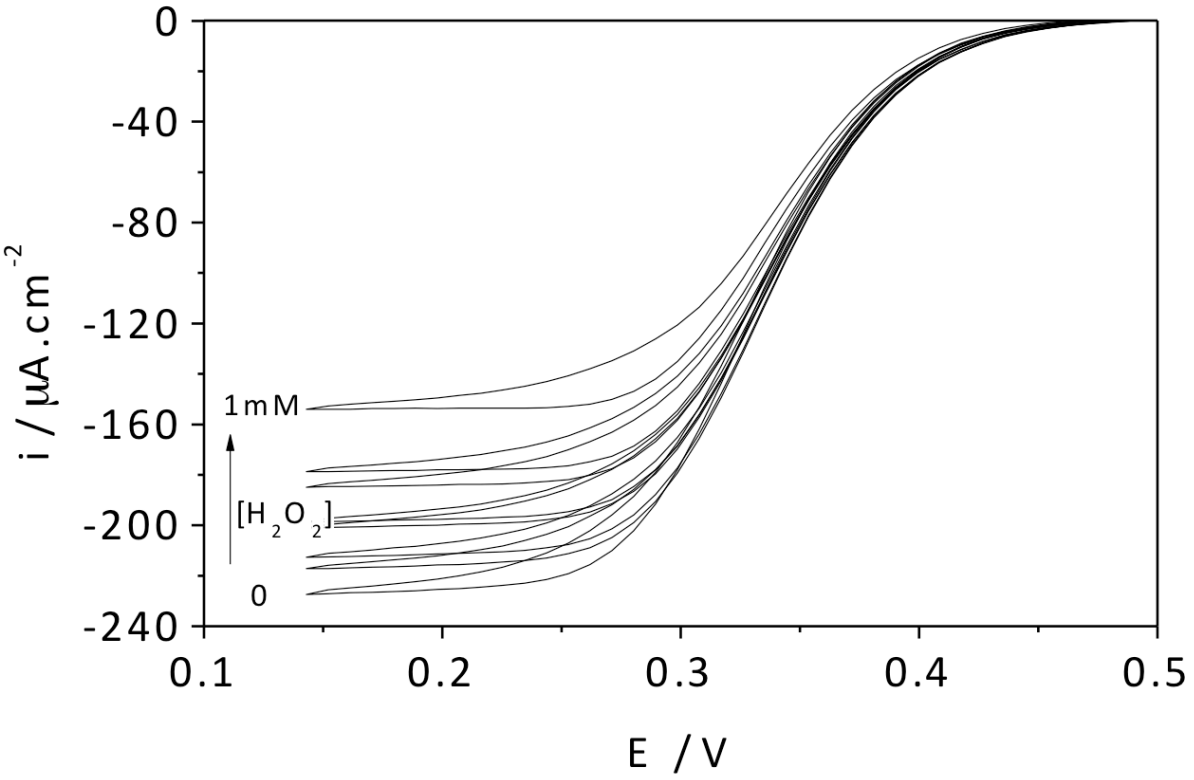

Figure 7.5 CyclicVoltammetry of $(Lac)_3(PAH\text{-}Os)_4$ at different H_2O_2 concentrations (0, 1, 10, 50, 100, 250, 500 and 1000 µM) for p_{O2} = 1.00 atm in 0.1 M acetate buffer (pH 4.7) + 0.2M KNO_3 at 25 mVs−1,RDE: ω = 16 Hz.

Figure 7.5 depicts current density-potential curves for the enzymatic reduction of oxygen mediated by the osmium polymer at different peroxide concentrations. The Nernstian potential dependence is identical with and without peroxide in solution and the decrease in the catalytic current is proportional to the peroxide concentration.

Larger inhibition is observed at higher oxygen partial pressures as can be seen in linear Dixon plots of Figure 7.6 with a decrease in the slopes at higher pO_2. Linearity of Dixon plots indicates that the enzyme-inhibitor complex cannot reduce oxygen (complete inhibition) [169]. It should be noticed that for thin films the current density is proportional to the enzyme reaction rate since diffusion effects are negligible in ultra thin films as previously discussed in chapter 7.1.

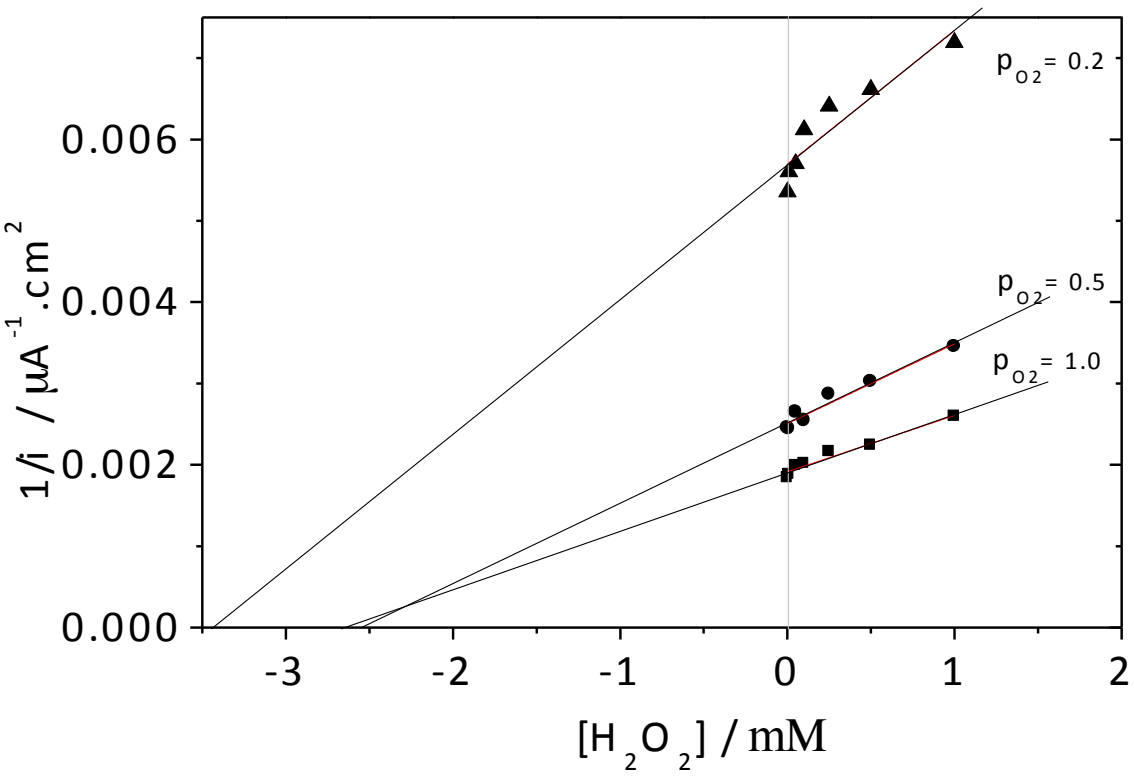

Figure 7.6 Dixon plot 1/i vs. [H_2O_2] at p_{O2} = 0.2, 0.5 and 1.00 for $(Lac)_3(PAH\text{-}Os)_4$ biocathode.

A complete set of catalytic waves at increasing inhibitor concentrations is shown in Figure 7.7 as a function of the oxygen partial pressure. The curves have been normalized to the limiting current at pO_2 = 1.00 atm in peroxide free solution, c.a. 114 μA cm^{-2}. The data was collected at 0.15 V where the complete reduction of the Os polymer can be reached.

For each peroxide concentration, the O_2 reduction bio-catalytic current density increases with oxygen concentration as it does in the absence of the inhibitor. The larger the concentration of peroxide in solution, the lower the biocathode current density. However, in all cases the characteristic enzyme electrode response is maintained. The reversible inhibition of laccase biocatalytic oxygen reduction by peroxide results in a decrease of i_{max} and the apparent Michaelis Menten constant, K_{O2} = 0.5–0.6 atm, c.a. below 250 μM.

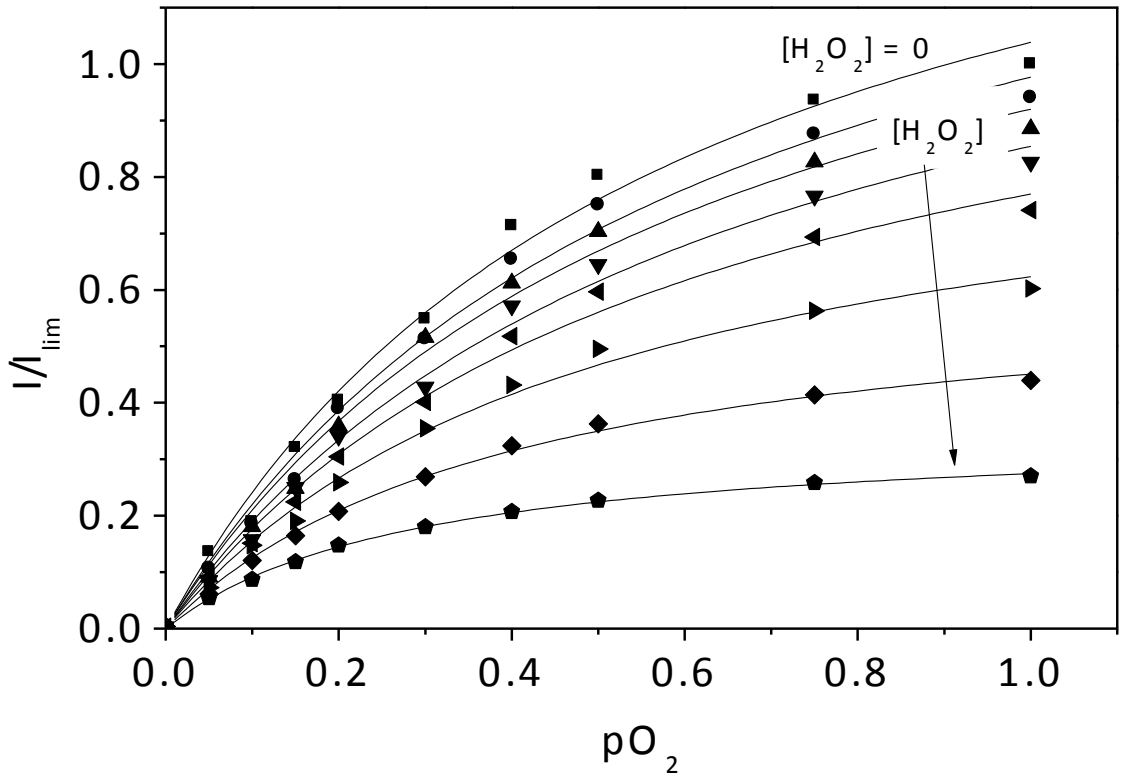

Figure 7.7 Normalized O_2 reduction catalytic currents at different peroxide concentrations (0, 1, 10, 50, 100, 250, 500 and 1000 μM) at E=0.15 V, RDE: ω = 16 Hz. Lines are best fit to Eq. 7.10.

In order to determine the type of inhibition on the catalytic current, the complex interplay between diffusion and non-linear enzyme kinetics needs to be taken into account, since the current density is not necessarily proportional to the rate of the enzyme reaction.

7.3.3 Discussion

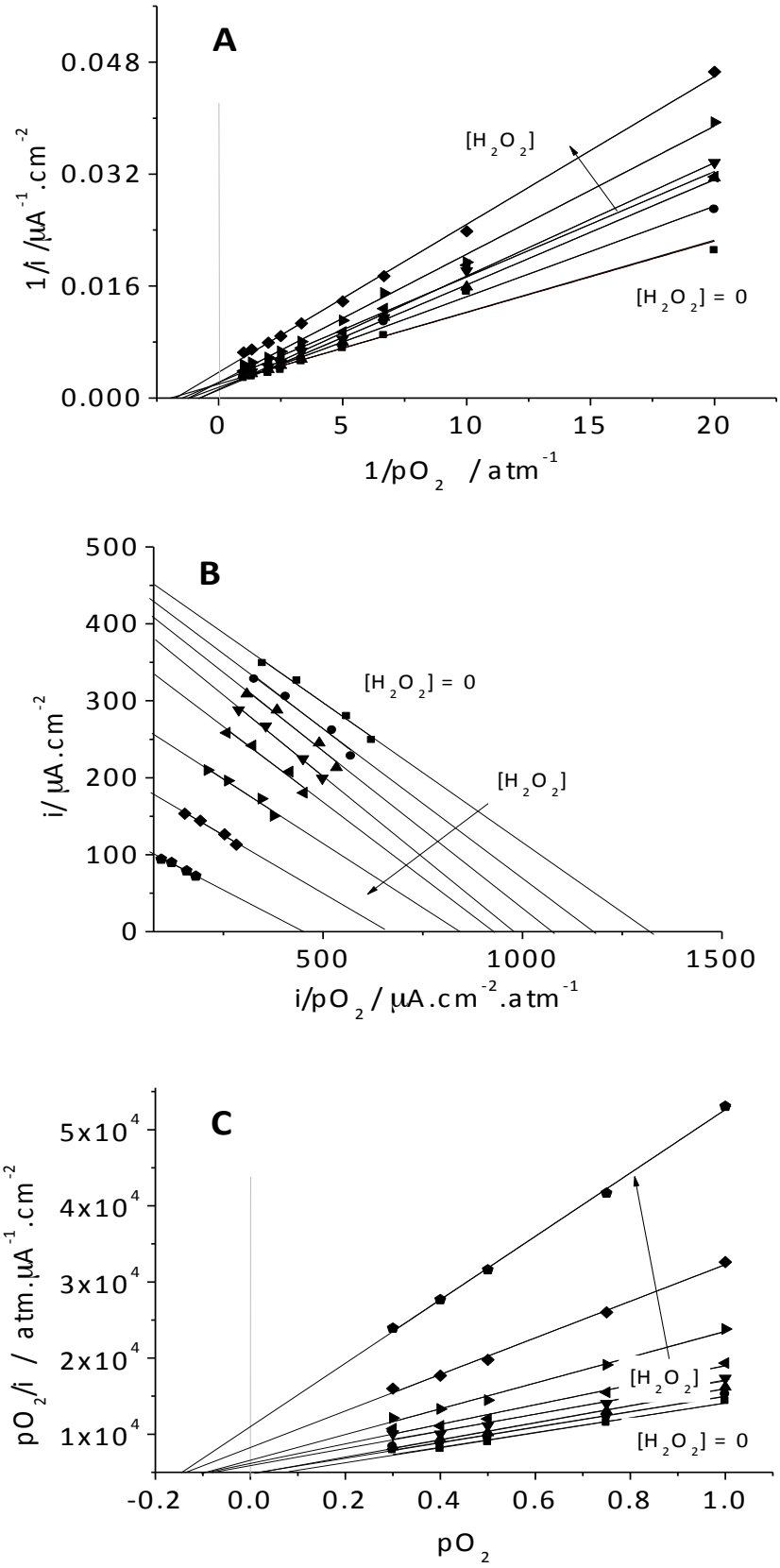

Figure 7.8 Lineweaver Burke plot (A), Eadie-Hofstee plot (B) and Hanes plot (C).

Figure 7.8 shows different diagnostic plots for the enzyme inhibition in thin films [169,170]. Linear Lineweaver Burke double reciprocal plots (Fig. 7.8A) with convergence on the x-axis corresponds to apparent non-competitive inhibition. However, convergence of data on the ordinate, characteristic of competitive inhibition, cannot be completely ruled out. Parallel linear Eadie-Hofstee plots (Fig. 7.8B) are characteristic of non-competitive inhibition which is confirmed by the non-parallel Hanes plots (Fig. 7.8C) [169]. In non-competitive enzyme inhibition mechanism, the inhibitor binds to a different site than the substrate-binding site. The inhibitor may bind to the free enzyme or to the enzyme-substrate complex [169,170]. Similar inhibition has been recently reported for another artificial mediator of laccase oxygen biocathodes (ABTS) by Prof. Minteer's group [164].

Furthemore, the $(Lac)_n(PAH\text{-}Os)_m$ biocathodes do not electrochemically reduce hydrogen peroxide [84]. A comparison of the CV in the absence and presence of peroxide in solution is shown in Figure 7.1 under anaerobic conditions and demonstrates that H_2O_2 cannot be reduced by laccase, since there is no difference after addition of peroxide to the electrolyte. We may conclude that soluble hydrogen peroxide is a non-competitive reversible inhibitor of laccase in oxygen biocathodes mediated by PAH-Os. It should be stressed that for thick films, i.e $L > 15$ nm, the diagnostic plots of Figure 7.8 are no longer valid, since the bio-catalytic current density is no longer proportional to the enzymatic rate because of diffusion limitations and the current dependence on oxygen substrate, enzyme and redox mediator is given by Eq. 7.10.

We demonstrate this behavior with data in Figure 7.9 for films with 4 and 12 enzyme-redox polymer bilayers, respectively. In the absence of peroxide inhibitor, the normalized current densities to the maximum current show no difference for thin and thick films. On the other hand, when 1 mM peroxide is present in the solution, the inhibited biocathode shows a larger current drop for a thin film (4 layers) than for a thick film (12 layers).

For the same fraction of inhibited enzyme molecules in the films, the current density dependence on enzyme concentration is weaker for thick films than for thin ones, i.e. $[Lac]^{1/2}$ in Eq. 7.10.

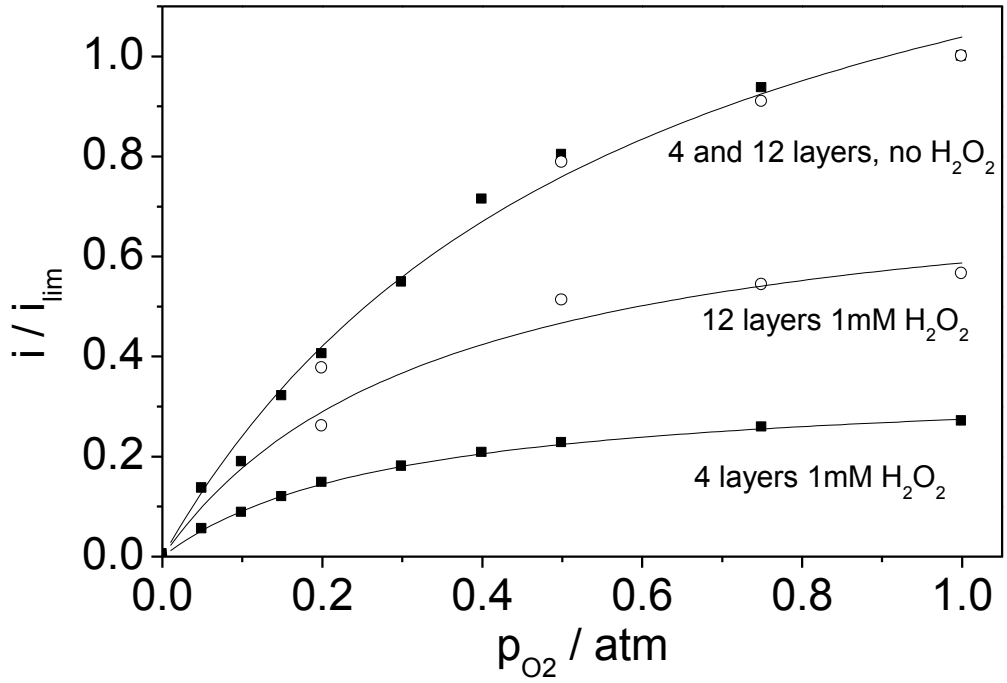

Figure 7.9 Normalized catalytic current vs. p_{O2} for thin (■) and thick (o) films and effect of addition of 1mM H_2O_2 Lines are best fit to Eq. 7.10.

On the basis of the experimental evidences, we will discuss possible mechanisms to explain the reversible non-competitive inhibition of laccase oxygen biocathodes by hydrogen peroxide. Solomon's group has extensively studied the mechanism of laccase oxygen catalysis [158,171,172]. Solomon's mechanism considers that oxygen binds to the fully reduced laccase forming the laccase peroxide intermediate with O_2 bridging between T2Cu(II) and T3Cu(II) and T3Cu(I). In order to explain H_2O_2 not binding to the O_2 binding site, we suggest that exogenous soluble H_2O_2 inhibits laccase by oxidizing T3Cu(I). Previous evidence that peroxide oxidizes the CuT3 site in laccase was provided by Solomon's group [167], and further disclosed that H_2O_2 binds with low affinity to the oxidized CuT2/T3 trinuclear center with the need of CuT2 center to bind peroxide [173], previously suggested by Vanngard [168].

Taking into account this mechanism, the inhibition reversibility was investigated. After inhibition, washing the electrode and immersing in a fresh peroxide free electrolyte no difference with the inhibited response was obtained. However, if the inhibited electrode was reduced at −0.4 V in peroxide free and oxygen free electrolyte for ten minutes, the response of the original non-inhibited bio-cathode was partially recovered. This suggests that peroxide oxidizes laccase, which needs fully reduced T3Cu sites to bind O_2 and that strong reduction of these sites recovers the catalytic activity.

Notice that laccase activity is recovered in the absence of oxygen and that the inhibition by peroxide is more important at the highest oxygen partial pressures. Therefore, we assume that in the reversible inhibition, peroxide competes for the electron injected at T1 copper center with the oxygen reduction at the trinuclear cluster and the reductive reactivation of laccase. In the absence of oxygen all electrons injected at T1 by Os(II) result in the reductive enzyme reactivation. However, at 1 mM peroxide concentration the initial response was no longer reached, which agrees with a previous study of Solomon's group who demonstrated that irreversible protein damage occurs at high H_2O_2 concentrations [167].

From the present experimental evidence and previous evidence of Kau et al. [167], we suggest that peroxide inhibits laccase by oxidizing T3Cu(I) and interfering in the Solomon 4-electron biocatalytic reduction of oxygen mechanism [172].

7.4 DET Laccase-based biocathodes

The first evidence of direct electron transfer (DET) from an electrode to the T1Cu of laccase was reported by Russian Scientists in 1978 and further confirmed in 1979 on carbon black electrodes [72,174]. Several other reports on DET to laccase biocatalyst have followed [62,68,90,175–177]. Based on the molecular structure and size of laccases the maximum surface concentration of the enzyme monolayer on electrode surfaces has been estimated $2\text{-}8\cdot10^{-12}$ moles·cm^{-2} [178]. The orientation of the T1Cu site with respect to the electrode is critical for catalysis, and since the population of enzyme molecules at tunneling distance is very low, the current densities reported for flat electrodes with enzyme monolayers are small, typically below 1µA·cm^{-2}. For these reason, large surface area carbon electrodes have been often employed to make DET electrodes.

7.4.1 Materials and Methods

Carbon Vulcan® XC-72 was obtained from Cabot Corporation. H_2O_2, H_2SO_4, HNO_3, KNO_3 and Poly(vynilchloride) (PVC) were purchased from Sigma-Aldrich Argentina. Sodium acetate and acetic acid (100 %) were obtained from Fluka. All reagents were analytical grade and used without further purification. Ultra pure water was obtained from a Milli-Q® purification system (nominal resistivity 18.2 MΩ at 25°C) and used to prepare all solutions.

7.4.1.1 DET Laccase-biocathode construction

To make the DET laccase-biocathode, a rotating gold discs (d = 5 mm) embedded in KelF® polymer was modified with successive deposition of Carbon Vulcan® and laccase. Carbon Vulcan® powder was cleaned with nitric acid before use. A suspension of carbon (90%) in poly(vinyl chloride) (PVC) (10%) in H_2O was prepared and diluted five times in the solvent and sonicated for 30 minutes. The gold disk electrode was first polished with alumina powder and tested in H_2SO_4 (1M). A drop of the carbon suspension is deposited on the gold electrode and allowed to dry completely. Before adsorption of the enzyme, cyclic voltammetry was performed in order to measure the capacity of the electrode. It is worth mentioning that this step is crucial for the successful adsorption of laccase. The electroactive area was estimated from the capacitive current and varies between 100 and 2000 cm^2. Adsorption of laccase was carried out by depositing a drop of enzyme solution in H_2O (0.3 mg·mL^{-1}) for 30 minutes and rinsed with MilliQ® water. Laccase

adsorption was identified by measuring the *ocp*, being higher than 0.5 V in presence of active laccase.

7.4.1.2 Electrochemistry

Cyclic voltammetry and chronoamperometry were performed using an Autolab PGSTAT 30 potentiostat in a three-electrode cell with platinum gauze as a counter electrode and Ag|AgCl (3M) as a reference electrode (all potentials herein are referred to this reference electrode). The working electrodes were the previously described gold discs modified with the carbon Vulcan®. All measurements were performed in 0.1 M acetate buffer of pH 4.7 containing 0.2 M KNO_3.

Before measurements, all solutions were degassed with pure nitrogen or saturated with gas mixtures of nitrogen/oxygen in different ratios. In order to control the oxygen partial pressure, the N_2/O_2 ratio of this gas mixture was controlled by means of precision flow meters and flow regulators (G. Bruno Schilling, Argentina).

7.4.2 Results and Discussion

7.4.2.1 Catalytic Oxygen Reduction on Carbon by Laccase

Very large surface area electrodes were employed in order to magnify the biocatalytic current response and to improve the contact between the electrode and the active sites of laccase by the carbon nanostructures.

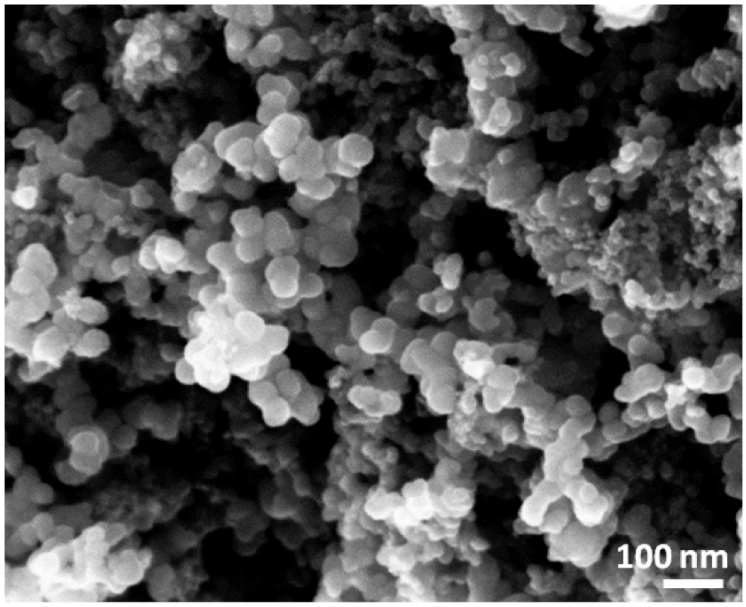

Figure 7.10 SEM micrographs of carbon Vulcan®-PVC deposited on gold.

Figure 7.10 depicts a scanning electron micrograph of a composite carbon Vulcan® XC-72 with adsorbed laccase. The large capacitive charging current $I_{cap} = C \cdot v$, observed in cyclic voltammetries depicted in figure 7.11, is due to a large surface area of the dispersed Vulcan® carbon as can be seen from figure 7.10. Comparing the capacitance obtained from the charging current at different potential sweep rates and the value for HOPG specific capacitance, c.a. 2 $\mu F \cdot cm^{-2}$ we obtain a surface area factor of 1500.

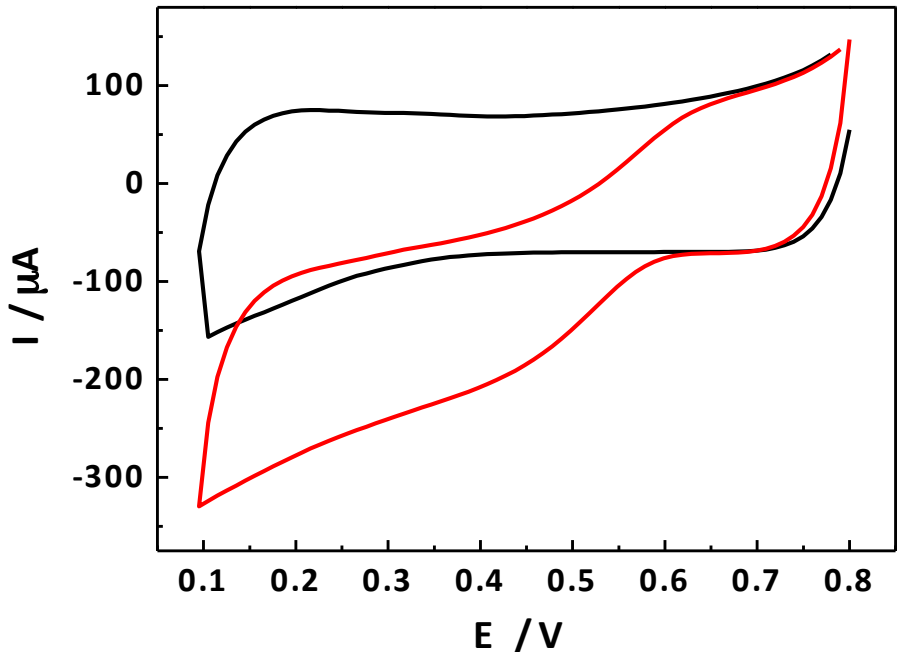

Figure 7.11 Cyclic voltammograms of the catalytic reduction of O_2 by laccase adsorbed on carbon Vulcan®-PVC deposited on the gold electrode in acetate buffer (pH = 4.7) in N_2 saturated electrolyte (black line) and in O_2 saturated electrolyte (red line) at 25 $mV \cdot s^{-1}$.

Figure 7.11 depicts current potential curves for carbon Vulcan®-adsorbed laccase composite cathode in nitrogen saturated and oxygen saturated electrolyte respectively. A clear onset of the bio-catalytic O_2 reduction current at 0.65 V is observed in good agreement with the high potential of *Trametes trogii* laccase T1 copper site (0.780 V) [179]. From the electrocatalytic response, two potential regions can be distinguished:

i) a potential dependent current, independent of the oxygen partial pressure at low overpotentials,

ii) a low potential dependent regime, strongly dependent on the oxygen concentration at high overpotentials. It should be noted that the current plateau at high overpotentials is well below the convective-diffusion controlled current.

It can be noted that oxygen electroreduction is present also for the N_2 saturated electrolyte below 0.30 V. Considering the high porosity of the electrode and the high affinity of laccase towards oxygen, traces of oxygen inside the porous electrode might be responsible for the obtained current response.

The biocatalytic nature of the cathodic currents in oxygen containing solutions was confirmed by the addition of fluoride as laccase inhibitor, since a complete offset of the catalysis was observed.

Figure 7.12 shows the polarization curves at different oxygen partial pressures and potentials, after subtracting of the capacitive charging current in N_2 saturated solution.

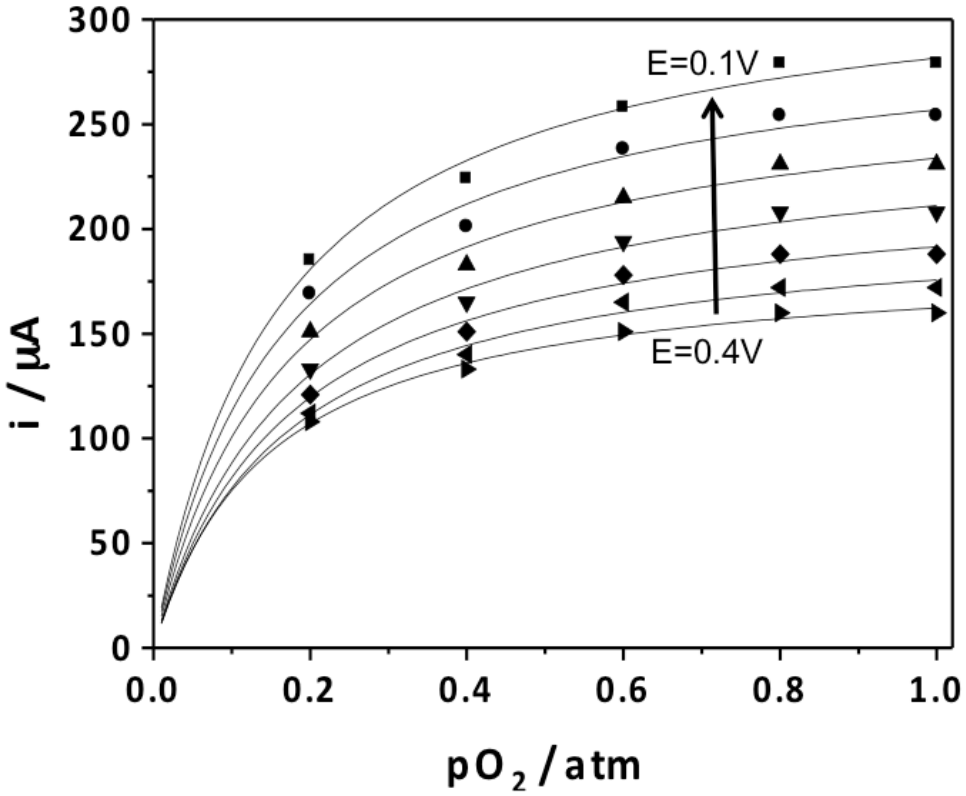

Figure 7.12 O_2 reduction catalytic currents at different electrochemical potential (E = 0.1, 0.15, 0.2, 0.25, 0.3, 0.35 and 0.4 V) Lines are best fit to eqn. 7.15.

Solomon has described the biocatalytic oxygen reduction by laccases, which can be represented by equations (7.11-7.13).

$$Lac(Cu^{II}_{T1}) + e^- \rightarrow Lac(Cu^{I}_{T1}) \quad \text{(eq. 7.11)}$$

$$Lac(Cu^{I}_{T1}) + Lac(Cu^{II}_{T2/T31}) \rightarrow Lac(Cu^{II}_{T1}) + Lac(Cu^{I}_{T2/T31}) \quad \text{(eq. 7.12)}$$

$$Lac(Cu^{I}_{T1}) + 3Lac(Cu^{I}_{T2/T3}) + O_2 \rightarrow Lac(Cu^{II}_{T1}) + 3Lac(Cu^{II}_{T2/T31}) + H_2O \quad \text{(eq. 7.13)}$$

The direct electron transfer (DET) from carbon to the T1 Cu atom represented by eqn. (7.11) is dependent on the electrode potential and is insensitive to the oxygen partial pressure.

$$k_{DET} = k^0_{DET} e^{-\frac{\alpha F}{RT}\left(E - E^0_{T1}\right)} \quad \text{(eq. 7.14)}$$

where E^0_{T1} is the formal redox potential of CuT1 center in laccase and α the charge transfer coefficient.

According to Solomon and Jones [172], the internal electron transfer from T1 Cu site to the tri-nuclear copper cluster T2/T3 across 1.3 nm (eqn. 7.12) is fast, then both T1Cu site and the oxygen reduction site at the T2/T3 Cu(I) which reacts with molecular oxygen according to eqn. (7.13) are in equilibrium. This enzymatic reaction is insensitive to the electrode potential and has a Michaelis-Menten dependence on oxygen partial pressure, pO_2:

$$V = \frac{V_{MAX} p_{O2}}{K_M + p_{O2}} \quad \text{(eq. 7.15)}$$

The experimental data at different oxygen partial pressures depicted in Figure 7.12 for different electrode potentials show a Michaelis-Menten behavior. However, the apparent K'_M values vary with electrode potential since these are apparent Michaelis Menten constants.

7.5 H_2O_2 Inhibition in DET Laccase-based Biocathodes

The interplay of the direct electron transfer from carbon electrodes to adsorbed laccase and the inhibition of the cathodic reaction by hydrogen peroxide plays a key role on the enzymatic electrocatalysis of the ORR. However, to the best of the writer's knowledge, only the research group of Prof. Minteer [164] has investigated the H_2O_2 inhibition on laccase electrodes in DET configuration, besides the importance of this process. Herein, the H_2O_2 inhibition on Laccase adsorbed on carbon Vulcan® electrodes was investigated.

7.5.1 Materials and Methods

For the inhibition study, the electrode was prepared as explained previously (chapter 7.4.1.1) with successive deposition of the Vulcan® carbon suspension and laccase. Chronoamperometry at 0.3 V was used in order to obtain the catalytic currents used for the inhibition mechanism study. All measurements were performed in acetate buffer (pH = 4.7) under rotation (6 Hz) with successive additions of freshly prepared hydrogen peroxide solution.

7.5.2 Results and Discussion

7.5.2.1 Inhibition of the Catalytic Activity by Hydrogen Peroxide

Figure 7.13 depicts the direct plot for the DET laccase-biocathode at different oxygen partial pressures and increasing H_2O_2 concentrations. The effect of the inhibitor on the biocatalytic current response can be clearly seen, influencing both the K_M and the V_{MAX}. In order to determine the inhibition mechanism on the DET electrode, linearization methods were employed and the results are reported below.

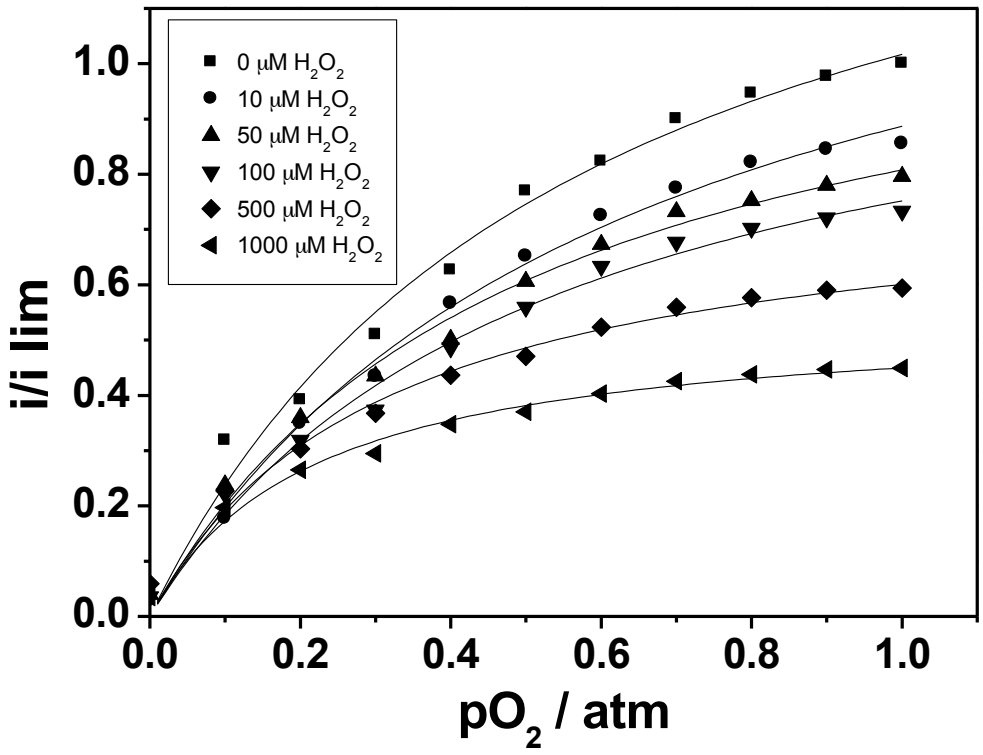

Figure 7.13 Normalized O_2 reduction catalytic currents at different peroxide concentrations (0, 10, 50, 100, 500 and 1000 μM) at E = 0.3 V, ω = 6 Hz.

7.5.2.2 Linearization Methods

Figure 7.14 depicts the Lineweaver Burke double reciprocal plots and the Eadie-Hofstee plots for the DET laccase-biocathode. Parallel double reciprocal Lineweaver Burk plots (Figure 7.14 A) are indicative of uncompetitive inhibition mechanism, unlike mediated mechanism previously reported (chapter 7.3). On the other hand, Eadie-Hofstee plots suggest non-competitive inhibition mechanism with parallel lines for low H_2O_2 inhibitor concentration [169]. However, for the Eadie-Hofstee plots at higher H_2O_2 concentrations, non-parallel lines are obtained, with a tendency for convergence in a joint intercept on the x-axis, corresponding to uncompetitive inhibition. These results indicate the presence of a mixed inhibition mechanism, with predominance of uncompetitive inhibition, especially at high H_2O_2 concentration. The results are consistent with similar findings from Prof. Minteer's group with multiwall carbon nanotubes laccase-biocathode [164].

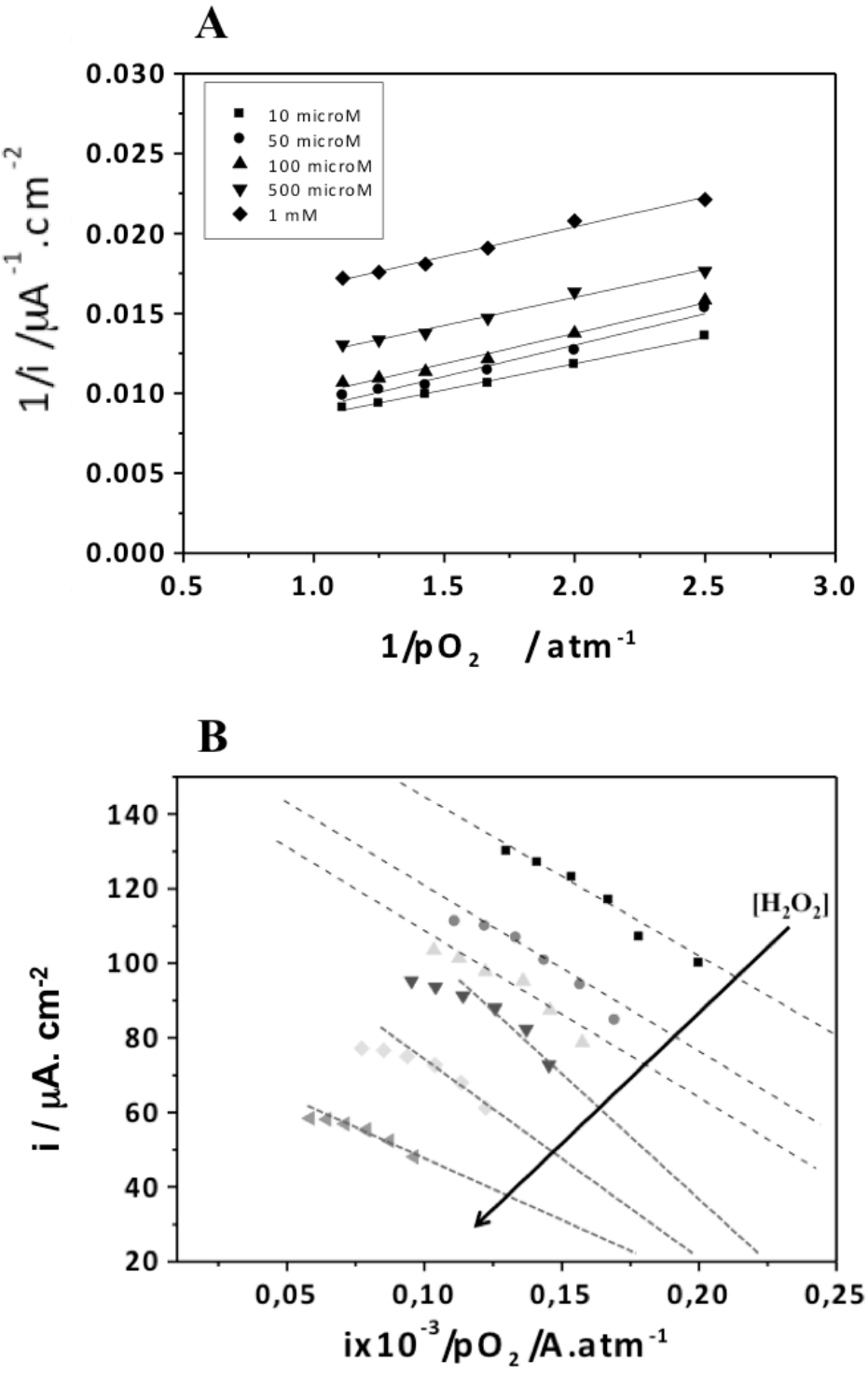

Figure 7.14 Double reciprocal Lineweaver-Burk plot (A) and Eadie-Hofstee plot (B).

8.

BIOANODE DEVELOPMENT

From: *E. Guerrini; P. Cristiani; **M. Grattieri**; C. Santoro; B. Li; S.P.M. Trasatti, Electrochemical Behavior of Stainless Steel Anodes in Membraneless Microbial Fuel Cells, Journal of The Electrochemical Society, 161(3) (**2014**) H62-H67.*

8.1 From Carbon Cloth to Stainless Steel

Carbon cloth sheets (CC) are the most common material for anode application in MFC laboratory studies due to low resistance and the physical structure of the material. The CC electrode consists of interwoven fibers that allow the free access of microorganisms and mediators to the electrode surface [11]. As a matter of fact, carbon cloth is still an expensive support, whose mechanical fragility prevents its widespread use especially for long term operations. Furthermore, resistivity of the tested carbon cloth was typically around 3–6 Ω·cm. A large projected surface area would have considerable power losses due to internal resistances. Thus, new materials need to be proposed as alternative to the carbonaceous based electrodes.

A more rugged and cost effective material AISI304 stainless steel has been proposed to overcome the weakness of carbon cloth for the scale-up of the MFC technology [180–182], especially for the application in microbial electrolysis cells where the cathodic reaction of hydrogen evolution is enhanced [47,183]. Despite a generally excellent corrosion behavior of this material [183], the effect of bacteria (microbial corrosion) can be considerable in specific electrochemical conditions and chemical environment, such as in the presence of sulfate reducing bacteria (SRBs) [184–186]. Literature studies of biocatalyzed anodes made of stainless steel, although still promising, did not bring to the production of scalable and cost effective MFC systems [180,181].

It is well known that a protective chromium enriched oxide layer forms on the surface of stainless steel exposed to a natural aerated environment. Nevertheless, the stability of this oxide layer on electrodes polarized far away from the free corrosion potential, in electrochemical systems like MFCs, might become critical, with and without the contribution of bacteria. Once stainless steel starts to corrode, it could act as a sacrificial electrode for providing electrons and eventually lose its electrode function.

From an electrochemical point of view, too high of potentials (anodic) could break metal passivity in transpassive regime, thus provoking massive dissolution of the metal [187]. Conversely, too low of potentials (cathodic) could destabilize the surface oxides, thus reducing the thickness of the protective layer or removing it completely [185]. In these circumstances, the surface of the metal might be unprotected from external chemical attacks. In contradiction, the absence of this oxides layer (normally considered insulating or semiconducting) could in principle increase the electron transfer from/to the bacterial biofilm, as a consequent decrease of resistivity at the metal/solution interface.

Previous experimentations with single chamber MFCs, using graphite bioanodes and biocathodes, revealed a relevant role of SRB at the cathode [188] and confirmed in the best performing systems in the presence of SRBs at the anode. In the perspective of extensive use of stainless steel in substitution of graphite electrodes for industrial application of single chamber MFC in wastewater plants, here, the microbial corrosion on AISI304 anodes was elucidated and the correlation of microbial corrosion with power generation of SCMFC was established.

8.2 Materials and Methods

The SCMFC (volume: 125 ml) was used in this study. The system had an opening on one side (area of 5 cm^2) to hold the cathodic materials, and two openings on the other side to insert the anodic materials. A plastic screw cap sealed the top opening of the system. The SCMFCs were filled with raw wastewater collected from the municipal wastewater treatment plant of Nosedo, Milan, Italy. Chemical oxygen demand (COD) of the wastewater was 0.3 $g \cdot L^{-1}$ [51]. Sodium acetate was periodically added into the SCMFCs as substrate for bacteria metabolism. The external resistor (R) connecting anode and cathode was 100 Ω for all tests (Figure 8.1).

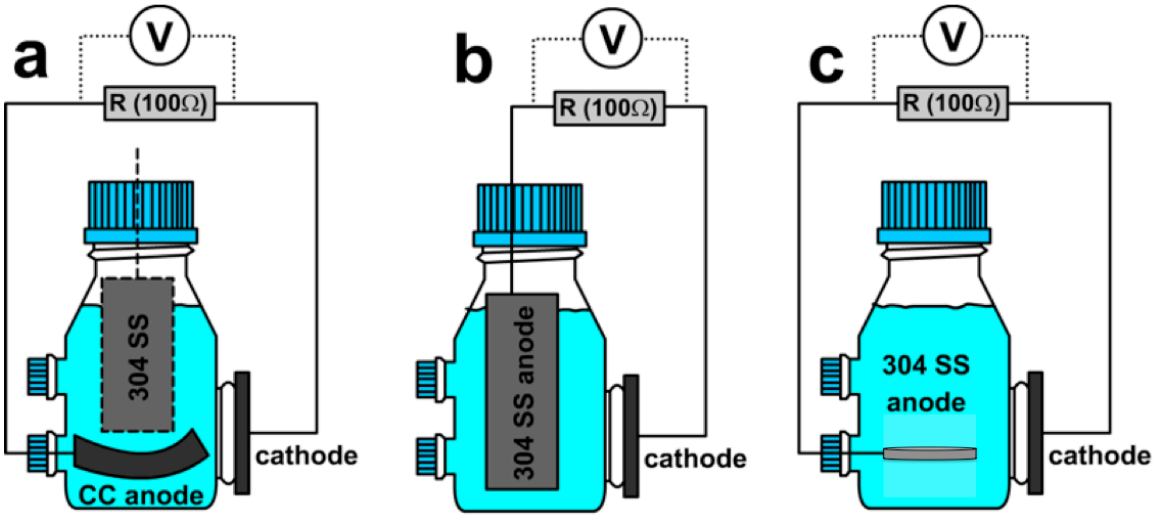

Figure 8.1 Sketch of the different SCMFC configurations used. SCMFC with CC anode and cathode, and a strip of AISI304 (A); SCMFC with a CC cathode and a strip of AISI304 anode in partially anaerobic conditions (B); SCMFC with CC cathode and anaerobic round AISI304 anode (C).

The cathode (geometric area: 5 cm^2) consisted of a carbon cloth sheet (Saati, Legnano Italy) with one side being covered by a slurry of carbon black powder (TIMCAL, ENSACO 350 G) and Nafion binder (5%w suspension in water/alcohols, Sigma Aldrich) to generate a micro porous layer (MPL) [189], and the other side being coated with a layer of graphite powder + Teflon suspension (70% w/w, Sigma Aldrich) to form a diffusion layer (GDL). No electrocatalyst was coated on the MPL layer, which directly contacted with wastewater in the anode chamber of SCMFC.

The AISI304 anodes (Table 8.1) were cut from a 2 mm thick foil. The thickness of the stripe was then reduced to 0.2 mm by cold working at room temperature. Cold working is the plastic deformation of metals below the recrystallization temperature. The deformation was obtained by passing the metal strip between two rolls with a gap of the selected dimension. The final anode products were obtained from the rolled steel. The degreasing of the anode surface was achieved by sonication in pure acetone first and in pure ethanol. Carbon-cloth (CC) based anodes (plain untreated CC without MPL or GDL, 5×3 cm^2) were used as the control throughout the experiments.

Table 8.1. Nominal composition of the AISI304 anode.

AISI No / Common Name	C	Si	Mn	P	S	Cr	Mo	Ni	Others
304	0.07	0.75	2.00	0.045	0.030	18.0	-	8.0	N 0.10

8.2.1 Experiment description

The experimentation was scheduled and divided in three consecutive steps:

1) setup of three SCMFCs with both electrodes (anode and cathode) in carbon cloth;
2) substitution of two anodes with AISI304 strips from top to bottom of the cells. In the third SCMFC, a strip of AISI304 was inserted, not connected and left at open circuit;
3) setup of two SCMFCs with the round AISI304 anode kept at the bottom of the cell, where anaerobic conditions are more easily met.

Step 1. Three SCMFCs with clean un-colonized carbon cloth anodes were set up at the beginning of the experiment. Fresh wastewater added with sodium acetate (COD: 3 $g \cdot L^{-1}$) was used as inoculum. The conductivity of the solution after the acetate addition was 4.5 $mS \cdot cm^{-1}$. Chemical and electrochemical measurements were conducted during the first 15 days of the operation.

Step 2. After these 15 days, an AISI304 strip (2×6.5 cm, area of 13 cm^2) was immersed into one of the three SCMFCs, and kept insulated from the carbon cloth anode (as in Figure 8.1a). The cell was refilled with fresh wastewater and acetate, and the open circuit potential (*ocp*) of the AISI304 anode was recorded during the next 15-days. In the other two SCMFCs, the carbon cloth anode was removed and replaced with an AISI304 anode (2 × 6.5 cm, area of 13 cm^2). The AISI304 anode strips were vertically immersed into the cell solution, with the upper part close to the solution surface and the lower part on the bottom of the solution (Figure 8.1b). The SCMFCs were then refilled with fresh wastewater and sodium acetate, and operated for 15 more days.

Step 3 To compare the microbial corrosion of stainless steel anodes under anaerobic and aerated conditions, two other SCMFCs were setup with circular AISI304 anodes (diameter of 4 cm, area of 12.6 cm^2) being positioned at the bottom of solution, in the strictly anaerobic zone (Figure 8.1c). As for all the previous cells, the wastewater was refreshed and added with the same quantity of sodium acetate.

8.2.2 Electrochemical measurements

A multi-channel multimeter (Graphtech midi Logger 820) was used to record the potential (E) over the external resistance (R_{ext}) every 15 minutes. The corresponding current (I) through the R_{ext} was calculated as previously indicated. The R_{ext} was disconnected twice a week for measuring the *ocp* of the anode and cathode. Unconnected AISI304 strip was continuously monitored during the 15 days

of operation, and the *ocp* was recorded each 15 minutes using Graphtech midi Logger 820, with a SCE as a reference electrode.

Polarization curves, more precisely quasi-stationary polarization curves, are a particular type of linear sweep voltammetry (LSV) measured at a low scan rate (0.166 $mV \cdot s^{-1}$) [131]. A three-electrode configuration was applied, with the testing electrode being connected to the working terminal of the potentiostat, a Pt wire being connected to the counter, and a Luggin capillary reference electrode being positioned close to the working electrode, so that no correction of the solution ohmic drops was needed. A linear potential ramp was applied from the *ocp* of the electrode to 0 V. All electrochemical potentials are reported vs. the saturated calomel electrode (SCE).

A scanning electron microscope (Leo 1430) was used to inspect the surface morphology of the AISI304 anode before and after the SCMFC operation. The anode samples were washed with Milli-Q water, gently scrubbed to remove the biofilms from the metallic surface, then sputtered with gold, and left under argon flow before the SEM observation.

8.3 Results

8.3.1 Carbon Cloth anode performance

All SCMFCs were operated with CC anodes in the first 15 days (Step 1). The *ocp* of the CC anode (as the control sample) dropped to −580 mV at the beginning stage of the tests, indicating that the anode chamber became completely anaerobic (Figure 8.2). The SCMFC generated useful current generation in correspondence with the *ocp* drops. The potential over R_{ext} was ∼50 mV, and the current density was 1 $A \cdot m^{-2}$. Anodic and cathodic polarization curves performed at the beginning and after 15 days of operation are overlapped in Figure 8.3 (absolute values). After 15 days of operation, great increase in the current sustained by both electrodes is evident. The cathodic shape did not change with time, while the current increased during the biocathode development in agreement with previous studies [51]. The anodic curve undergoes a more complex variation, with a current peak at the intersection with the cathodic curve. The anodic curve crosses at its maximum the cathodic curve also in the case of the other two SCMFCs (data not reported). The anodic *ocp* (the potential at zero current of each curve) decreases from the initial value of −280 mV down to the value of about −500 mV. This is consistent with the open circuit measurements shown in Figure 8.2.

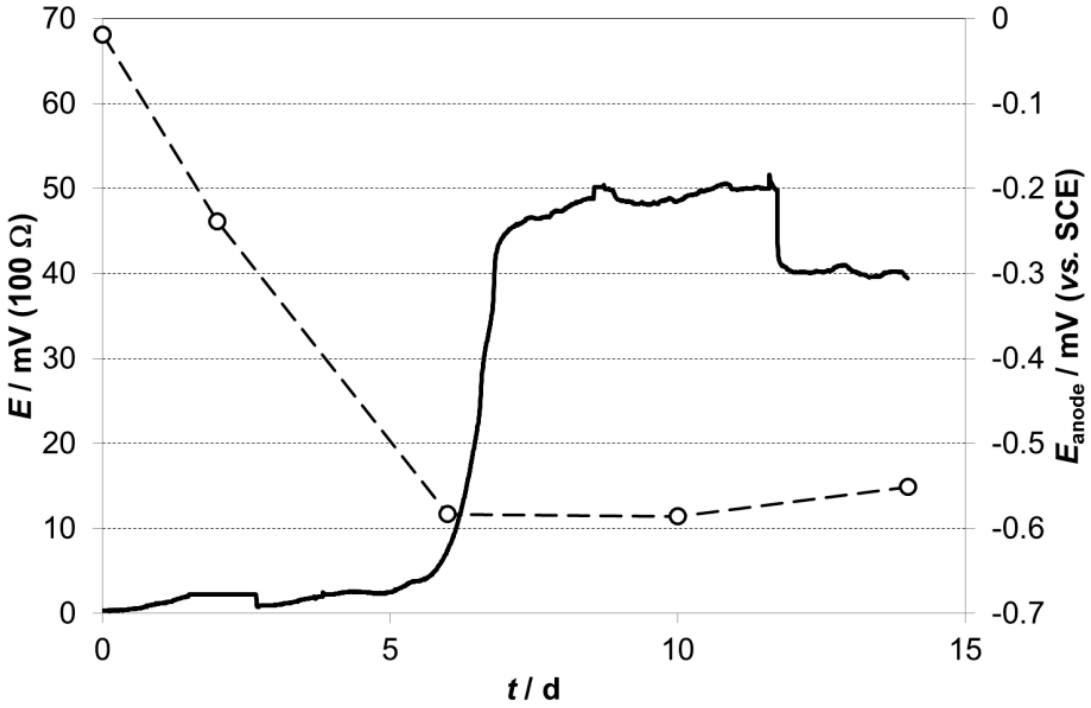

Figure 8.2 Trend of the potential (over 100 Ω R_{ext}) of the SCMFCs with CC anodes (solid line, the left axis) and the corresponding anodic ocp (dashed line, the right axis) during the 15 days of operation.

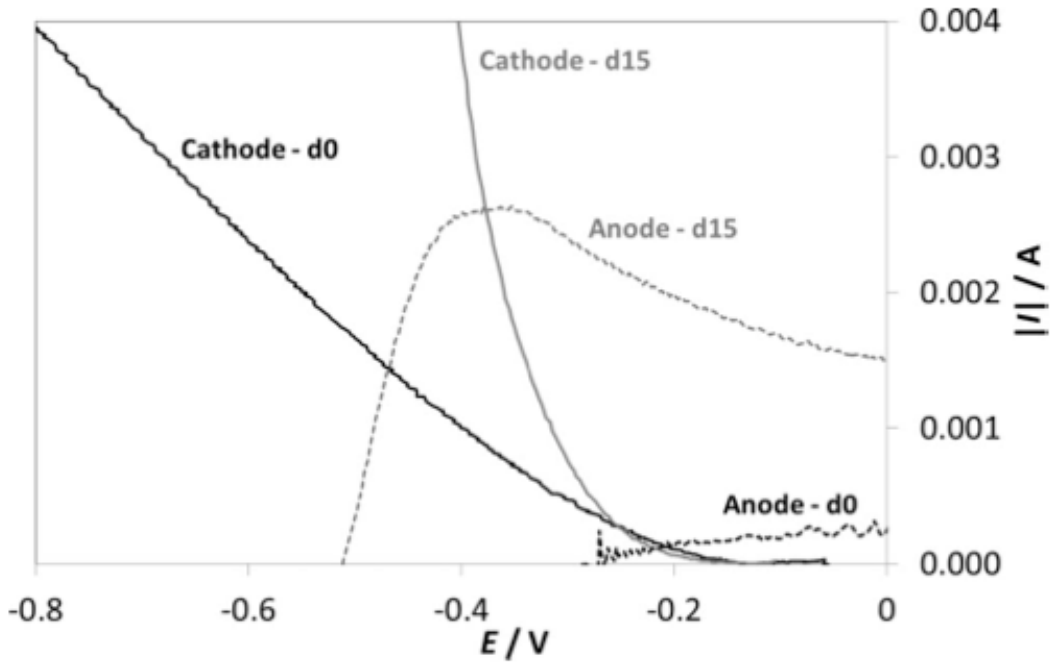

Figure 8.3 Polarization curves (linear sweep, 0.166 $mV \cdot s^{-1}$) of anode and cathode in SCMFCs with CC anodes at day 0 and day 15. (Currents are expressed as the absolute values for Anode/Cathode comparison and overlay).

8.3.2 AISI304 anode performance

After 15 days, a AISI304 strip was immersed into the solution of a SCMFC (Step 2). The free corrosion potential (*ocp*) of the AISI304 strip decreased constantly to −380 mV (Figure 8.4), 200 mV less negative than that of the CC anodes, as the wastewater becomes anaerobic, simply following the redox potential of the solution and settled to a constant value in 10 days. No macroscopic biofilms were observed on the AISI304 surface.

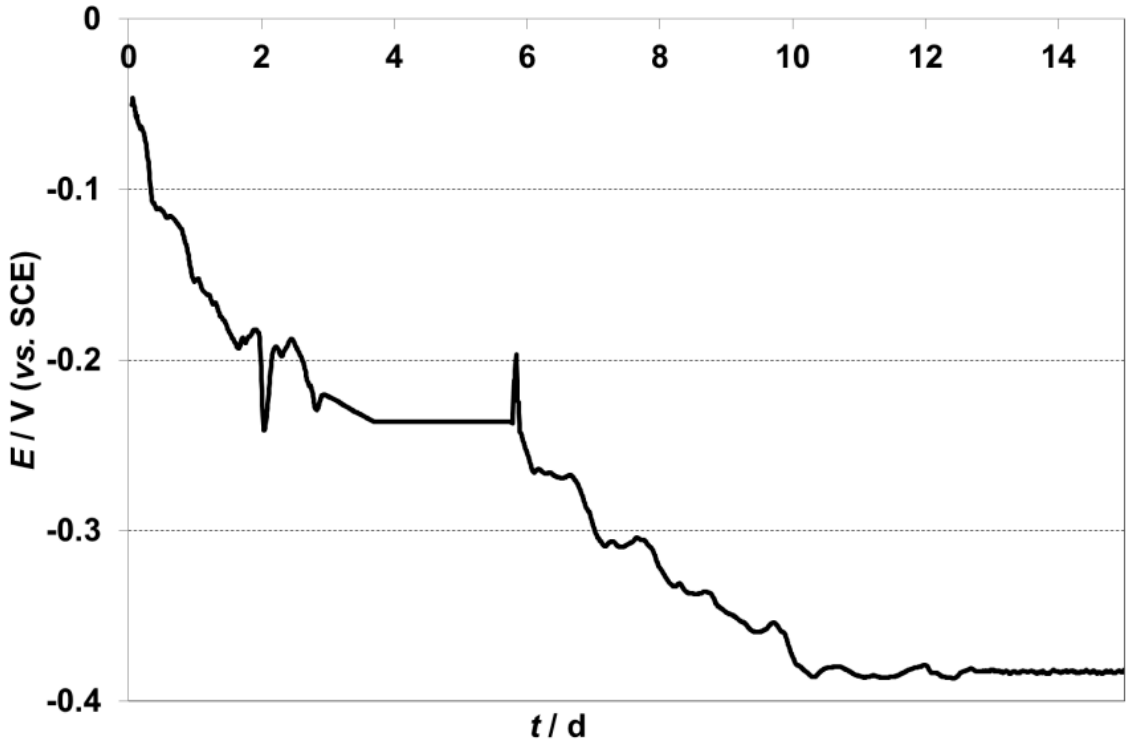

Figure 8.4 Free corrosion potential trend of the AISI304 strip immersed close to the anode in a SCMFC.

In the other MFCs, the carbon cloth anode was replaced with a new AISI304 stainless steel strip (the biocathode was unchanged). Due to the rectangular geometry of the strip, the upper part of the new anode operated near the surface of the solution and the lower part was in the deeper zone (Figure 8.1B). During tests an occasional contact with oxygen happened on the surface, due to the opening and handling of the SCMFC for electrochemical analyzes and sampling.

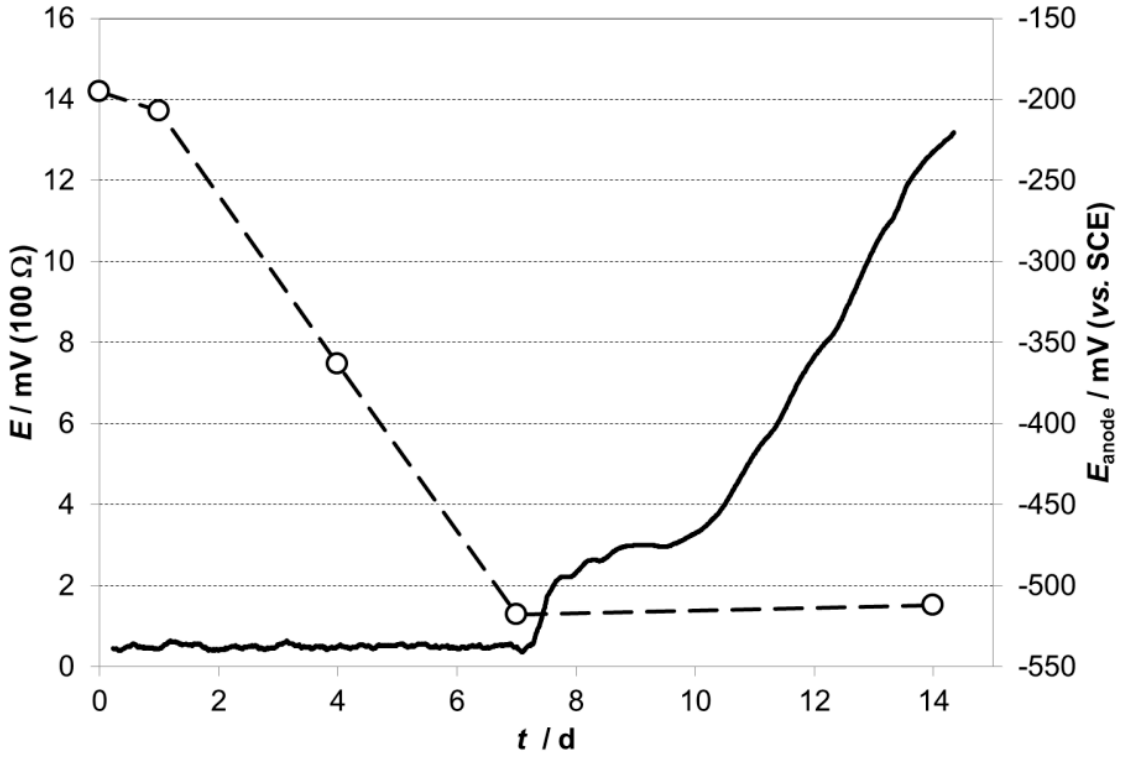

Figure 8.5 Trend of the potential (over 100 Ω R_{ext}) of the SCMFCs with AISI304 anode (solid line, the left axis) and the corresponding anodic ocp (dashed line, the right axis) during the 15 days of

The *ocp* trend decreased within a week of operation (Figure 8.5), indicating that the anaerobic condition was recovered in the chamber, and the SCMFCs started producing power. The *ocp* of the AISI304 anode reached −510 mV, becoming more negative than AISI304 left in wastewater solution and less negative than the carbon cloth anode, in two weeks. An increase of SCMFC productivity is observed during the second week, correlated to the decrease of the *ocp* of the AISI304 anode, up to a maximum at day 15.

The potential output was three times lower than the one exhibited by the SCMFC with carbon cloth anode, and it did not reach a plateau. It must be noted that, despite the metal and carbon cloth anodes have the same projected surface area, a considerably higher real surface is due to the weaving of carbon fibers. Hence, the current output might partially be attributed to difference in the real surface area.

Anodic polarization curves performed over time (0, 1, 4, 7, and 14 days) are shown in Figure 8.6. The current intensity increased monotonically over time when biofilms started growing on AISI304 surfaces. The current output was low on day 0 and day 1, indicating the effect of the passive layer controlling the stainless steel corrosion.

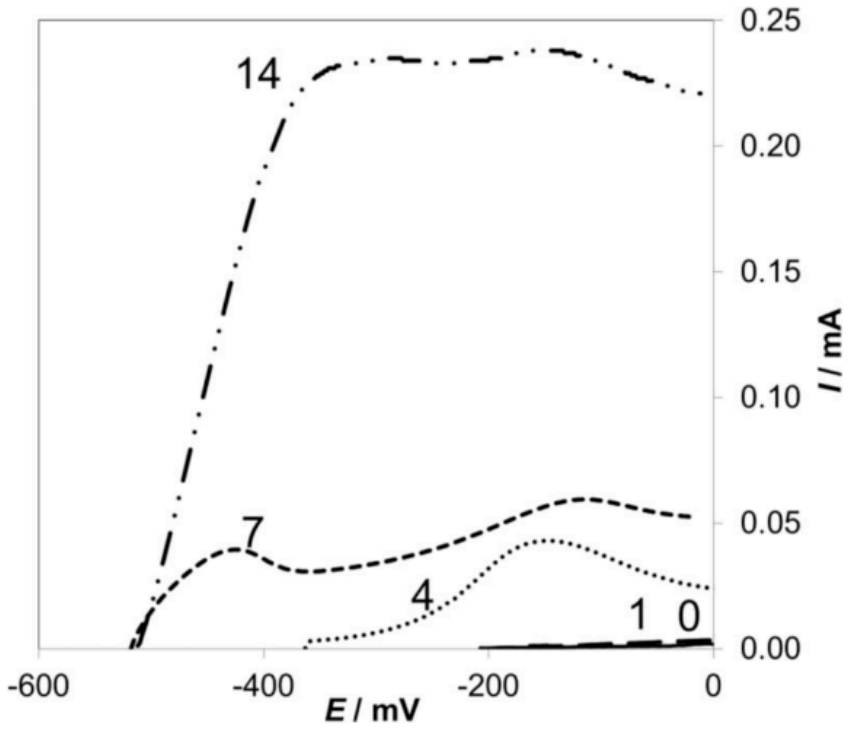

Figure 8.6 Evolution over time of the anodic polarization curves of the AISI304 anode kept as in Fig. 8.1B, in partially oxygenated conditions. (Numbers next to the curves refer to the day of the polarization measurement).

After day 2, the behavior of the passive layer disappeared, and two current peaks (one at −180 mV (typical of stainless steel corrosion) and the other at −380 mV) evolved and persisted in the plateau till the end of the experiment (15 days). The first peak appeared on day 4, a couple of days before SCMFCs started to produce power. The second peak appeared on day 7, when SCMFCs had measurable power output. Even though there was no evidence associated with power production in the first peak, it was still apparent that the peak was correlated to the anaerobic progression in the solution and/or to the modifications of the *ocp* of the metal.

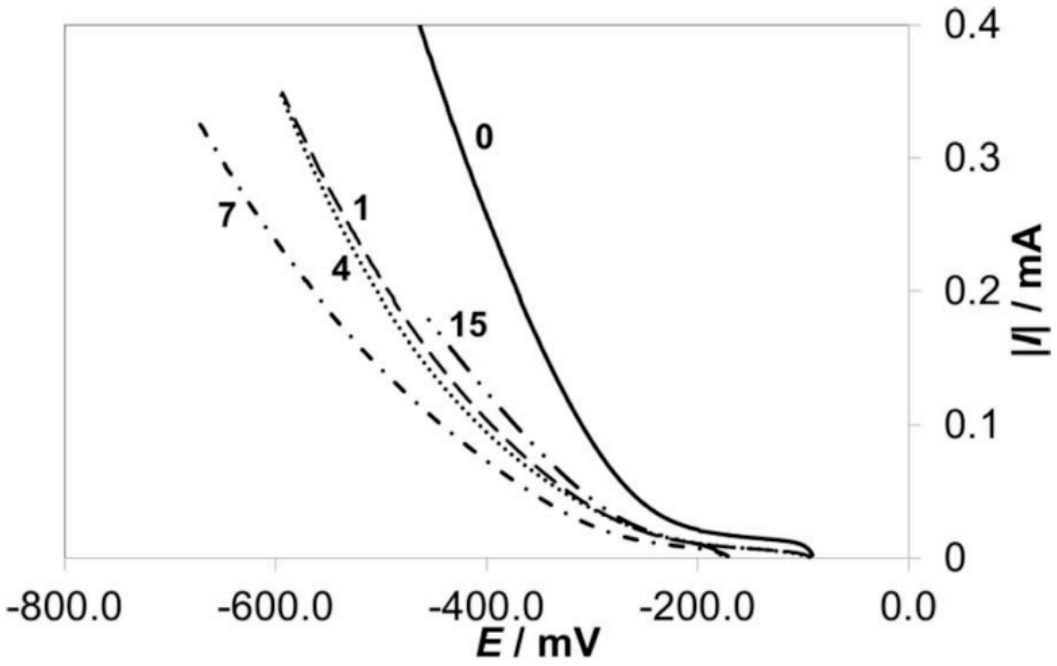

Figure 8.7 Evolution over time of the polarization curves of the carbon cloth cathode in the SCMFC with the AISI304 anode. Numbers next to the curves refer to the day of the polarization experiment.

Figure 8.7 illustrates the response of the biocathode, already operating from the previous experiment with graphite-based anode. The polarization curve on day zero, right after the anode exchange and wastewater refreshment, shows high currents. This points to effective capacity of the biocathode to maintain the catalysis of oxygen reduction also in the new environment.

Polarization curves for cathode (Figure 8.8, curve a) and anode (Figure 8.8, curve b) after 15 days showed an increase in current response. The AISI304 anodic curves showed the evolution of the anodic peak at a potential close to −380 mV. No typical stainless steel corrosion peak was visible at around −180 mV. The *ocp* of the anode on day 15 reached to −580 mV, close to the potential exhibited by the CC anode (Figure 8.2).

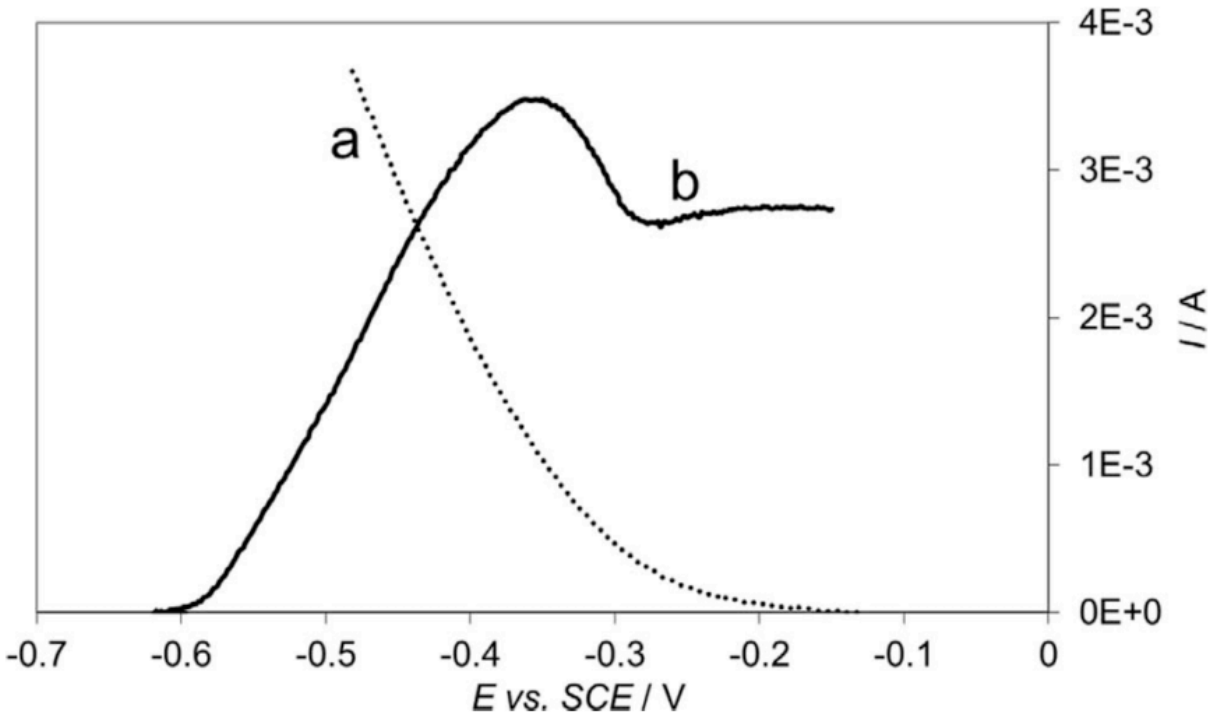

Figure 8.8 Cathode (a) and anode (b) polarization curves at day 15 of a SCMFC with anode AISI304 positioned as in Fig. 8.1C, in the presence of strictly anaerobic conditions.

8.3.3 Polarized AISI304

In another comparative experiment to confirm the passive layer chemical stability, a new AISI304 strip was exposed to fresh wastewater with acetate. The metal was kept at −600 mV (SCE) by means of a potentiostat for one day. After this period, a polarization curve was recorded, from −600 mV up to 0 mV, at 0.166 $mV \cdot s^{-1}$. The resulting graph was similar to the curves at day 0 and 1 in Figure 8.6. No peak was observed and the metal exhibited low currents. This test confirmed that the first peak (day 4) was not caused by the chemical dissolution of oxides on the metal, if exposed to wastewater at potentials of −600 mV. If the protecting oxide of the AISI304 would be modified by the low potential, then a peak (at −180 mV) would have formed on the polarization. The low currents demonstrate the presence of an effective oxide layer, protecting the metal.

8.3.4 AISI304 anodes under partially aerated and strictly anaerobic conditions

The CC anodes were replaced with the rectangular AISI304 anodes (the biocathodes were intact). In one case, the AISI304 anode was placed on the bottom of the MFC guaranteeing always strictly anaerobic condition (Step 3). Instead, another AISI304 anode (the upper part) was occasionally in contact with oxygen during the opening and handling of the SCMFCs for sampling and analyzes, while the lower part was always anaerobic (Step 3). The results showed that the AISI304 anode in the complete anaerobic environment had the power density comparable to the CC anodes (Figure 8.9, curve a).

Power production started after 3 days, and reached a stable plateau of 40 mV (0.4 mA). After the acetate depletion on day 8, the power production dropped rapidly zero. Once acetate (3 $g \cdot L^{-1}$) was added, the current production regained a potential of 50 mV (0.5 mA). In contrast, the AISI304 anode with the upper part occasionally exposed to air had much lower power density (Figure 8.9, curve b).

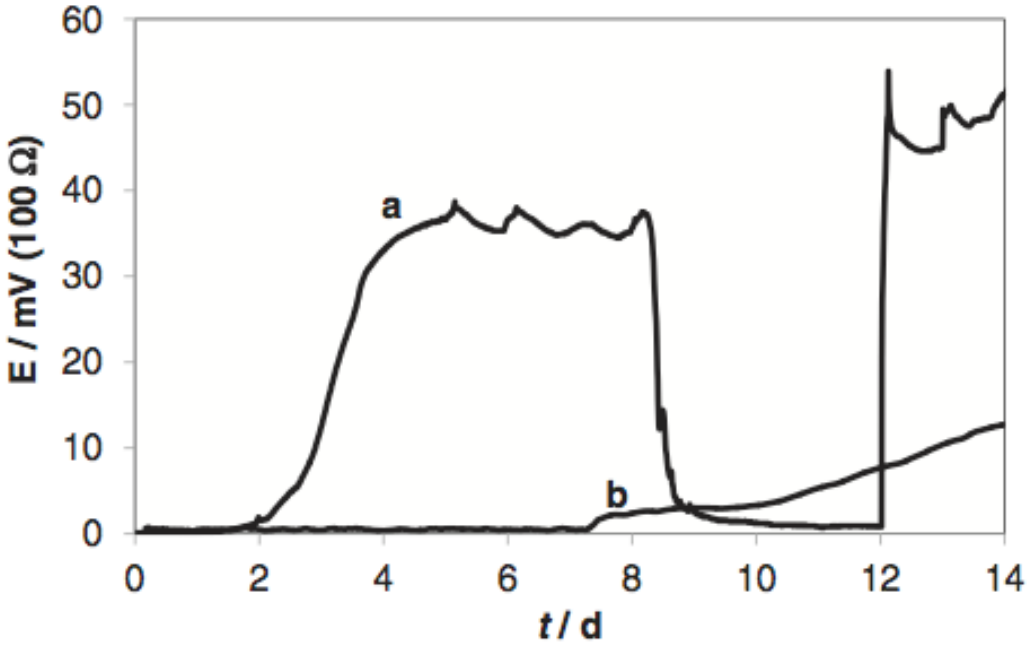

Figure 8.9 Trend of the potential at 100 Ω exhibited by the MFC with an AISI304 anode completely immerged in anaerobic conditions (a) and partially immerged in the anodic solution (b).

8.3.5 SEM observations of AISI304 anode surfaces after 15-day operation

After the 15 days of operation, the AISI304 anodes exposed to aerobic/anaerobic environment in the anode solution were extracted from SCMFCs for SEM observation. Images A, C, and E (Figure 8.10) were for the lower part of the anode that was in strictly anaerobic status, while the images B, D, and F were for the upper part of the anode that was occasionally exposed to air during refilling and sampling. The SEM images showed that there was no change on the lower part surface, and the oxide layer homogeneously covered the metal surface without damage. In contrast, spots on the upper part surface were observed (Figure 8.10B), and two morphologies of corrosion pits were revealed at higher magnifications (Figure 8.10D), with one being large and shallow and the other being scale-like deposits over the pits. These deposits were probably morphologically attributable to iron sulfide precipitates (using EDX analysis, data not shown). Analogous pits had been found on AISI316 surface with the presence of SRB [190].

The SCMFCs with the AISI304 anode in strictly anaerobic environment had a long operational period (up to two months), and the SEM micrographs showed there was no pitting on the surface after two months of continuous current production (Figure 8.11). Moreover, grooves due to the stainless steel sheet fabrication were still present on the used anode surface, indicating the good anti-corrosion of the AISI304 anode under strictly anaerobic condition.

8.4 Discussion

The results clearly demonstrated that under the strictly anaerobic condition, the AISI304 anode achieved similar power generation as the CC anode, and the corrosion of the stainless steel became negligible. Three relevant concerns were

i) the mechanism of anode activation in anaerobic environment,
ii) the possible correlation between bioanode and biocathode performance,
iii) the AISI304 corrosion mechanisms.

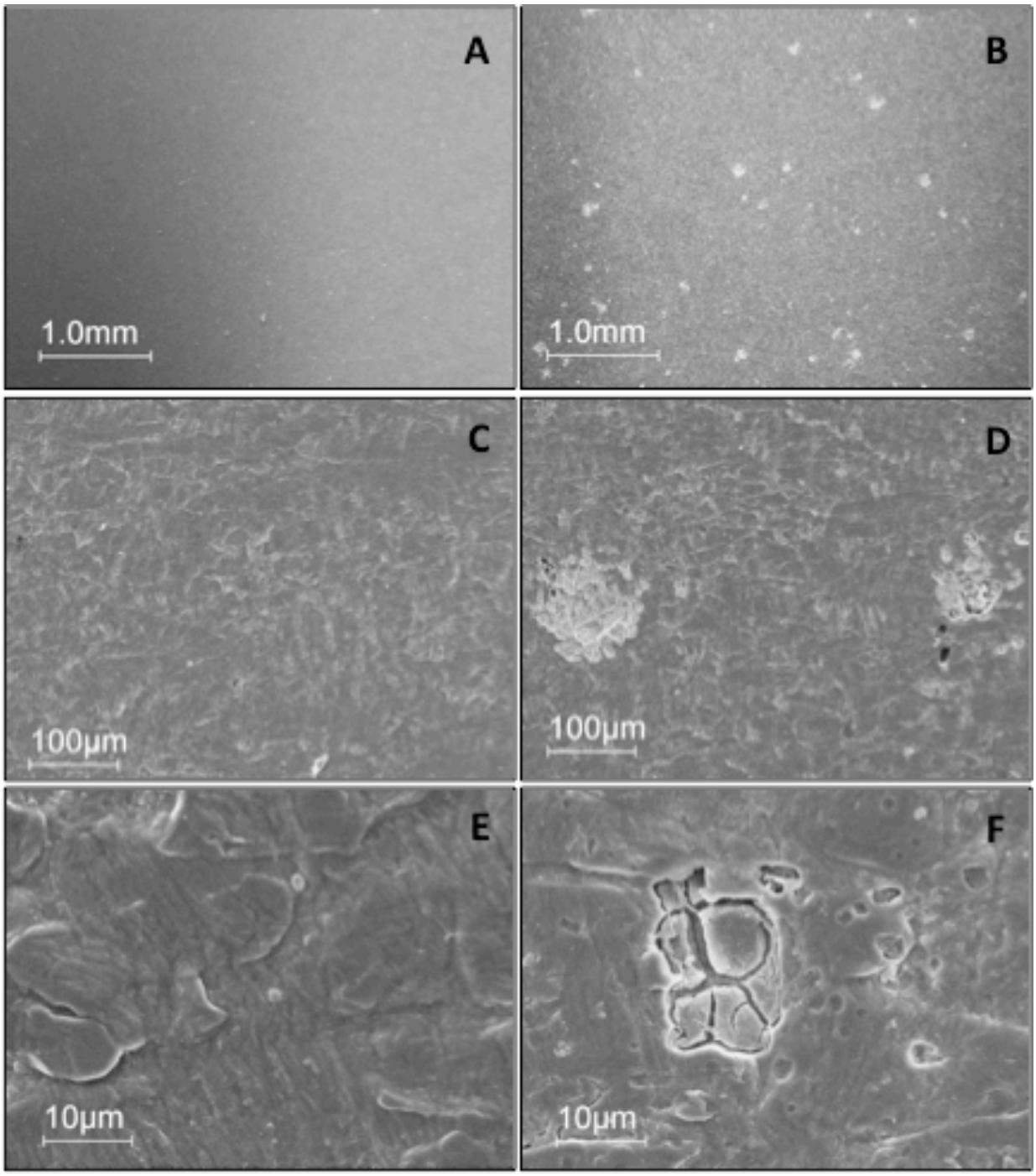

Figure 8.10 SEM images at three magnifications of the AISI304 used as anode for 15 days. Left images (A,C,E) refer to the lower part of the plate, exposed to anoxic conditions. Right images (B,D,F) refer to the upper part of the plate, exposed to residual oxygen concentrations.

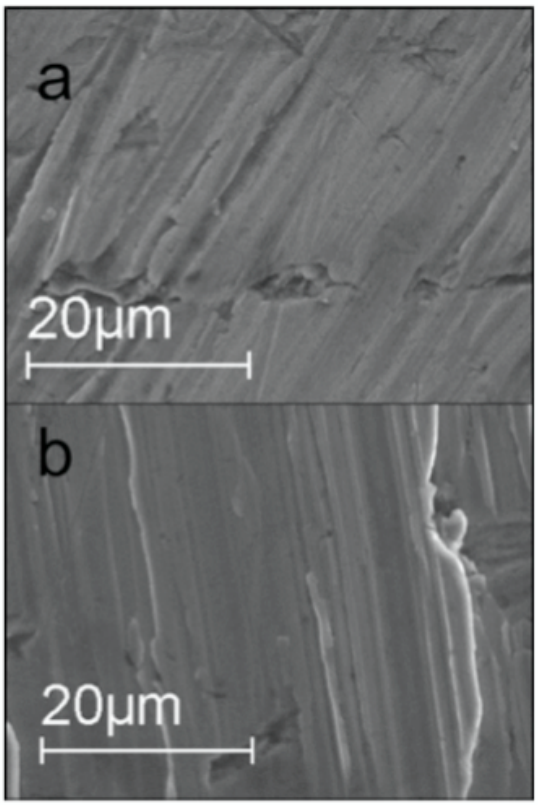

Figure 8.11 SEM images of AISI304 before the immersion (a) and after 2 months immersion (b) in completely anaerobic conditions.

8.4.1 Anode activation in SCMFC

After inoculation, a SCMFC normally needs several days to acclimate, during which the anodic potential decreased to a negative value associated with the anaerobic conditions. The *ocp* of AISI304 anode and CC anode reached −580 mV (SCE), approaching the thermodynamic redox potential of the acetate/CO_2 couple (about −600 mV at pH 8). Anodic polarization on day 0 showed low current production (Figure 8.3 and 8.6), that is condition of kinetically inhibited electron transfer. The SCMFC was under anodic control, since an increase in the cathodic polarization would not give a higher current generation, whereas an increase in the anodic polarization curve would cause an increase of current density in SCMFC. The anodic polarization on day 15 showed a current peak close to the anodic *ocp* on both CC (Figure 8.3) and AISI304 anodes (Figure 8.6). Such peaks, corresponding to active redox couples, were already detected in microbial fuel cells and in microbial electrolyzers by cyclic voltammetry [191–194]. The shape of the polarizations curves reported, despite the low scan rate (0.166 $mV \cdot s^{-1}$), resembles closely the forward scan of the cyclic voltammetry at 1 $mV \cdot s^{-1}$ [194] or more [192,193].

A general mechanism modeled recently by Strycharz et al. [194] splits the acetate oxidation pathway on a bioanode into five steps with no assumption about the bacterial consortium, or the type of mediators involved in electron transfer. The results in this study implied the presence of mediators in the anodic biofilms. The peaks in the polarization curve on day 15 (Figure 8.3) pointed unequivocally to a rate-determining step due to the transfer of electrons from the bacteria to the electroactive mediators, since no similar peak of current was observed in the calculated cyclic voltammetries of the other steps. The second peak on the AISI304 anode polarization (Figure 8.6) had the same maximum peak potential as on the CC anode (Figure 8.3). Therefore, it is reasonable to hypothesize that this is the same rate-determining step between the same mediators.

8.4.2 Bioanode biocathode mutual influence

The evolution of anodic and cathodic curves (Figure 8.3) determined the amount of electrons exchanged via the external circuit and suggests a strong influence between anodic and cathodic biofilm metabolisms. Previous observations had found that the development of biocathodes was closely associated with the functionality of bioanodes [56]. The behavior of the biocathodes (Figure 8.7) supports this statement. On the other hand, the interconnection between anode and cathode is a further proof of biologically activated cathodic reduction.

After day 0, the electrochemical response of the well-developed biocathode started to decrease, lowering its activity from day 1, to 4, and finally 7. Current exchange capability decreased steadily over time. At day 7, the new AISI304 anode started to collect electrons and the SCMFC generated power. At day 14, the biocathode reversed its trend and showed to develop again, but it did not reach the currents of day 0, since the current generation of the SCMFC was three times lower than in the previous cycle. This behavior was a further qualitative evidence of a possible cooperation between anodic and cathodic biofilms. Hypotheses on cooperation are often invoked to explain the increase in power production frequently observed in MFCs inoculated with a consortium of bacteria [182,186,189], although in the same biofilm and not in different biofilms. The first peak of current in the polarization curves of the AISI304 anode (Figure 8.6) might be correlated to the mutual influence of anode and cathode. The potential of this first peak is at the *ocp* of the unproductive anode. The interaction of bacterial mediators with the oxidized metal at the initial *ocp* would have started the electron exchange and biofilm growth, which was in agreement with previous results [181].

It was also noticed that the anodic curve intersected the cathodic curve near its peak at −380 mV (SCE) (Figure 8.3). The low *ocp* of the cathode suggests that the electrochemical reaction carried

out at the cathode is not the direct oxygen reduction reaction, most likely is a reduction of SO_4 to S^{-2} by sulfate-reducing bacteria, as studied in detail previously [51,188]. Bacteria grew on biocathodes to obtain more electrons from the electrode (free of chemical catalyst), and anodophilic bacteria, similarly, developed a specific anodic redox couple to exploit this electronic request. In reverse, bioanode developed a peak to increase the electron exchange with the electrode at the required potential, stimulated the cathodic electron exchange of the biocathode, and enhanced the growth of electrogenic bacteria. At the same time, if either anode or cathode stopped electron transfer (as in the case of replacing CC anode with stainless steel anode), the other electrode would suffer a lower electroactivity. Bio-electrode development resumed only after the restoration of the electron flux in the external circuit.

8.4.3 AISI 304 corrosion mechanisms

For the rectangular AISI304 anode vertically installed in SCMFCs, the upper part directly in contact with residual oxygen (if any) in the head space of the anode chamber, which established a mixed potential in the metal, and achieved a less negative *ocp* value (−380 mV). In fact, under mixed-potential conditions, a zone of the metallic surface (the oxygenated part) became more cathodic than the strictly anaerobic status, and thus a localized corrosion might occur. This is the case in which pitting corrosion became evident (Figure 8.10B), and nucleation of cathodic centers started to sustain the formation of pits. More pits showed up from bottom to top of the AISI304 anode, where oxygen was not completely consumed by bacteria. Observation inside the pits of iron sulfide and the presence of SRB (documented previously on both the electrodes) [51,118,188] might establish a correlation between localized corrosion and bacteria metabolism in the well-known phenomenon of biocorrosion [195–197]. The pitting corrosion might be carried out by bacteria, since the cathodic polarization at −600 mV (Par. 3.2.1) excluded the possibility of a purely electrochemical corrosion.
In contrast, the strict and homogeneous anaerobic conditions (the bottom of the solution in SCMFC) inhibited corrosion on the AISI304 anodes. The negative potential prevented metal oxidation, allowing current production that became comparable to CC anodes over time (Figure 8.3). Furthermore, the SEM images demonstrated the effectiveness of using a AISI304 as a cheaper anode material. Its corrosion resistance was well preserved under strict anaerobic conditions and the passive layer was stable at the normal anodic potentials (less than −500 mV vs. SCE).

9.

CONCLUSIONS AND OUTLOOK

Microbial fuel cells are a fascinating biotechnology that still presents several issues for their widespread application. The objectives of this dissertation have been focused to investigate four urgent topics:

- oxygen consumption in Single Chamber Microbial Fuel Cells;
- PTFE influence on the oxygen reduction reaction in open-air biocathode;
- H_2O_2 inhibition in enzyme electrodes for improved biocathodes;
- application of stainless steel anodes instead of carbon cloth-based anodes.

The results obtained along the three years research activity allowed clarifying the open issues in these four topics and the most important achievements are highlighted below.

9.1 Oxygen consumption in Single Chamber Microbial Fuel Cells

The designed hand-made bilirubin oxidase enzymatic microsensor was successfully built, calibrated and applied in SCMFCs. The microsensor was not poisoned by wastewater and the encapsulation step with TMOS provided a diffusional barrier improving reproducibility and stability of the sensor. The microsensor allowed for the understanding of the bioelectrochemical mechanism of oxygen consumption and the key role of cathodic biofilm that develops on the open-air cathode electrode to maintain the anaerobic condition in the anode chamber. The biofilm acts as “natural barrier” for the oxygen diffusion to the anode. The oxygen profiles allowed correlating the oxygen concentration inside the SCMFC with the start-up and the evolution of the power production of the cell. Moreover, based on the obtained oxygen profiles, it can be proposed that the cathode biofilm has a thickness around 3 mm.

9.2 Biocathode Development

The effect of PTFE content in the cathodes of operating MFCs on ORR was evaluated by electrocatalysis parameters. The results show that SCMFCs with the lower PTFE percentages in the GDL had a prompt startup and high current outputs. Electro-activation of the cathodes was shown by a change of the Tafel slope from 120 mV/decade of current (corresponding to no electrocatalysis), down to a lower limit of around 80 mV/decade of current (electrocatalytic behavior). Activation is reversible, related to the biological consumption of acetate in the MFCs. The ORR is not related to the surface area, neither affected by diffusion-limitations, nor by ohmic drops. It seems mostly related to biologically-assisted electron transfer activation, inhibited by the PTFE presence in the triple-contact zone.

9.3 Laccase-based Biocathodes

Trametes trogii laccase-based biocathodes were developed, allowing for catalyzing oxygen reduction reaction at high potential (0.4 V and 0.6V vs. Ag|AgCl 3M for the MET and DET electrode respectively). The critical role of H_2O_2 on the electrocatalytic performances was demonstrated. The study of H_2O_2 inhibition showed two different mechanisms depending on the wiring technique utilized for the sensor development. The inhibitor binds with no preference to the free enzyme or to the enzyme-substrate complex, obtaining a non-competitive reversible inhibition for the MET biocathode. The inhibitor binds preferentially to the enzyme-substrate complex in the case of the DET biocathode, obtaining an uncompetitive inhibition, especially at high H_2O_2 concentration. It is important to remark that unlike competitive inhibition, where at high substrate concentrations (oxygen) the effect of the inhibitor is minimized or completely eliminated, for non-competitive and uncompetitive inhibition mechanisms the effect of the inhibitor is present at all substrate concentrations, thus strongly affecting the performances of the biocathode operating in a hybrid-microbial fuel cell.

9.4 Bioanode Development

AISI304 stainless steel in SCMFCs was extensively examined under aerobic/anaerobic conditions. As first estimation, stainless steel anode material is a couple of orders of magnitude cheaper than carbon cloth (CC). AISI304 anodes and CC anodes had similarities in terms of power generation, current peaks (at −380 mV) and acetate oxidation. AISI304 anodes suffered from pitting corrosion with the presence of residual oxygen in the anode chamber. Microbial corrosion did not occur under strictly anaerobic conditions. CC anodes had higher power generation than AISI304 anodes at the beginning stage of SCMFC operation, and AISI304 anodes approached the CC anodes over time.
Due to the mechanical stability, low cost, and anti-corrosion capability of AISI304, anodes with the combined stainless steel and CC should be developed to enhance power generation, prolong the MFC operational duration, and reduce the costs.

9.5 Outlook

The results presented in this dissertation, together with future improvements, will allow the development and scale-up of optimized Single Chamber Microbial Fuel Cells. The performances of SCMFC could be greatly improved if a proper design of the cell is provided and the device is operated under specific conditions. Stacks of miniaturized microbial fuel cells are gaining interest due to the possibility to improve power output utilizing small-volume devices. However, the oxygen diffusion and the dimension of the cathodic biofilm studied in chapter 5 will have to be taken into consideration when designing the device. If the distance between anode and cathode electrodes is lower than the 3 mm measured for the cathode biofilm, short circuit will be obtained, with no power production. The amount of PTFE in the GDL of the air-breathing cathodes must be properly controlled to avoid leakage of the solution and, at the same time, to do not decrease the ORR performances. The applicability of enzymatic-cathodes will have to consider the H_2O_2 role and the larger inhibition obtained at high oxygen pressures. Application of hybrid-MFC in conditions of medium/low oxygen content could allow limiting the H_2O_2 inhibition effects. AISI 304 could substitute carbon cloth as support for the bioanode, with good cost-effectiveness. More research is needed to further optimize the anode support and inexpensive carbon-based conductive paints may be used on AISI304 to increase the conductivity and the biofilm adhesion on the electrode.

BIBLIOGRAPHY

[1] M.C. Potter, Electrical effects accompanying the decomposition of organic compounds, Proc. R. Soc. London. (1911) 260–276.

[2] S. Kadoshin, T. Nishiyama, T. Ito, The trend in current and near future energy consumption from a statistical perspective, Appl. Energy. 67 (2000) 407–417. doi:10.1016/S0306-2619(00)00033-7.

[3] S.M. Sarathy, P. Oßwald, N. Hansen, K. Kohse-Höinghaus, Alcohol combustion chemistry, Prog. Energy Combust. Sci. 44 (2014) 40–102. doi:10.1016/j.pecs.2014.04.003.

[4] U S Environmental Protection Agency, Municipal Solid Waste Generation, Recycling, and Disposal in the United States: Facts and Figures for 2010, (2010) 1–12. http://www.epa.gov/osw/nonhaz/municipal/pubs/msw_2010_rev_factsheet.pdf.

[5] K. Miksch, G. Cema, P.F.X. Corvini, E. Felis, A. Sochacki, J. Surmacz-Górska, et al., R&D priorities in the field of sustainable remediation and purification of agro-industrial and municipal wastewater, N. Biotechnol. 32 (2015) 128–132. doi:10.1016/j.nbt.2013.11.002.

[6] M. Alcalde, M. Ferrer, F.J. Plou, A. Ballesteros, Environmental biocatalysis: from remediation with enzymes to novel green processes, Trends Biotechnol. 24 (2006) 281–287. doi:10.1016/j.tibtech.2006.04.002.

[7] D. Paul, G. Pandey, J. Pandey, R.K. Jain, Accessing microbial diversity for bioremediation and environmental restoration, Trends Biotechnol. 23 (2005) 135–142. doi:10.1016/j.tibtech.2005.01.001.

[8] R.M. Dell, D.A.J. Rand, Energy storage - A key technology for global energy sustainability, J. Power Sources. 100 (2001) 2–17. doi:10.1016/S0378-7753(01)00894-1.

[9] D.R. Lovley, Bug juice: harvesting electricity with microorganisms., Nat. Rev. Microbiol. 4 (2006) 497–508. doi:10.1038/nrmicro1442.

[10] W. Gellett, M. Kesmez, J. Schumacher, N. Akers, S.D. Minteer, Biofuel cells for portable power, Electroanalysis. 22 (2010) 727–731. doi:10.1002/elan.200980013.

[11] R.M. Allen, H.P. Bennetto, Microbial fuel cells: Electricity production from carbohydrates, Appl. Biochem. Biotechnol. 39 (1993) 27–40. doi:10.1007/BF02918975.

[12] S. Venkata Mohan, G. Velvizhi, J.A. Modestra, S. Srikanth, Microbial fuel cell : Critical factors regulating bio-catalyzed electrochemical process and recent advancements, Renew. Sustain. Energy Rev. 40 (2014) 779–797. doi:10.1016/j.rser.2014.07.109.

[13] B. Capdeville, K.M. Nguyen, J.L. Rols, Biofilm Modelling: Structural, Reactional and diffusional aspects, in: L.F. Melo, T.R. Bott, M. Fletcher, B. Capdeville (Eds.), Biofilms – Sci. Technol., Kluwer Academic Publishers, Amsterdam, 1992: pp. 251–276. doi:10.1007/s13398-014-0173-7.2.

[14] D. Pant, G. Van Bogaert, L. Diels, K. Vanbroekhoven, A review of the substrates used in microbial fuel cells (MFCs) for sustainable energy production, Bioresour. Technol. 101 (2010) 1533–1543. doi:10.1016/j.biortech.2009.10.017.

[15] S.K. Chaudhuri, D.R. Lovley, Electricity generation by direct oxidation of glucose in mediatorless microbial fuel cells, Nat. Biotechnol. 21 (2003) 1229–1232. doi:10.1038/nbt867.

[16] K.-J. Chae, M.-J. Choi, J.-W. Lee, K.-Y. Kim, I.S. Kim, Effect of different substrates on the performance, bacterial diversity, and bacterial viability in microbial fuel cells, Bioresour. Technol. 100 (2009) 3518–3525. doi:10.1016/j.biortech.2009.02.065.

[17] S. Venkata Mohan, G. Mohanakrishna, B.P. Reddy, R. Saravanan, P.N. Sarma, Bioelectricity generation from chemical wastewater treatment in mediatorless (anode) microbial fuel cell (MFC) using selectively enriched hydrogen producing mixed culture under acidophilic microenvironment, Biochem. Eng. J. 39 (2008) 121–130. doi:10.1016/j.bej.2007.08.023.

[18] P. Clauwaert, D. Van Der Ha, N. Boon, K. Verbeken, M. Verhaege, K. Rabaey, et al., Open Air Biocathode Enables Effective Electricity Generation with Microbial Fuel Cells, Environ. Sci. Technol. 41 (2007) 7564–7569.

[19] A.K. Manohar, F. Mansfeld, The internal resistance of a microbial fuel cell and its dependence on cell design and operating conditions, Electrochim. Acta. 54 (2009) 1664–1670. doi:10.1016/j.electacta.2008.06.047.

[20] Y. Feng, X. Wang, B.E. Logan, H. Lee, Brewery wastewater treatment using air-cathode microbial fuel cells, Appl. Microbiol. Biotechnol. 78 (2008) 873–880. doi:10.1007/s00253-008-1360-2.

[21] A. Gálvez, J. Greenman, I. Ieropoulos, Landfill leachate treatment with microbial fuel cells; scale-up through plurality, Bioresour. Technol. 100 (2009) 5085–5091. doi:10.1016/j.biortech.2009.05.061.

[22] A. Bard, L. Faulkner, Electrochemical Methods: Fundamentals and applications, Second Edi, John Wiley & Sons, Inc., New York, 2001.

[23] B. Erable, D. Féron, A. Bergel, Microbial catalysis of the oxygen reduction reaction for microbial fuel cells: A review, ChemSusChem. 5 (2012) 975–987. doi:10.1002/cssc.201100836.

[24] U. Schröder, Anodic electron transfer mechanisms in microbial fuel cells and their energy efficiency., Phys. Chem. Chem. Phys. 9 (2007) 2619–2629. doi:10.1039/b703627m.

[25] L. Gorton, A. Lindgren, T. Larsson, F.D. Munteanu, T. Ruzgas, I. Gazaryan, Direct electron transfer between heme-containing enzymes and electrodes as basis for third generation biosensors, Anal. Chim. Acta. 400 (1999) 91–108. doi:10.1016/S0003-2670(99)00610-8.

[26] N.S. Malvankar, D.R. Lovley, Microbial nanowires for bioenergy applications, Curr. Opin. Biotechnol. 27 (2014) 88–95. doi:10.1016/j.copbio.2013.12.003.

[27] D.R. Lovley, N.S. Malvankar, Seeing is believing: novel imaging techniques help clarify microbial nanowire structure and function, Environ. Microbiol. 17 (2015) 2209–2215. doi:10.1111/1462-2920.12708.

[28] M.E. Hernandez, D.K. Newman, Extracellular electron transfer, Cell. Mol. Life Sci. 58 (2001) 1562–1571.

[29] G.M. Delaney, H.P. Bennetto, J.R. Mason, S.D. Roller, J.L. Stirling, C.F. Thurston, Electron-transfer Coupling in Microbial Fuel Cells. 2. Performance of Fuel Cells Containing Selected Microorganism-Mediator-Substrate Combinations, J. Chem. Technol. Biotechnol. 34B (1984) 13–27.

[30] D.K. Newman, R. Kolter, A role for excreted quinones in extracellular electron transfer., Nature. 405 (2000) 94–97. doi:10.1038/35011098.

[31] K.B. Gregory, D.R. Bond, D.R. Lovley, Graphite electrodes as electron donors for anaerobic respiration, Environ. Microbiol. 6 (2004) 596–604. doi:10.1111/j.1462-2920.2004.00593.x.

[32] J.C. Thrash, J.D. Coates, Review: Direct and Indirect Electrical Stimulation of Microbial Metabolism, Environ. Sci. Technol. 42 (2008) 3921–3931.

[33] D.R. Lovley, Powering microbes with electricity : direct electron transfer from electrodes to microbes, Environ. Microbiol. Rep. 3 (2011) 27–35. doi:10.1111/j.1758-2229.2010.00211.x.

[34] C.R. Myers, K.H. Nealson, Bacterial manganese reduction and growth with manganese oxide as the sole electron acceptor, Science (80-.). 240 (1988) 1319–1321.

doi:10.1126/science.240.4857.1319.

[35] O. Bretschger, A. Obraztsova, C. a. Sturm, S.C. In, Y. a. Gorby, S.B. Reed, et al., Current production and metal oxide reduction by Shewanella oneidensis MR-1 wild type and mutants, Appl. Environ. Microbiol. 73 (2007) 7003–7012. doi:10.1128/AEM.01087-07.

[36] J.K. Fredrickson, M.F. Romine, A.S. Beliaev, J.M. Auchtung, M.E. Driscoll, T.S. Gardner, et al., Towards environmental systems biology of Shewanella., Nat. Rev. Microbiol. 6 (2008) 592–603. doi:10.1038/nrmicro1947.

[37] D.A. Finkelstein, L.M. Tender, J.G. Zeikust, Effect of electrode potential on electrode reducing microbiota, Environ.Sci.Technol. 40 (2006) 6990–6995.

[38] N.S. Malvankar, J. Lau, K.P. Nevin, A.E. Franks, M.T. Tuominen, D.R. Lovley, Electrical Conductivity in a Mixed-Species Biofilm, Appl. Environ. Microbiol. 78 (2012) 5967–5971. doi:10.1128/AEM.01803-12.

[39] E. Antolini, Structural parameters of supported fuel cell catalysts: The effect of particle size, inter-particle distance and metal loading on catalytic activity and fuel cell performance, Appl. Catal. B Environ. 181 (2016) 298–313. doi:10.1016/j.apcatb.2015.08.007.

[40] B.E. Logan, B. Hamelers, R. Rozendal, U. Schröder, J. Keller, S. Freguia, et al., Microbial fuel cells: Methodology and technology, Environ. Sci. Technol. 40 (2006) 5181–5192. doi:10.1021/es0605016.

[41] G. Antonopoulou, K. Stamatelatou, S. Bebelis, G. Lyberatos, Electricity generation from synthetic substrates and cheese whey using a two chamber microbial fuel cell, Biochem. Eng. J. 50 (2010) 10–15. doi:10.1016/j.bej.2010.02.008.

[42] B. Erable, L. Etcheverry, A. Bergel, Increased power from a two-chamber microbial fuel cell with a low-pH air-cathode compartment, Electrochem. Commun. 11 (2009) 619–622. doi:10.1016/j.elecom.2008.12.058.

[43] S. Venkata Mohan, R. Saravanan, S.V. Raghavulu, G. Mohanakrishna, P.N. Sarma, Bioelectricity production from wastewater treatment in dual chambered microbial fuel cell (MFC) using selectively enriched mixed microflora: Effect of catholyte, Bioresour. Technol. 99 (2008) 596–603. doi:10.1016/j.biortech.2006.12.026.

[44] B. Min, S. Cheng, B.E. Logan, Electricity generation using membrane and salt bridge microbial fuel cells, Water Res. 39 (2005) 1675–1686. doi:10.1016/j.watres.2005.02.002.

[45] A. Bergel, D. Féron, A. Mollica, Catalysis of oxygen reduction in PEM fuel cell by seawater

biofilm, Electrochem. Commun. 7 (2005) 900–904. doi:10.1016/j.elecom.2005.06.006.

[46] K. Chung, I. Fujiki, S. Okabe, Effect of formation of biofilms and chemical scale on the cathode electrode on the performance of a continuous two-chamber microbial fuel cell, Bioresour. Technol. 102 (2011) 355–360. doi:10.1016/j.biortech.2010.04.091.

[47] A.W. Jeremiasse, H.V.M. Hamelers, C.J.N. Buisman, Microbial electrolysis cell with a microbial biocathode, Bioelectrochemistry. 78 (2010) 39–43. doi:10.1016/j.bioelechem.2009.05.005.

[48] E. Guerrini, M. Grattieri, S.P. Trasatti, M. Bestetti, P. Cristiani, Performance explorations of single chamber microbial fuel cells by using various microelectrodes applied to biocathodes, Int. J. Hydrogen Energy. 39 (2014) 21837–21846. doi:10.1016/j.ijhydene.2014.06.132.

[49] H. Liu, B.E. Logan, Electricity generation using an air-cathode single chamber microbial fuel cell in the presence and absence of a proton exchange membrane., Environ. Sci. Technol. 38 (2004) 4040–4046. doi:Doi 10.1021/Es0499344.

[50] C. Santoro, Y. Lei, B. Li, P. Cristiani, Power generation from wastewater using single chamber microbial fuel cells (MFCs) with platinum-free cathodes and pre-colonized anodes, Biochem. Eng. J. 62 (2012) 8–16. doi:10.1016/j.bej.2011.12.006.

[51] P. Cristiani, M.L. Carvalho, E. Guerrini, M. Daghio, C. Santoro, B. Li, Cathodic and anodic biofilms in Single Chamber Microbial Fuel Cells, Bioelectrochemistry. 92 (2013) 6–13. doi:10.1016/j.bioelechem.2013.01.005.

[52] S. Cheng, H. Liu, B.E. Logan, Power densities using different cathode catalysts (Pt and CoTMPP) and polymer binders (Nafion and PTFE) in single chamber microbial fuel cells, Environ. Sci. Technol. 40 (2006) 364–369. doi:10.1021/es0512071.

[53] H. Dong, H. Yu, X. Wang, Q. Zhou, J. Feng, A novel structure of scalable air-cathode without Nafion and Pt by rolling activated carbon and PTFE as catalyst layer in microbial fuel cells., Water Res. 46 (2012) 5777–87. doi:10.1016/j.watres.2012.08.005.

[54] Y. Luo, F. Zhang, B. Wei, G. Liu, R. Zhang, B.E. Logan, Power generation using carbon mesh cathodes with different diffusion layers in microbial fuel cells, J. Power Sources. 196 (2011) 9317–9321. doi:10.1016/j.jpowsour.2011.07.077.

[55] S. Cheng, H. Liu, B.E. Logan, Increased performance of single-chamber microbial fuel cells using an improved cathode structure, Electrochem. Commun. 8 (2006) 489–494. doi:10.1016/j.elecom.2006.01.010.

[56] E. Guerrini, P. Cristiani, S.P. Trasatti, Relation of anodic and cathodic performance to pH

variations in membraneless microbial fuel cells, Int. J. Hydrogen Energy. 38 (2013) 345–353. doi:10.1016/j.ijhydene.2012.10.001.

[57] M. Zhou, M. Chi, H. Wang, T. Jin, Anode modification by electrochemical oxidation: A new practical method to improve the performance of microbial fuel cells, Biochem. Eng. J. 60 (2012) 151–155. doi:10.1016/j.bej.2011.10.014.

[58] J. Luo, M. Chi, H. Wang, H. He, M. Zhou, Electrochemical surface modification of carbon mesh anode to improve the performance of air-cathode microbial fuel cells., Bioprocess Biosyst. Eng. 36 (2013) 1889–96. doi:10.1007/s00449-013-0963-x.

[59] G.G. Kumar, V.G.S. Sarathi, K.S. Nahm, Recent advances and challenges in the anode architecture and their modifications for the applications of microbial fuel cells, Biosens. Bioelectron. 43 (2013) 461–475. doi:10.1016/j.bios.2012.12.048.

[60] C. Santoro, I. Ieropoulos, J. Greenman, P. Cristiani, T. Vadas, A. Mackay, et al., Current generation in membraneless single chamber microbial fuel cells (MFCs) treating urine, J. Power Sources. 238 (2013) 190–196. doi:10.1016/j.jpowsour.2013.03.095.

[61] T. Chen, S.C. Barton, G. Binyamin, Z. Gao, Y. Zhang, H.H. Kim, et al., A miniature biofuel cell., J. Am. Chem. Soc. 123 (2001) 8630–8631. doi:10.1021/ja0163164.

[62] M.R. Tarasevich, V.A. Bogdanovskaya, L.N. Kuznetsova, Bioelectrocatalytic Reduction of Oxygen in the Presence of Laccase Adsorbed on Carbon Electrodes, Russ. J. Electrochem. 37 (2001) 833–837. http://www.springerlink.com/index/H064402K8P350774.pdf.

[63] N. Mano, V. Soukharev, A. Heller, A laccase-wiring redox hydrogel for efficient catalysis of O 2 electroreduction, J. Phys. Chem. B. 110 (2006) 11180–11187. doi:10.1021/jp055654e.

[64] E.I. Solomon, D.E. Heppner, E.M. Johnston, J.W. Ginsbach, J. Cirera, M. Qayyum, et al., Copper active sites in biology, Chem. Rev. 114 (2014) 3659–3853. doi:10.1021/cr400327t.

[65] T. Sakurai, K. Kataoka, Basic and applied features of multicopper oxidases, cueo, bilirubin oxidase, and laccase, Chem. Rec. 7 (2007) 220–229. doi:10.1002/tcr.20125.

[66] M. Alcalde, Laccases: Biological functions, molecular structure and industrial applications, in: J. Polaina, A.P. MacCabe (Eds.), Ind. Enzym. Struct. Funct. Appl., Springer, Dordrecht, 2007: pp. 461–476.

[67] O. V Morozova, G.P. Shumakovich, M. a Gorbacheva, S. V Shleev, a I. Yaropolov, “Blue” laccases., Biochemistry. (Mosc). 72 (2007) 1136–1150. doi:10.1134/S0006297907100112.

[68] G. Gupta, C. Lau, B. Branch, V. Rajendran, D.M. Ivnitski, P. Atanassov, Direct bio-

electrocatalysis by multi-copper oxidases: Gas-diffusion laccase-catalyzed cathodes for biofuel cells, Electrochim. Acta. 56 (2011) 10767–10771. doi:10.1016/j.electacta.2011.01.089.

[69] S. Shleev, M. Pita, A.I. Yaropolov, T. Ruzgas, L. Gorton, Direct heterogeneous electron transfer reactions of Trametes hirsuta laccase at bare and thiol-modified gold electrodes, Electroanalysis. 18 (2006) 1901–1908. doi:10.1002/elan.200603600.

[70] R. Szamocki, V. Flexer, L. Levin, F. Forchiassin, E.J. Calvo, Oxygen cathode based on a layer-by-layer self-assembled laccase and osmium redox mediator, Electrochim. Acta. 54 (2009) 1970–1977. doi:10.1016/j.electacta.2008.09.002.

[71] F. Giroud, R.D. Milton, B.-X. Tan, S.D. Minteer, Simplifying Enzymatic Biofuel Cells: Immobilized Naphthoquinone as a Biocathodic Orientational Moiety and Bioanodic Electron Mediator, ACS Catal. 5 (2015) 1240–1244. doi:10.1021/cs501940g.

[72] M.R. Tarasevich, A.I. Yaropolov, V.A. Bogdanovskaya, S.D. Varfolomeev, Electrocatalysis of a cathodic oxygen reduction by laccase, Bioelectrochemistry Bioenerg. 6 (1979) 393–403. doi:http://dx.doi.org/10.1016/0302-4598(79)80006-9.

[73] N. Mano, Features and applications of bilirubin oxidases, Appl. Microbiol. Biotechnol. 96 (2012) 301–307. doi:10.1007/s00253-012-4312-9.

[74] N. Tanaka, S. Murao, Reaction of Bilirubin Oxidase Produced by Myrothecium verrucaria MT-1, Agric. Biol. Chem. 49 (1985) 843–844.

[75] S. Tsujimura, H. Tatsumi, J. Ogawa, S. Shimizu, K. Kano, T. Ikeda, Bioelectrocatalytic reduction of dioxygen to water at neutral pH using bilirubin oxidase as an enzyme and 2,2′-azinobis (3-ethylbenzothiazolin-6-sulfonate) as an electron transfer mediator, J. Electroanal. Chem. 496 (2001) 69–75. doi:10.1016/S0022-0728(00)00239-4.

[76] S. Shleev, J. Tkac, A. Christenson, T. Ruzgas, A.I. Yaropolov, J.W. Whittaker, et al., Direct electron transfer between copper-containing proteins and electrodes, Biosens. Bioelectron. 20 (2005) 2517–2554. doi:10.1016/j.bios.2004.10.003.

[77] G. Gupta, C. Lau, V. Rajendran, F. Colon, B. Branch, D. Ivnitski, et al., Direct electron transfer catalyzed by bilirubin oxidase for air breathing gas-diffusion electrodes, Electrochem. Commun. 13 (2011) 247–249. doi:10.1016/j.elecom.2010.12.024.

[78] S. Brocato, C. Lau, P. Atanassov, Mechanistic study of direct electron transfer in bilirubin oxidase, Electrochim. Acta. 61 (2012) 44–49. doi:10.1016/j.electacta.2011.11.074.

[79] N. Mano, L. Edembe, Bilirubin oxidases in bioelectrochemistry: Features and recent

findings, Biosens. Bioelectron. 50 (2013) 478–485. doi:10.1016/j.bios.2013.07.014.

[80] O. Schaetzle, F. Barrière, U. Schröder, An improved microbial fuel cell with laccase as the oxygen reduction catalyst, Energy Environ. Sci. 2 (2009) 96–99. doi:10.1039/B815331K.

[81] H. Luo, S. Jin, P.H. Fallgren, H.J. Park, P. a. Johnson, A novel laccase-catalyzed cathode for microbial fuel cells, Chem. Eng. J. 165 (2010) 524–528. doi:10.1016/j.cej.2010.09.061.

[82] S.R. Higgins, C. Lau, P. Atanassov, S.D. Minteer, M.J. Cooney, Hybrid Biofuel Cell: Microbial Fuel Cell with an Enzymatic Air-Breathing Cathode, ACS Catal. 1 (2011) 994–997. doi:10.1021/cs2003142.

[83] C. Santoro, S. Babanova, P. Atanassov, B. Li, I. Ieropoulos, P. Cristiani, High Power Generation by a Membraneless Single Chamber Microbial Fuel Cell (SCMFC) Using Enzymatic Bilirubin Oxidase (BOx) Air-Breathing Cathode, J. Electrochem. Soc. 160 (2013) H720–H726. doi:10.1149/2.058310jes.

[84] P. Scodeller, R. Carballo, R. Szamocki, L. Levin, F. Forchiassin, E.J. Calvo, Laccase Oxygen Cathodes for Biofuel Cells : The Role of Hydrogen Peroxide, J. Am. Chem. Soc. 123 (2010) 11132–11140. doi:10.1021/ja1020487.

[85] R.D. Milton, F. Giroud, A.E. Thumser, S.D. Minteer, R.C.T. Slade, Bilirubin oxidase bioelectrocatalytic cathodes: the impact of hydrogen peroxide., Chem. Commun. (Camb). 50 (2014) 94–6. doi:10.1039/c3cc47689h.

[86] R.D. Milton, F. Giroud, A.E. Thumser, S.D. Minteer, R.C.T. Slade, Hydrogen peroxide produced by glucose oxidase affects the performance of laccase cathodes in glucose/oxygen fuel cells: FAD-dependent glucose dehydrogenase as a replacement., Phys. Chem. Chem. Phys. 15 (2013) 19371–9. doi:10.1039/c3cp53351d.

[87] F.A. Armstrong, G.S. Wilson, Recent developments in faradaic bioelectrochemistry, Electrochim. Acta. 45 (2000) 2623–2645. doi:10.1016/S0013-4686(00)00342-X.

[88] M. Rasmussen, S. Abdellaoui, S.D. Minteer, Enzymatic biofuel cells: 30 years of critical advancements, Biosens. Bioelectron. 76 (2016) 91–102. doi:10.1016/j.bios.2015.06.029.

[89] E.J. Calvo, F. Battaglini, C. Danilowicz, A. Wolosiuk, M. Otero, Layer-by-layer electrostatic deposition of biomolecules on surfaces for molecular recognition, redox mediation and signal generation., Faraday Discuss. (2000) 47–65; discussion 67–75. doi:10.1039/b001665i.

[90] A. Shrier, F. Giroud, M. Rasmussen, S.D. Minteer, Operational Stability Assays for Bioelectrodes for Biofuel Cells: Effect of Immobilization Matrix on Laccase Biocathode

Stability, J. Electrochem. Soc. 161 (2014) H244–H248. doi:10.1149/2.087404jes.

[91] G. Gupta, S.B. Rathod, K.W. Staggs, L.K. Ista, K.A. Oucherif, P. Atanassov, et al., CVD for the facile synthesis of hybrid nanobiomaterials integrating functional supramolecular assemblies, Langmuir. 25 (2009) 13322–13327. doi:10.1021/la903475d.

[92] J.M. Harris, C. Reyes, G.P. Lopez, Common causes of glucose oxidase instability in in vivo biosensing: a brief review, J. Diabetes Sci. Technol. 7 (2013) 1030–8. doi:10.1177/193229681300700428.

[93] S. Abdellaoui, B.C. Corgier, C.A. Mandon, B. Doumèche, C.A. Marquette, L.J. Blum, Biomolecules Immobilization Using the Aryl Diazonium Electrografting, Electroanalysis. 25 (2013) 671–684. doi:10.1002/elan.201200334.

[94] R.D. Milton, F. Wu, K. Lim, S. Abdellaoui, D.P. Hickey, S.D. Minteer, Promiscuous Glucose Oxidase: Electrical Energy Conversion of Multiple Polysaccharides Spanning Starch and Dairy Milk, ACS Catal. 5 (2015) 7218–7225. doi:10.1021/acscatal.5b01777.

[95] S. Borgmann, A. Schulte, S. Neugebauer, W. Schuhmann, Amperometric Biosensors, in: R.C. Alkire, D.M. Kolb, J. Lipkowski (Eds.), Adv. Electrochem. Sci. Eng., WILEY-VCH Verlag GmbH, Weinheim, 2011: pp. 1–83.

[96] F. Ricci, G. Palleschi, Sensor and biosensor preparation, optimisation and applications of Prussian Blue modified electrodes, Biosens. Bioelectron. 21 (2005) 389–407. doi:10.1016/j.bios.2004.12.001.

[97] A.A. Karyakin, O. V Gitelmacher, E.E. Karyakina, Prussian Blue-Based First-Generation Biosensor. A Sensitive Amperometric Electrode for Glucose, Anal. Chem. 67 (1995) 2419–2423.

[98] F. Ricci, G. Palleschi, Y. Yigzaw, L. Gorton, T. Ruzgas, A.A. Karyakin, Investigation of the Effect of Different Glassy Carbon Materials on the Performance of Prussian Blue Based Sensors for Hydrogen Peroxide, Electroanalysis. 15 (2003) 175–182. doi:10.1002/elan.200390021.

[99] A.L. Ghindilis, P. Atanassov, E. Wilkins, Enzyme-catalyzed direct electron transfer: Fundamentals and analytical applications, Electroanalysis. 9 (1997) 661–674. doi:10.1002/elan.1140090902.

[100] R.A. Marcus, N. Sutin, Electron transfers in chemistry and biology, Biochim. Biophys. Acta. 811 (1985) 265–322. doi:10.1016/0304-4173(85)90014-X.

[101] D.M. Ivnitski, P. Atanassov, C. Apblett, Direct bioelectrocatalysis of PQQ-dependent

glucose dehydrogenase, Electroanalysis. 19 (2007) 1562–1568. doi:10.1002/elan.200703899.

[102] A. Christenson, N. Dimcheva, E.E. Ferapontova, L. Gorton, T. Ruzgas, L. Stoica, et al., Direct electron transfer between ligninolytic redox enzymes and electrodes, Electroanalysis. 16 (2004) 1074–1092. doi:10.1002/elan.200403004.

[103] P. Ramírez, N. Mano, R. Andreu, T. Ruzgas, A. Heller, L. Gorton, et al., Direct electron transfer from graphite and functionalized gold electrodes to T1 and T2 / T3 copper centers of bilirubin oxidase, Biochim. Biophys. Acta. 1777 (2008) 1364–1369. doi:10.1016/j.bbabio.2008.06.010.

[104] R.J. Chen, Y. Zhang, D. Wang, H. Dai, Noncovalent sidewall functionalization of single-walled carbon nanotubes for protein immobilization, J. Am. Chem. Soc. 123 (2001) 3838–3839. doi:10.1021/ma021417n.

[105] J. Liu, A. Chou, W. Rahmat, M.N. Paddon-Row, J.J. Gooding, Achieving direct electrical connection to glucose oxidase using aligned single walled carbon nanotube arrays, Electroanalysis. 17 (2005) 38–46. doi:10.1002/elan.200403116.

[106] R.P. Ramasamy, H.R. Luckarift, D.M. Ivnitski, P. Atanassov, G.R. Johnson, High electrocatalytic activity of tethered multicopper oxidase-carbon nanotube conjugates., Chem. Commun. 46 (2010) 6045–6047. doi:10.1039/c0cc00911c.

[107] P.J. Goodhew, F.J. Humphreys, R. Beanland, Microscopy with light and electrons, in: P.J. Goodhew, F.J. Humphreys, R. Beanland (Eds.), Electron Microsc. Anal., Third Edit, Taylor & Francis Inc, New York, 2001: pp. 1–19.

[108] E. Guerrini, S. Trasatti, Recent developments in understanding factors of electrocatalysis, Russ. J. Electrochem. 42 (2006) 1017–1025. doi:10.1134/S1023193506100053.

[109] D.W. Banham, J.N. Soderberg, V.I. Birss, Pt/Carbon Catalyst Layer Microstructural Effects on Measured and Predicted Tafel Slopes for the Oxygen Reduction Reaction, J. Phys. Chem. 113 (2009) 10103–10111.

[110] S. Trasatti, O.A. Petrii, Real Surface Area Measurements in Electrochemistry, J. Electroanal. Chem. 327 (1992) 353–376.

[111] J.N. Roy, S. Babanova, K.E. Garcia, J. Cornejo, L.K. Ista, P. Atanassov, Catalytic biofilm formation by Shewanella oneidensis MR-1 and anode characterization by expanded uncertainty, Electrochim. Acta. 126 (2014) 3–10. doi:10.1016/j.electacta.2013.07.075.

[112] C. Danilowicz, E. Cortón, F. Battaglini, Osmium complexes bearing functional groups:

building blocks for integrated chemical systems, J. Electroanal. Chem. 445 (1998) 89–94. doi:http://dx.doi.org/10.1016/S0022-0728(97)00484-1.

[113] E.J. Calvo, R. a. Etchenique, L. Pietrasanta, A. Wolosiuk, Layer-By-Layer Self-Assembly of Glucose Oxidase and Os (Bpy) 2 ClPyCH 2 NH - poly (Allylamine) Bioelectrode, Anal. Chem. 73 (2001) 1161–1168. doi:10.1021/ac0011686.

[114] G. Decher, Fuzzy Nanoassemblies: Toward Layered Polymeric Multicomposites, Science (80-.). 277 (1997) 1232–1237. doi:10.1126/science.277.5330.1232.

[115] P. Lavalle, V. Vivet, N. Jessel, G. Decher, J.-C. Voegel, P.J. Mesini, et al., Direct evidence for vertical diffusion and exchange processes of polyanions and polycations in polyelectrolyte multilayer films, Macromolecules. 37 (2004) 1159–1162. doi:10.1021/ma035326h.

[116] G.G. Anderson, G.A. O'Toole, Innate and Induced Resistance Mechanisms of Bacterial Biofilms, in: T. Romeo (Ed.), Bact. Biofilms, Springer, Heidelberg, 2008: pp. 85–91. doi:10.1007/s13398-014-0173-7.2.

[117] J.T. Babauta, H.D. Nguyen, O. Istanbullu, H. Beyenal, Microscale gradients of oxygen, hydrogen peroxide, and pH in freshwater cathodic biofilms, ChemSusChem. 6 (2013) 1252–1261. doi:10.1002/cssc.201300019.

[118] C. Santoro, M. Cremins, U. Pasaogullari, M. Guilizzoni, A. Casalegno, A. Mackay, et al., Evaluation of Water Transport and Oxygen Presence in Single Chamber Microbial Fuel Cells with Carbon-Based Cathodes, J. Electrochem. Soc. 160 (2013) G3128–G3134. doi:10.1149/2.020307jes.

[119] N.P. Revsbech, Analysis of microbial communities with electrochemical microsensors and microscale biosensors., Methods Enzymol. 397 (2005) 147–166. doi:10.1016/S0076-6879(05)97009-2.

[120] C.-C. Wu, T. Yasukawa, H. Shiku, T. Matsue, Fabrication of miniature Clark oxygen sensor integrated with microstructure, Sensors Actuators B Chem. 110 (2005) 342–349. doi:10.1016/j.snb.2005.02.014.

[121] L. Hedstrom, Enzyme specificity and selectivity, Encycl. Life Sci. (2001) 1–7. doi:10.1002/9780470015902.a0000716.pub2.

[122] O. Kirk, T.V. Borchert, C.C. Fuglsang, Industrial enzyme applications, Curr. Opin. Biotechnol. 13 (2002) 345–351. doi:10.1016/S0958-1669(02)00328-2.

[123] E.J. Calvo, A. Wolosiuk, Wiring enzymes in nanostructures built with electrostatically self-

assembled thin films, ChemPhysChem. 6 (2005) 43–47. doi:10.1002/cphc.200400312.

[124] N.G. Tognalli, P. Scodeller, V. Flexer, R. Szamocki, A. Ricci, M. Tagliazucchi, et al., Redox molecule based SERS sensors., Phys. Chem. Chem. Phys. 11 (2009) 7412–7423. doi:10.1039/b905600a.

[125] J. Hirose, K. Inoue, H. Sakuragi, M. Kikkawa, M. Minakami, T. Morikawa, et al., Anions binding to bilirubin oxidase from Trachyderma tsunodae K-2593, Inorganica Chim. Acta. 273 (1998) 204–212. doi:10.1016/S0020-1693(97)06183-5.

[126] B. Shoham, Y. Migron, A. Riklin, I. Willner, B. Tartakovsky, A bilirubin biosensor based on a multilayer network enzyme electrode, Biosens. Bioelectron. 10 (1995) 341–352. doi:10.1016/0956-5663(95)96852-P.

[127] Y. Zhang, A. Pothukuchy, W. Shin, Y. Kim, A. Heller, Detection of ~10^3 copies of DNA by an electrochemical enzyme-amplified sandwich assay with ambient O2 as the substrate, Anal. Chem. 76 (2004) 4093–4097. doi:10.1021/ac0495034.

[128] D. Avnir, S. Braun, O. Lev, M. Ottolenghi, Enzymes and Other Proteins Entrapped in Sol-Gel Materials, Chem. Mater. 6 (1994) 1605–1614. doi:10.1021/cm00046a008.

[129] J.K. McIninch, E.R. Kantrowitz, Use of silicate sol-gels to trap the R and T quaternary conformational states of pig kidney fructose-1,6-bisphosphatase, Biochim. Biophys. Acta. 1547 (2001) 320–328. <Go to ISI>://000169535700015.

[130] J.R. Stetter, W.R. Penrose, S. Yao, Sensors, Chemical Sensors, Electrochemical Sensors, and ECS, J. Electrochem. Soc. 150 (2003) S11. doi:10.1149/1.1539051.

[131] E. Guerrini, S. Trasatti, Electrocatalysis in Water Electrolysis, in: P. Barbaro, C. Bianchini (Eds.), Catal. Sustain. Energy Prod., WILEY-VCH Verlag GmbH, Weinheim, 2009: pp. 235–270.

[132] B. Wang, Recent development of non-platinum catalysts for oxygen reduction reaction, J. Power Sources. 152 (2005) 1–15. doi:10.1016/j.jpowsour.2005.05.098.

[133] C. Sealy, The problem with platinum, Mater. Today. 11 (2008) 65–68. doi:10.1016/S1369-7021(08)70254-2.

[134] G. Gotti, K. Fajerwerg, D. Evrard, P. Gros, Electrodeposited gold nanoparticles on glassy carbon: Correlation between nanoparticles characteristics and oxygen reduction kinetics in neutral media, Electrochim. Acta. 128 (2014) 412–419. doi:10.1016/j.electacta.2013.10.172.

[135] R. Renslow, C. Donovan, M. Shim, J. Babauta, S. Nannapaneni, J. Schenk, et al., Oxygen

reduction kinetics on graphite cathodes in sediment microbial fuel cells, Phys. Chem. Chem. Phys. 13 (2011) 21573–21584. doi:10.1039/c1cp23200b.

[136] T. Kuwahara, T. Asano, M. Kondo, M. Shimomura, Bioelectrocatalytic O(2) reduction with a laccase-bearing poly(3-methylthiophene) film based on direct electron transfer from the polymer to laccase., Bioelectrochemistry. 91 (2013) 28–31. doi:10.1016/j.bioelechem.2012.12.002.

[137] I. Asano, Y. Hamano, S. Tsujimura, O. Shirai, K. Nano, Improved Performance of Gas-diffusion Biocathode for Oxygen Reduction, Electrochemistry. 80 (2012) 324–326. http://dx.doi.org/10.5796/electrochemistry.80.324.

[138] T. Zhang, Y. Zeng, S. Chen, X. Ai, H. Yang, Improved performances of E. coli-catalyzed microbial fuel cells with composite graphite/PTFE anodes, Electrochem. Commun. 9 (2007) 349–353. doi:10.1016/j.elecom.2006.09.025.

[139] Y. Luo, F. Zhang, B. Wei, G. Liu, R. Zhang, B.E. Logan, The use of cloth fabric diffusion layers for scalable microbial fuel cells, Biochem. Eng. J. 73 (2013) 49–52. doi:10.1016/j.bej.2013.01.011.

[140] K. Ben Liew, W.R.W. Daud, M. Ghasemi, J.X. Leong, S. Su Lim, M. Ismail, Non-Pt catalyst as oxygen reduction reaction in microbial fuel cells: A review, Int. J. Hydrogen Energy. 39 (2014) 4870–4883. doi:10.1016/j.ijhydene.2014.01.062.

[141] S.D. Minteer, P. Atanassov, H.R. Luckarift, G.R. Johnson, New materials for biological fuel cells, Mater. Today. 15 (2012) 166–173. doi:10.1016/S1369-7021(12)70070-6.

[142] F. Zhao, F. Harnisch, U. Schröder, F. Scholz, P. Bogdanoff, I. Herrmann, Challenges and constraints of using oxygen cathodes in microbial fuel cells., Environ. Sci. Technol. 40 (2006) 5193–5199. doi:10.1021/es060332p.

[143] K. Rabaey, S.T. Read, P. Clauwaert, S. Freguia, P.L. Bond, L.L. Blackall, et al., Cathodic oxygen reduction catalyzed by bacteria in microbial fuel cells., ISME J. 2 (2008) 519–527. doi:10.1038/ismej.2008.1.

[144] L. De Schamphelaire, P. Boeckx, W. Verstraete, Evaluation of biocathodes in freshwater and brackish sediment microbial fuel cells, Appl. Microbiol. Biotechnol. 87 (2010) 1675–1687. doi:10.1007/s00253-010-2645-9.

[145] L. Huang, J.M. Regan, X. Quan, Electron transfer mechanisms, new applications, and performance of biocathode microbial fuel cells, Bioresour. Technol. 102 (2011) 316–323. doi:10.1016/j.biortech.2010.06.096.

[146] C. Wu, X.-W. Liu, W.-W. Li, G.-P. Sheng, G.-L. Zang, Y.-Y. Cheng, et al., A white-rot fungus is used as a biocathode to improve electricity production of a microbial fuel cell, Appl. Energy. 98 (2012) 594–596. doi:10.1016/j.apenergy.2012.02.058.

[147] L. Zhuang, Y. Yuan, G. Yang, S. Zhou, In situ formation of graphene/biofilm composites for enhanced oxygen reduction in biocathode microbial fuel cells, Electrochem. Commun. 21 (2012) 69–72. doi:10.1016/j.elecom.2012.05.010.

[148] T. Nakagawa, H. Mita, H. Kumita, H. Sakai, Y. Tokita, S. Tsujimura, Water-repellent-treated enzymatic electrode for passive air-breathing biocathodic reduction of oxygen, Electrochem. Commun. 36 (2013) 46–49. doi:10.1016/j.elecom.2013.09.012.

[149] Z. Wang, Y. Zheng, Y. Xiao, S. Wu, Y. Wu, Z. Yang, et al., Analysis of oxygen reduction and microbial community of air-diffusion biocathode in microbial fuel cells, Bioresour. Technol. 144 (2013) 74–79. doi:10.1016/j.biortech.2013.06.093.

[150] M. Sharma, P. Jain, J.L. Varanasi, B. Lal, J. Rodríguez, J.M. Lema, et al., Enhanced performance of sulfate reducing bacteria based biocathode using stainless steel mesh on activated carbon fabric electrode, Bioresour. Technol. 150 (2013) 172–180. doi:10.1016/j.biortech.2013.09.069.

[151] W.G. Characklis, K.C. Marshall, Biofilms, John Wiley & Sons, New York, 1990.

[152] M.C.M. Van Loosdrecht, D. Eikelboom, A. Gjaltema, A. Mulder, L. Tijhuis, J.J. Heijnen, Biofilm structures, Water Sci. Technol. 32 (1995) 35–43. doi:10.1016/0273-1223(96)00005-4.

[153] T.R. Bott, Fouling of Heat Exchangers, Elsevier, Amsterdam, 1995.

[154] V. Flexer, K.F.E. Pratt, F. Garay, P.N. Bartlett, E.J. Calvo, Relaxation and Simplex mathematical algorithms applied to the study of steady-state electrochemical responses of immobilized enzyme biosensors: Comparison with experiments, J. Electroanal. Chem. 616 (2008) 87–98. doi:10.1016/j.jelechem.2008.01.006.

[155] P.N. Bartlett, C.S. Toh, E.J. Calvo, V. Flexer, Modelling Biosensor Responses, in: P.N. Barlett (Ed.), Bioelectrochemistry Fundam. Exp. Tech. Appl., John Wiley & Sons, Chichester, 2008: pp. 267–325.

[156] D.N. Blauch, J.-M. Savéant, Dynamics of Electron Hopping in Assemblies of Redox Centers . Percolation and Diffusion, J. Am. Chem. Soc. 114 (1992) 3323–3332. doi:10.1021/ja00035a025.

[157] D.N. Blauch, J.-M. Savéant, Effects of Long-Range Electron Transfer on Charge Transport in Static Assemblies of Redox Centers, J. Phys. Chem. 97 (1993) 6444–6448.

[158] E.I. Solomon, A.J. Augustine, J. Yoon, O2 Reduction to H2O by the multicopper oxidases, Dalt. Trans. 9226 (2008) 3921. doi:10.1039/b800799c.

[159] J.W. Gallaway, S. a C. Barton, Kinetics of redox polymer-mediated enzyme electrodes, J. Am. Chem. Soc. 130 (2008) 8527–8536. doi:10.1021/ja0781543.

[160] P.N. Bartlett, K.F.E. Pratt, Theoretical treatment of diffusion and kinetics in amperometric immobilized enzyme electrodes Part I: Redox mediator entrapped within the film, J. Electroanal. Chem. 397 (1995) 61–78. doi:10.1016/0022-0728(95)04236-7.

[161] P.N. Bartlett, K.F.E. Pratt, Modelling of processes in enzyme electrodes, Biosens. Bioelectron. 8 (1993) 451–462. doi:10.1016/0956-5663(93)80030-S.

[162] V. Flexer, E.J. Calvo, P.N. Bartlett, The application of the relaxation and simplex method to the analysis of data for glucose electrodes based on glucose oxidase immobilised in an osmium redox polymer, J. Electroanal. Chem. 646 (2010) 24–32. doi:10.1016/j.jelechem.2009.11.017.

[163] L. Levin, F. Forchiassin, A. Viale, Ligninolytic enzyme production and dye decolorization by Trametes trogii: Application of the Plackett-Burman experimental design to evaluate nutritional requirements, Process Biochem. 40 (2005) 1381–1387. doi:10.1016/j.procbio.2004.06.005.

[164] R.D. Milton, S.D. Minteer, Investigating the Reversible Inhibition Model of Laccase by Hydrogen Peroxide for Bioelectrocatalytic Applications, J. Electrochem. Soc. 161 (2014) 3011–3014. doi:10.1149/2.0031413jes.

[165] P. Scodeller, F.J. Williams, E.J. Calvo, XPS Analysis of Enzyme and Mediator at the Surface of a Layer-by-Layer Self-Assembled Wired Enzyme Electrode, Anal. Chem. 86 (2014) 12180–12184. doi:10.1021/ac503147c.

[166] P. Scodeller, V. Flexer, R. Szamocki, E.J. Calvo, N.G. Tognalli, H. Troiani, et al., Wired-Enzyme Core-Shell Au Nanoparticle Biosensor, J. Am. Chem. Soc. 130 (2008) 12690–12697. doi:10.1021/ja802318f.

[167] L.-S. Kau, D.J. Spira-Solomon, J.E. Penner-Hahn, K.O. Hodgson, E.I. Solomon, X-ray absorption edge determination of the oxidation state and coordination number of copper. Application to the type 3 site in Rhus vernicifera laccase and its reaction, J. Am. Chem. Soc. 109 (1987) 6433–6442. doi:10.1021/ja00255a032.

[168] R. Branden, B.G. Malmstrom, T. Vanngard, The Interaction of Fungal Laccase with Hydrogen Peroxide and the Removal of Fluoride from the Inhibited Enzyme, Eur. J. Biochem. 18 (1971) 238–241.

[169] H. Bisswanger, Enzyme kinetics: Principles and methods, WILEY-VCH Verlag GmbH, Weinheim, 2002.

[170] N.C. Price, L. Stevens, Fundamentals of Enzymology, Oxford University Press, Oxford, 1996.

[171] E.I. Solomon, U.M. Sundaram, T.E. Machonkin, Multicopper Oxidases and Oxygenases., Chem. Rev. 96 (1996) 2563–2606. doi:10.1021/cr950046o.

[172] S.M. Jones, E.I. Solomon, Electron transfer and reaction mechanism of laccases, Cell. Mol. Life Sci. 72 (2015) 869. doi:10.1007/s00018-014-1826-6.

[173] U.M. Sundaram, H.H. Zhang, B. Hedman, K.O. Hodgson, E.I. Solomon, S. Synchrotron, et al., Spectroscopic Investigation of Peroxide Binding to the Trinuclear Copper Cluster Site in Laccase : Correlation with the Peroxy-Level Intermediate and Relevance to Catalysis, J. Am. Chem. Soc. 119 (1997) 12525–12540. doi:10.1021/ja972039i.

[174] I. V. Berezin, V.A. Bogdanovskaya, S.D. Varfolomeev, M.R. Tarasevich, A.I. Iaropolov, Bioelectrocatalysis - Equilibrium Oxygen Potential in Presence of Laccase, Dokl. Akad. Nauk SSSR. 240 (1978) 615–18.

[175] C.F. Blanford, R.S. Heath, F. a Armstrong, A stable electrode for high-potential, electrocatalytic O(2) reduction based on rational attachment of a blue copper oxidase to a graphite surface., Chem. Commun. (Camb). (2007) 1710–1712. doi:10.1039/b703114a.

[176] S. Shleev, A. Jarosz-Wilkolazka, A. Khalunina, O. Morozova, A. Yaropolov, T. Ruzgas, et al., Direct electron transfer reactions of laccases from different origins on carbon electrodes, Bioelectrochemistry. 67 (2005) 115–124. doi:10.1016/j.bioelechem.2005.02.004.

[177] C.F. Blanford, C.E. Foster, R.S. Heath, F. a Armstrong, Efficient electrocatalytic oxygen reduction by the “blue” copper oxidase, laccase, directly attached to chemically modified carbons, Faraday Discuss. 140 (2008) 319–335. doi:10.1039/b808939f.

[178] V. Climent, J. Zhang, E.P. Friis, L.H. Østergaard, J. Ulstrup, Voltammetry and Single-Molecule in Situ Scanning Tunneling Microscopy of Laccases and Bilirubin Oxidase in Electrocatalytic Dioxygen Reduction on Au(111) Single-Crystal Electrodes, J. Phys. Chem. C. 116 (2012) 1232–1243. doi:10.1021/jp2086285.

[179] A.M. Garzillo, M.C. Colao, V. Buonocore, R. Oliva, L. Falcigno, M. Saviano, et al., Structural and kinetic characterization of native laccases from Pleurotus ostreatus, Rigidoporus lignosus, and Trametes trogii, J. Protein Chem. 20 (2001) 191–201. doi:10.1023/A:1010954812955.

[180] C. Dumas, R. Basseguy, A. Bergel, Electrochemical activity of *Geobacter sulfurreducens* biofilms on stainless steel anodes, Electrochim. Acta. 53 (2008) 5235–5241. doi:10.1016/j.electacta.2008.02.056.

[181] B. Erable, A. Bergel, First air-tolerant effective stainless steel microbial anode obtained from a natural marine biofilm., Bioresour. Technol. 100 (2009) 3302–7. doi:10.1016/j.biortech.2009.02.025.

[182] S. Chen, Y. Chen, G. He, S. He, U. Schröder, H. Hou, Stainless steel mesh supported nitrogen-doped carbon nanofibers for binder-free cathode in microbial fuel cells., Biosens. Bioelectron. 34 (2012) 282–5. doi:10.1016/j.bios.2011.10.049.

[183] D.F. Call, M.D. Merrill, B.E. Logan, High surface area stainless steel brushes as cathodes in microbial electrolysis cells, Environ. Sci. Technol. 43 (2009) 2179–2183. doi:10.1021/es803074x.

[184] M. Mehanna, R. Basseguy, M.L. Delia, R. Gubner, N. Sathirachinda, A. Bergel, Geobacter species enhances pit depth on 304L stainless steel in a medium lacking with electron donor, Electrochem. Commun. 11 (2009) 1476–1481. doi:10.1016/j.elecom.2009.05.035.

[185] J.J. Santana Rodríguez, F.J. Santana Hernández, J.E. González González, Comparative study of the behaviour of AISI 304 SS in a natural seawater hopper, in sterile media and with SRB using electrochemical techniques and SEM, Corros. Sci. 48 (2006) 1265–1278. doi:10.1016/j.corsci.2005.04.007.

[186] a. M. Awad, E. a. Ghazy, S. a. Abo El-Enin, M.G. Mahmoud, Electropolishing of AISI-304 stainless steel for protection against SRB biofilm, Surf. Coatings Technol. 206 (2012) 3165–3172. doi:10.1016/j.surfcoat.2011.11.046.

[187] S.E. Werner, C. a Johnson, N.J. Laycock, P.T. Wilson, B.J. Webster, Pitting of type 304 stainless steel in the presence of a biofilm containing sulphate reducing bacteria, Corros. Sci. 40 (1998) 465–480. doi:10.1016/S0010-938X(97)00160-1.

[188] P. Cristiani, A. Franzetti, I. Gandolfi, E. Guerrini, G. Bestetti, Bacterial DGGE fingerprints of biofilms on electrodes of membraneless microbial fuel cells, Int. Biodeterior. Biodegrad. 84 (2013) 211–219. doi:10.1016/j.ibiod.2012.05.040.

[189] C. Santoro, A. Agrios, U. Pasaogullari, B. Li, Effects of gas diffusion layer (GDL) and micro porous layer (MPL) on cathode performance in microbial fuel cells (MFCs), Int. J. Hydrogen Energy. 36 (2011) 13096–13104. doi:10.1016/j.ijhydene.2011.07.030.

[190] C. Xu, Y. Zhang, G. Cheng, W. Zhu, Localized corrosion behavior of 316L stainless steel in the presence of sulfate-reducing and iron-oxidizing bacteria, Mater. Sci. Eng. A. 443 (2007) 235–241. doi:10.1016/j.matchar.2007.01.001.

[191] T. Zhang, C. Cui, S. Chen, H. Yang, P. Shen, The direct electrocatalysis of Escherichia coli through electroactivated excretion in microbial fuel cell, Electrochem. Commun. 10 (2008) 293–297. doi:10.1016/j.elecom.2007.12.009.

[192] K. Rabaey, N. Boon, M. Höfte, W. Verstraete, Microbial phenazine production enhances electron transfer in biofuel cells, Environ. Sci. Technol. 39 (2005) 3401–3408. doi:10.1021/es048563o.

[193] D. Pocaznoi, B. Erable, L. Etcheverry, M.L. Delia, A. Bergel, Forming microbial anodes under delayed polarisation modifies the electron transfer network and decreases the polarisation time required, Bioresour. Technol. 114 (2012) 334–341. doi:10.1016/j.biortech.2012.03.042.

[194] S.M. Strycharz, A.P. Malanoski, R.M. Snider, H. Yi, D.R. Lovley, L.M. Tender, Application of cyclic voltammetry to investigate enhanced catalytic current generation by biofilm-modified anodes of Geobacter sulfurreducens strain DL1 vs. variant strain KN400, Energy Environ. Sci. 4 (2011) 896. doi:10.1039/c0ee00260g.

[195] G. Chen, C.R. Clayton, Influence of Sulfate-Reducing Bacteria on the Passivity of Type 304 Austenitic Stainless Steel, J. Electrochem. Soc. 144 (1997) 3140–3146.

[196] I.B. Beech, Corrosion of technical materials in the presence of biofilms—current understanding and state-of-the art methods of study, Int. Biodeterior. Biodegradation. 53 (2004) 177–183. doi:10.1016/S0964-8305(03)00092-1.

[197] J.J. Santana, F.J. Santana, J.E. González, R.M. Souto, S. González, J. Morales, Electrochemical Analysis of the Microbiologically Influenced Corrosion of AISI 304 Stainless Steel by Sulphate Reducing Bacteria Associated with Bacillus Cereus, Int. J. Electrochem. Sci. 7 (2012) 711–724.

[198] T. Palmer, P.L. Bonner, ENZYMES: Biochemistry, Biotechnology and Clinical Chemistry, Woodhead Publishing Limited, Cambridge, 2007.

APPENDIX ONE

Enzymes

Enzymes (*E*) are biological catalysts. They are classified as biomacromolecules that act in numerous chemical transformations. Proteins, linear polymers of twenty different amino acids, constitute the majority of enzymes. *Substrates* (*S*) are the reactants of the enzyme-catalyzed reactions. Enzymes contain one or more *active site*, where the substrates (*S*) are chemically transformed into products (*P*). One active site may comprise only a few amino acid residues, while the rest of the protein maintains the three-dimensional integrity of the network. *S* are transformed into *P* with a velocity that is 10^8-10^{20} times faster than the reaction in the absence of the bio-catalyst. It is important to remark that the most important characteristics of enzymes are the high specificity for the catalyzed reaction and for the substrates selection, which varies from molecule to molecule. For the sake of simplicity and to avoid confusion, the enzyme commission have divided enzymes into six major classes, depending on the total reaction catalyzed, utilizing a code number that unambiguously identify each enzyme [198].

Redox Enzymes

Redox Enzymes, or oxidoreductases, are the first class of enzyme accordingly to the enzyme commission. They catalyze redox reactions, where one molecule is oxidized while one is reduced as depicted in figure A1.1.

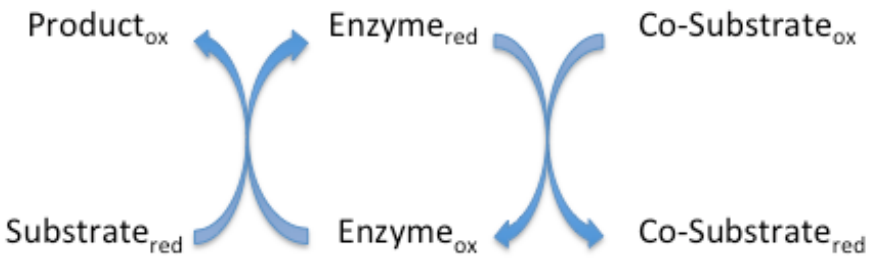

Figure A1.1 Schematic representation of the catalytic mechanism of an oxidoreductase enzyme. "ox" and "red" indicate the oxidized and reduced form respectively.

The enzyme is reduced accepting electrons from the substrate. Following, the enzyme delivers the electrons to a co-substrate (or a mediator) and comes back to the oxidized state. The presence of both the reduced substrate and the oxidized co-substrate will continuously switch the enzyme between the oxidized and the reduced states. In this way the bio-catalytic process is repeated, obtaining a stationary state. This mechanism is named *ping-pong* as the enzyme switches between the two-redox states to convert the substrate into product. It is possible to use an artificial co-substrate, which means a co-substrate different from the one that the enzyme uses in nature, using an electrode as electron acceptor and obtaining an electrons flow that allow to develop amperometric biosensors. The enzyme can deliver the electrons to redox active molecules or can directly communicate with the electrode surface.

Enzyme kinetics

The simplest description of the steady-state enzymatic kinetics is based on the Michaelis-Menten model. It is assumed that *S* forms a complex enzyme-substrate (*ES*) with *E* in a reversible step and *E*, *S* and *ES* maintain equilibrium until an irreversible break of the complex *ES* gives the products *P*.

$$E + S \underset{}{\overset{k_M}{\rightleftharpoons}} ES \xrightarrow{k_2} E + P \qquad \text{(A1.1)}$$

The second assumption of the model is that the *ES* concentration can be considered with the steady-state conditions. This is not true immediately after the addition of the substrate, as the *ES* concentration is increasing at his step (called pre-steady state conditions).

Briggs and Haldane proposed a more general mechanism where the direct and the reverse rate constant (k_1 and k_{-1}) for the formation of the complex ES are included:

$$E + S \underset{k_{-1}}{\overset{k_1}{\rightleftharpoons}} ES \xrightarrow{k_2} E + P \qquad \text{(A1.2)}$$

If we define e_Σ as the total concentration of the enzyme and e_{ES} as the concentration of the enzyme-substrate complex, the concentration of the free enzyme e is:

$$e = e_\Sigma - e_{ES} \qquad \text{(A1.3)}$$

Assuming that the concentration of the substrate is considerably greater than the concentration of the enzyme, the concentration of the free substrate can be considered equal to the initial concentration *S*.

It is now possible to define

$$\frac{de_{ES}}{dt} = k_1(e_\Sigma - e_{ES})S - k_{-1}e_{ES} - k_{cat}e_{ES} \qquad \text{(A1.4)}$$

but when the steady-state is obtained ($de_{ES}/dt=0$)

$$e_{ES} = \frac{k_1 e_\Sigma S}{k_1 S + k_{-1} + k_{cat}} \qquad \text{(A1.5)}$$

the reaction rate, *V*, is $V = k_{cat}e_{ES}$ thus:

$$V = \frac{k_1 k_{cat} e_\Sigma S}{k_1 S + k_{-1} + k_{cat}} \qquad \text{(A1.6)}$$

that can be rearranged to obtain the Michaelis-Menten equation

$$V = \frac{dS}{dt} = \frac{k_{cat}e_\Sigma S}{K_{MS} + S} = k_E S \qquad \text{(A1.7)}$$

where

$$k_E = \frac{k_{cat}e_\Sigma}{K_{MS} + S} \qquad \text{(A1.8)}$$

and

$$K_{MS} = \frac{k_{-1} + k_{cat}}{k_1} = Constant\ of\ Michaelis - Menten \qquad \text{(A1.9)}$$

$k_{cat}e_\Sigma$ is the maximum reaction rate of the process, V_{MAX}, and the Michaelis-Menten equation can be written as:

$$V = \frac{V_{MAX} S}{K_{MS} + S} \qquad \text{(A1.10)}$$

The graph for the Michaelis-Menten equation (equation 10) is reported in figure A1.2.

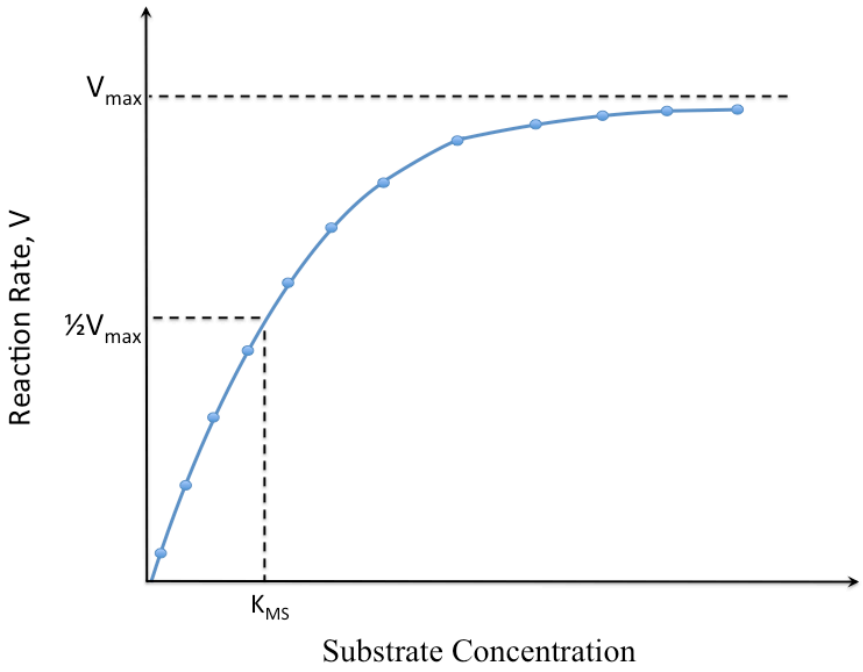

Figure A1.2 Graph of the Michaelis-Menten equation.

This is the expected shape for the calibration of an enzymatic sensor made with an enzyme that follows the Michaelis-Menten model. At low substrate concentration ($S << K_{MS}$), the reaction rate increases linearly with the substrate concentration and the Michaelis-Menten equation can be simplified to

$$V = \frac{V_{MAX} S}{K_{MS}} \qquad \text{(A1.11)}$$

When $S = K_{MS}$ the reaction rate is exactly half of the V_{MAX}.

When $k_{-1} >> k_{cat}$ thus

$$K_{MS} = \frac{k_{-1}}{k_1} \qquad \text{(A1.12)}$$

and K_{MS} can be considered as an indicator of the affinity of the enzyme for the substrate. A low K_{MS} value corresponds to a strong *ES* complex whereas if the K_{MS} value is high, the enzyme has low affinity for the substrate and the *ES* complex is weak. The disadvantage of the direct plot (non-linear) is that K_{MS} and V_{MAX} can be determined only with difficulty. Linearized representations are preferred to overcome this problem. There are different ways to find K_{MS} and V_{MAX} from the conversion of the Michaelis-Menten equation, such as Lineweaver Burke double reciprocal plot, Eadie-Hofstee plot and Hanes plot [169].

Lineweaver Burke Double Reciprocal Plot

By taking the reciprocal of the Michaelis-Menten equation:

$$\frac{1}{V} = \frac{(K_{MS} + S)}{V_{MAX} S} \tag{A1.13}$$

that can be rearranged to obtain

$$\frac{1}{V} = \left(\frac{K_{MS}}{V_{MAX}}\right)\left(\frac{1}{S}\right) + \frac{1}{V_{MAX}} \tag{A1.14}$$

applied to a straight line equation $y = mx + q$

$$y = \frac{1}{V} \text{ and } x = \frac{1}{S} \tag{A1.15}$$

Thus:

$$m = slope = \frac{K_{MS}}{V_{MAX}} \; ; \; y\text{–}intercept = \frac{1}{V_{MAX}} \text{ and } x\text{–}intercept = \frac{-1}{K_{MS}}$$

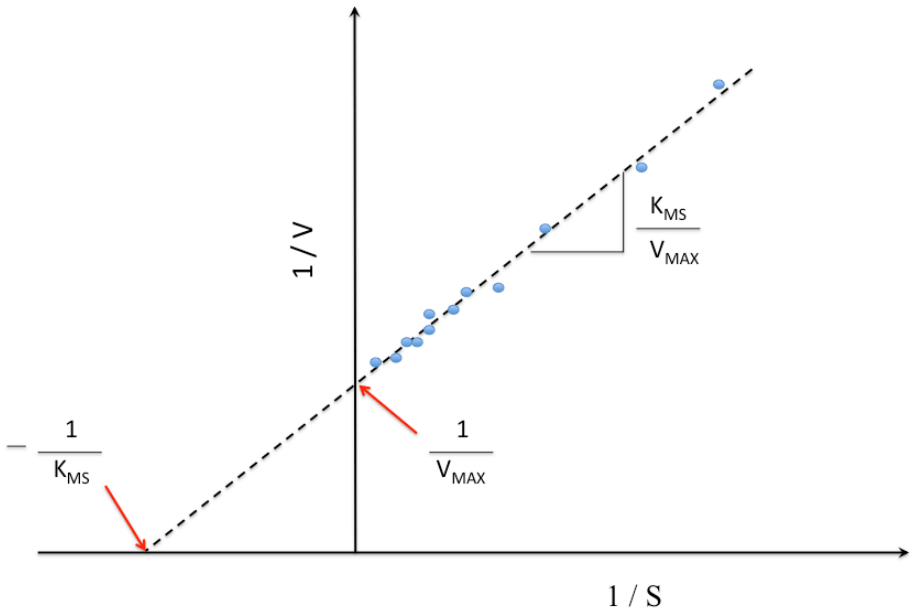

Figure A1.3 Lineweaver Burke Double Reciprocal Plot

Eadie-Hofstee Plot

The Michaelis-Menten equation also can be rearranged into

$$V\left(K_{MS}+S\right)=V_{MAX}S \tag{A1.16}$$

$$VK_{MS}+VS=V_{MAX}S \tag{A1.17}$$

$$VS=-VK_{MS}+V_{MAX}S \tag{A1.18}$$

and dividing through by S

$$V=-K_{MS}\frac{V}{S}+V_{MAX} \tag{A1.19}$$

Thus:

$$m=slope=-K_{MS};\ y\text{–}intercept=V_{MAX}\ \text{and}\ x\text{–}intercept=\frac{V_{MAX}}{K_{MS}}$$

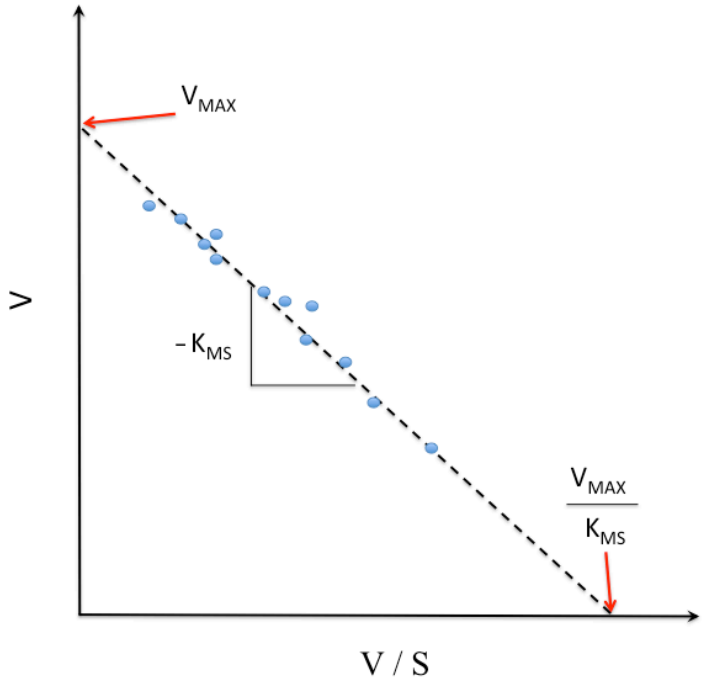

Figure A1.4 Eadie-Hofstee Plot

Hanes Plot

By taking the reciprocal of the Michaelis-Menten equation and multiply by *S*:

$$\frac{S}{V} = \frac{S\left(K_{MS} + S\right)}{V_{MAX} S} = \frac{K_{MS} + S}{V_{MAX}} \tag{A1.20}$$

The equation is rearranged to

$$\frac{S}{V} = \frac{1}{V_{MAX}} S + \frac{K_{MS}}{V_{MAX}} \tag{A1.21}$$

Thus:

$$m = slope = \frac{1}{V_{MAX}};\ y\text{–}intercept = \frac{K_{MS}}{V_{MAX}};\ x\text{–}intercept = -K_{MS}$$

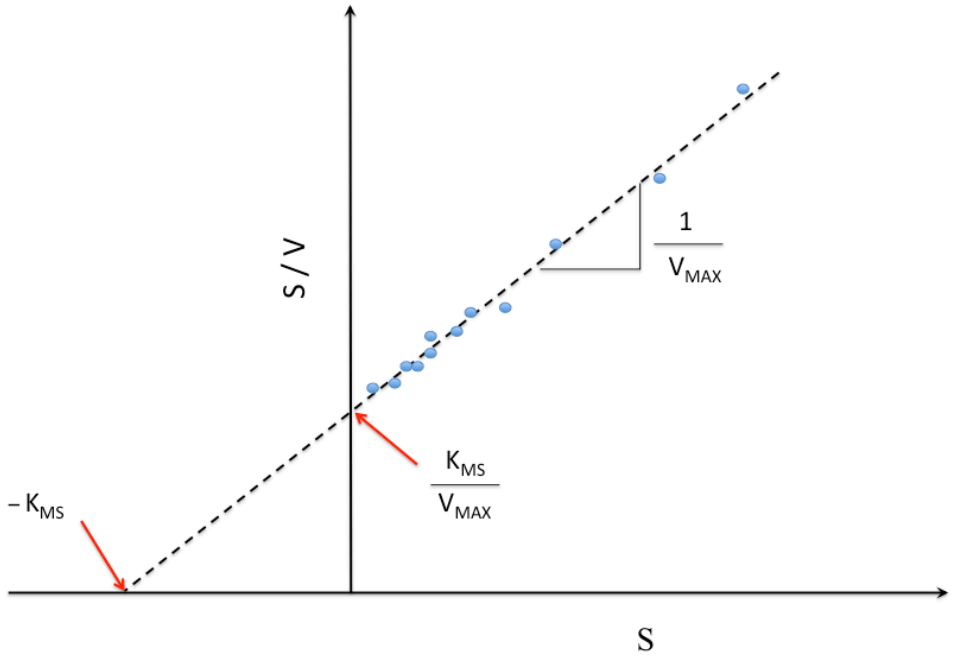

Figure A1.5 Hanes Plot

APPENDIX TWO

Enzyme Inhibition

Enzyme inhibition is defined as the negative effect on enzyme activity by ligands (inhibitors) specifically binding to defined catalytic or regulatory centers. In the majority of the cases, the inhibitor binds reversibly to the enzyme and can be released or displaced, obtaining reversible inhibition. On the other hand, certain inhibitors bind so strong to the enzyme that they cannot be detached, obtaining irreversible inhibition. This last case can be caused by covalent binding of the inhibitor, i.e. suicide substrates that initially follow the catalytic process but subsequently form a covalent bond with a functional group of the active center and block the enzyme. Reversible and irreversible inhibitors have to be discussed separately, thus, it is imperative to determine the nature of inhibition in advance. One possible way to distinguish between reversible and irreversible inhibition is to separate the inhibitor from the enzyme by dialysis, gel filtration, ultrafiltration, etc. In the case of reversible inhibition, total enzyme activity should be restored, while no reactivation may be expected for irreversible inhibition. However, the enzyme may suffer from activity loss due to the separation procedure, making it difficult to distinguish inactivation from inhibition.

A reliable test to achieve this goal is the determination of the time dependence of the inhibition effect (figure A2.1). In the case of reversible inhibition, the inhibitor immediately reduces enzyme activity to a constant time-independent value. On the other hand, for irreversible inhibition the inhibitor exponentially reduce enzyme activity with a pseudo first order reaction. If the concentration of the inhibitor is the same of the enzyme, the inhibitor will finally inactivate all enzyme molecules (stoichiometric binding to the enzyme) [169].

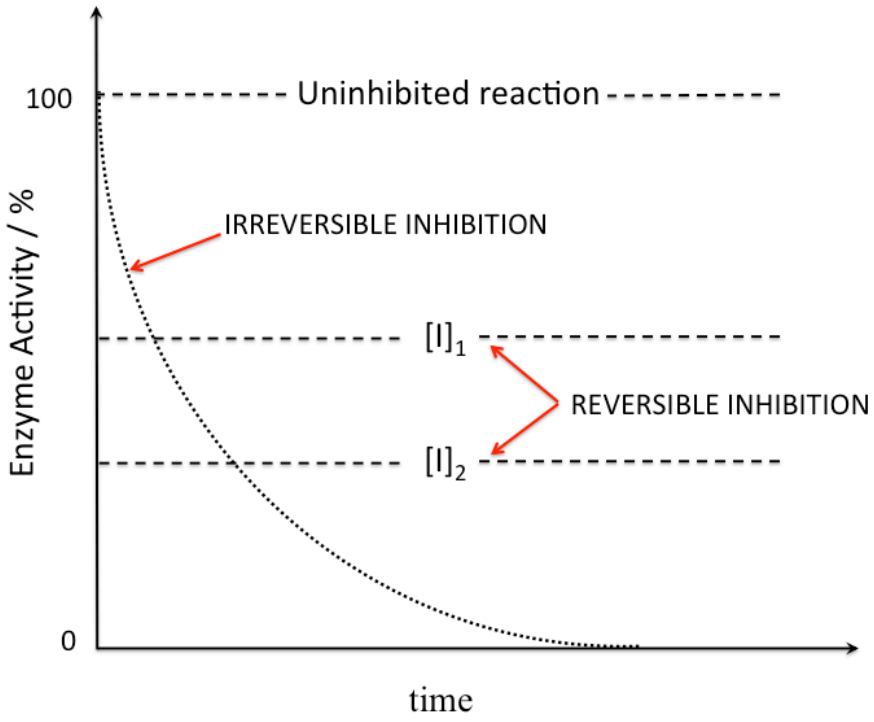

Figure A2.1 Time course for an irreversible and reversible inhibition. $[I]_1$ and $[I]_2$ refer to increasing concentration of reversible inhibitor.

Enzyme Inhibition Mechanisms

Irreversible inhibition

The irreversible binding of inhibitor (*I*) to an enzyme can be described as

$$E + I \underset{k_{-1}}{\overset{k_1}{\rightleftharpoons}} EI \xrightarrow{k_2} EI_i \qquad \text{(A2.1)}$$

There is an initial formation of a non-covalent *EI* complex, which is then transformed by an irreversible process into the inactive complex EI_i.

Reversible Partial and Complete Inhibition

The general description mechanism for reversible inhibitors can be schematized as follow (A2.2)

$$\begin{array}{ccc} E + S & \underset{k_{-1}}{\overset{k_1}{\rightleftharpoons}} & ES \xrightarrow{k_2} E + P \\ + & & + \\ I & & I \\ k_3 \uparrow\downarrow k_{-3} & & k_4 \uparrow\downarrow k_{-4} \\ EI + A & \underset{k_{-5}}{\overset{k_5}{\rightleftharpoons}} & EIS \xrightarrow{k_6} EI + P \end{array} \qquad \text{(A2.2)}$$

where $V_1 = k_2 E$ and $(S \to \infty)$ and $V_2 = k_6 E$. Among the reversible inhibition mechanisms, the first distinction is made between partial and complete inhibition. In the case of partial inhibition, $V_2 \neq 0$, thus the enzyme remains active even after the binding of the inhibitor and it is still possible to obtain the product, but the activity of the enzyme may be affected by the inhibitor.

For complete inhibition, $V_2 = 0$, thus the enzyme forms an inactive *dead-end complex* and the product is not obtained. It is not easy to distinguish between partial and complete reversible inhibition. A possible way is related to the graphical representation of the experimental data with the Dixon plot, where the reciprocal of the reaction rate is plotted versus the inhibitor concentration (figure A2.2). For partial inhibition the Dixon plot does not yield straight lines, whereas for complete inhibition a linear graph is obtained.

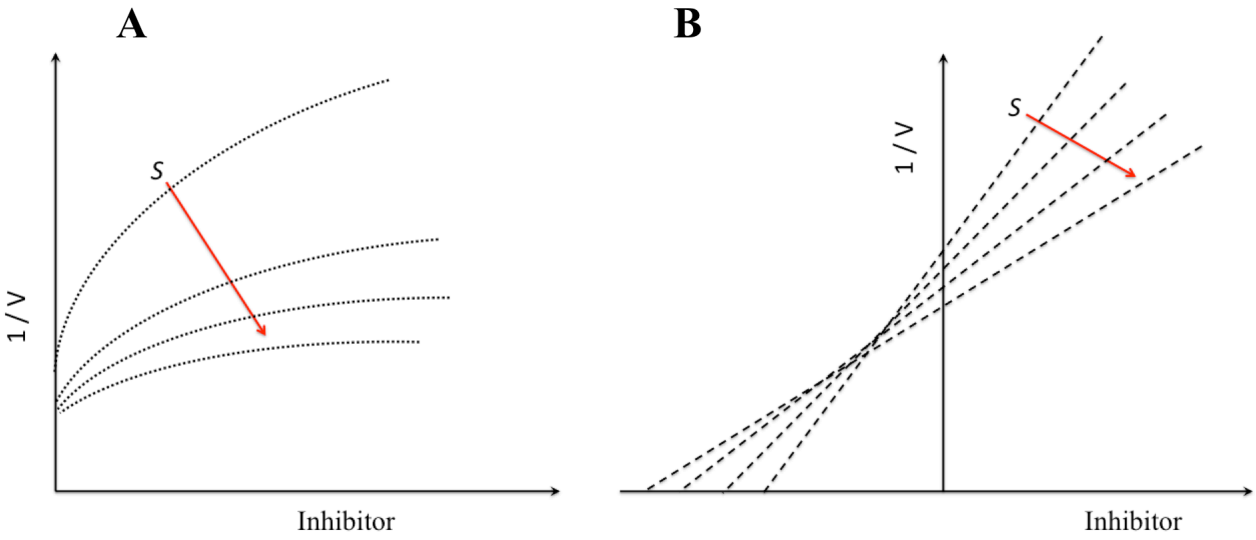

Figure A2.2 Dixon plot for partial inhibition (A) and complete inhibition (B).

Graphic Representation for Reversible Complete inhibitions

To characterize the inhibition types, the turnover rates of several measuring series with varying substrate concentrations have to be performed, each series containing a constant amount of the inhibitor. Moreover, as control test, one series without inhibitor have to be measured, for the determination of K_{MS} and V_{MAX}.

Non-competitive inhibition

In the case of non-competitive inhibition, the inhibitor binds in a different binding site than the enzyme substrate, either to the free enzyme or to the enzyme-substrate complex.

$$\begin{array}{ccc} E + S & \underset{k_{-1}}{\overset{k_1}{\rightleftharpoons}} & ES \xrightarrow{k_2} E + P \\ + & & + \\ I & & I \\ k_3 \downarrow\uparrow k_{-3} & & k_4 \downarrow\uparrow k_{-4} \\ EI + A & \underset{k_{-5}}{\overset{k_5}{\rightleftharpoons}} & EIS \end{array} \qquad \text{(A2.3)}$$

In non-competitive inhibition the apparent Michaelis constant and the maximum velocity are both affected by the inhibitor. The linearized plots for the experimental evidence will give the behavior reported in figure A2.3

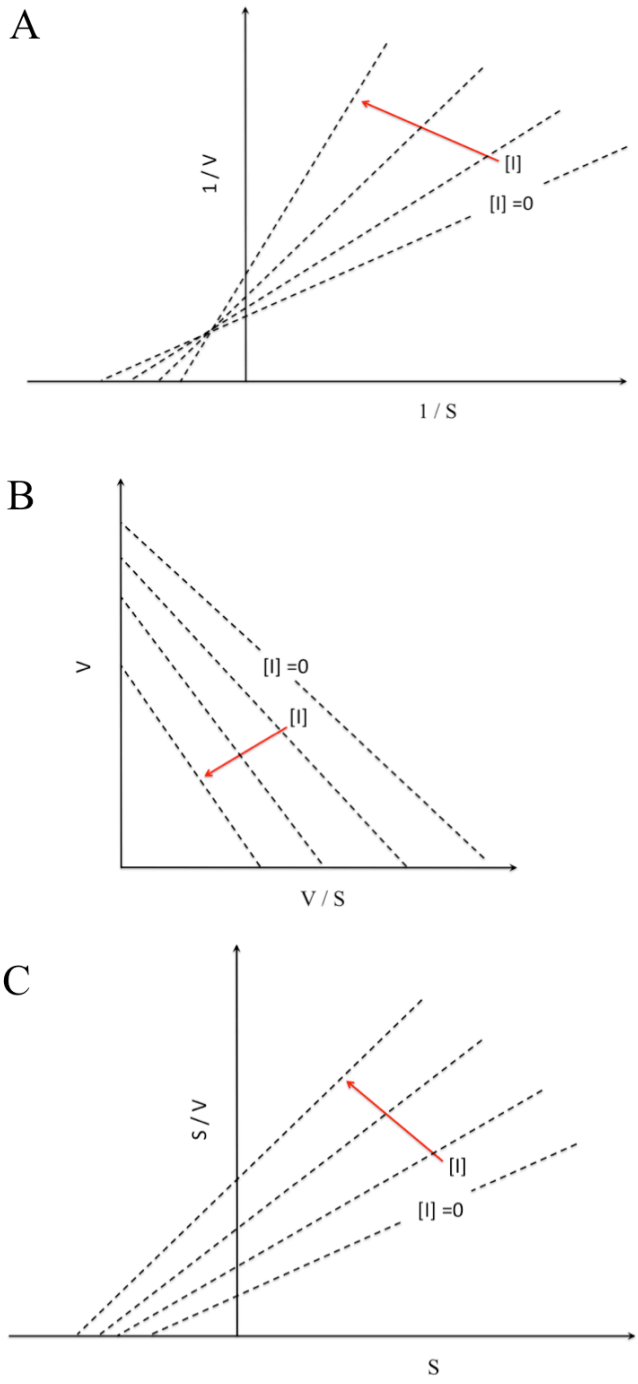

Figure A2.3 Lineweaver Burke double reciprocal (A) Eadie-Hofstee (B) and Hanes plot (C) for reversible complete non-competitive inhibition.

The Lineweaver Burke double reciprocal plot presents all straight lines that meet in a joint intercept left of the ordinate. The lines differ in gradient and ordinate intercept, because the inhibitor influences both the apparent Michaelis constant and the maximum velocity. When the binding of substrate and inhibitor occur completely independent of each other, the joint intercept is located on the abscissa and this case (where Km is not changed) is named as "pure non-competitive inhibition". On the other hand, the shift of the joint intercept up or down, away from the abscissa, is characteristic of "mixed non-competitive inhibition". In particular, when the joint intercept is shifted above the abscissa the substrate tends to impede binding of the inhibitor, thus the inhibitor binds with a slight preference to the free enzyme. When the joint intercept is shifted below the abscissa the inhibitor and the substrate support each other in their binding to the enzyme.

The Eadie-Hofstee plot may present parallel or non-parallel lines, but always with different y-intercepts and x-intercepts. The Hanes plot present non-parallel lines.

Competitive inhibition

In the case of competitive inhibition, the inhibitor competes with the enzyme substrate for its binding site at the active centre of the enzyme.

$$\begin{array}{ccccc} E + S & \underset{k_{-1}}{\overset{k_1}{\rightleftharpoons}} & ES & \xrightarrow{k_2} & E + P \\ + & & & & \\ I & & & & \\ k_3 \downarrow\uparrow k_{-3} & & & & \\ EI & & & & \end{array} \qquad \text{(A2.4)}$$

V_{MAX} is not changed in this case, as substrate is in large surplus $(S \to \infty)$ and displaces the inhibitor (as reversely large quantities of inhibitor displace the substrate). The linearized plots for the experimental evidence will give the behavior reported in figure A2.4.

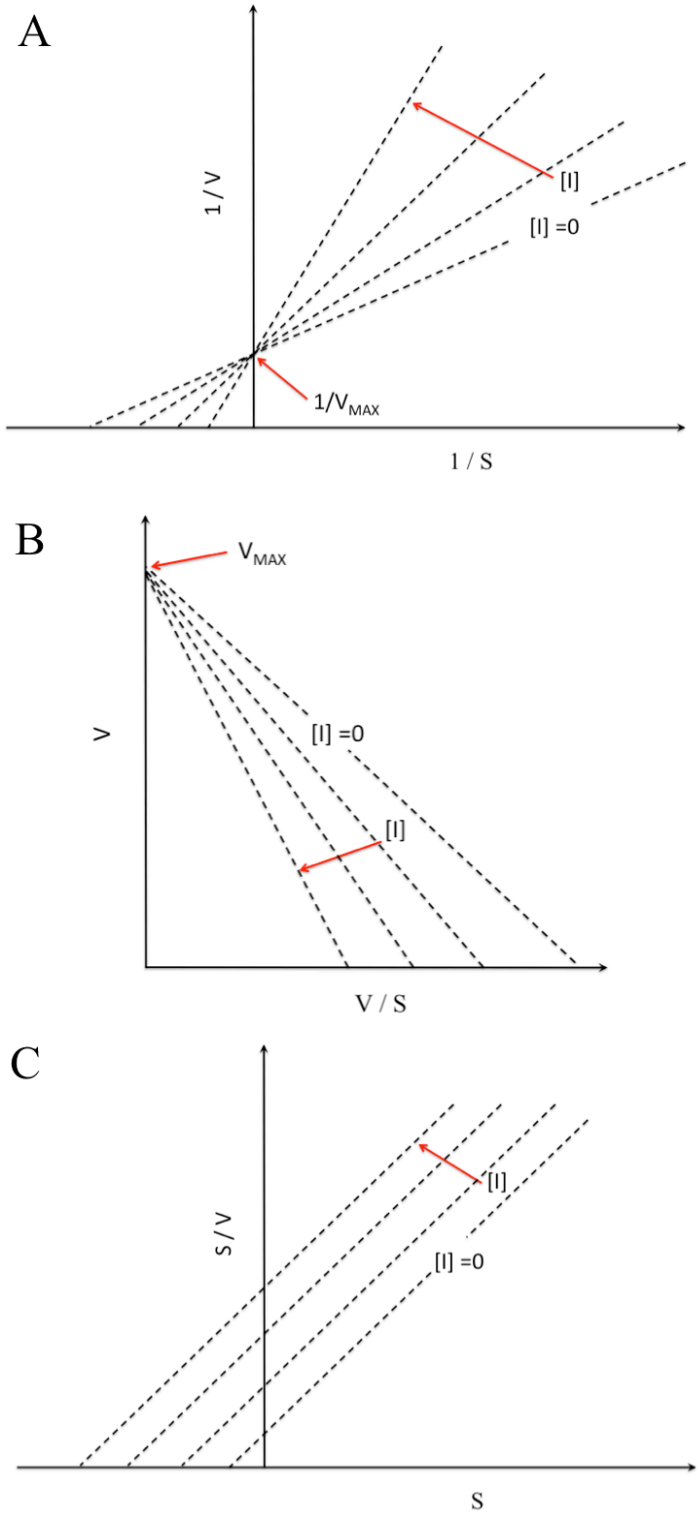

Figure A2.4 Lineweaver Burke double reciprocal (A) Eadie-Hofstee (B) and Hanes plot (C) for reversible complete competitive inhibition.

The Lineweaver Burke double reciprocal plot presents all straight lines that meet in a joint intercept on the ordinate, and the y-intercept corresponds to $1/V_{MAX}$. The Eadie-Hofstee plot presents non-parallel lines that meet in a joint intercept on the ordinate, and the y-intercept this time corresponds to V_{MAX}. The Hanes plot for competitive inhibition present parallel lines. It has to be remarked that Competitive inhibition is important for the analysis of enzyme specificity by substrate analog as competitive inhibitors (antagonists) serve as targeted blockers of enzyme reactions in therapy.

Uncompetitive inhibition

Uncompetitive inhibition is a rare type of inhibition. The inhibitor binds exclusively to the enzyme-substrate complex, thus, such a mechanism will be obtained when the binding site for the inhibitor is only formed in interaction with substrate:

$$\begin{array}{ccccc} E + S & \underset{k_{-1}}{\overset{k_1}{\rightleftharpoons}} & ES & \xrightarrow{k_2} & E + P \\ & & + & & \\ & & I & & \\ & & k_4 \downarrow\uparrow k_{-4} & & \\ & & ESI & & \end{array} \qquad \text{(A2.5)}$$

The linearized plots for the experimental evidence will give the behavior reported in figure A2.5.

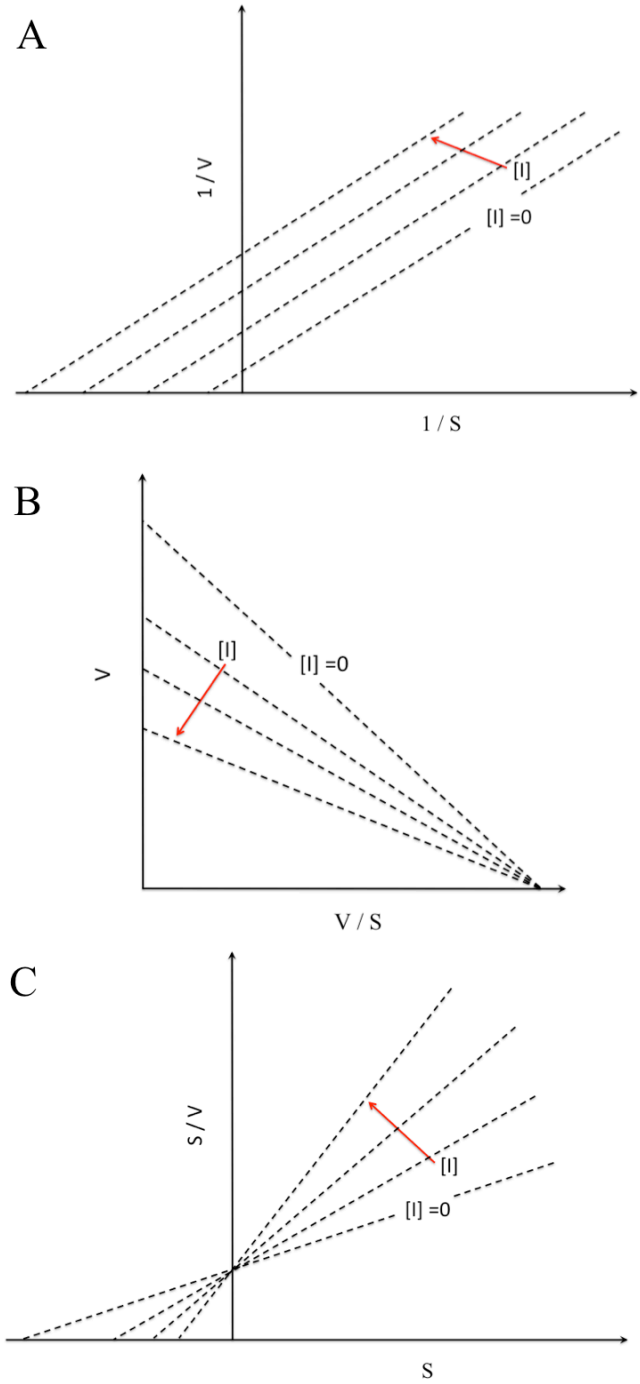

Figure A2.5 Lineweaver Burke double reciprocal (A) Eadie-Hofstee (B) and Hanes plot (C) for reversible complete uncompetitive inhibition.